

OPTIMIZATION OF VARIABLE STIFFNESS
CURVED COMPOSITE PANELS UTILIZING NURBS REFERENCE PATHS

A THESIS SUBMITTED TO
THE GRADUATE SCHOOL OF NATURAL AND APPLIED SCIENCES
OF
MIDDLE EAST TECHNICAL UNIVERSITY

BY

KAAN ÇİMEN

IN PARTIAL FULFILLMENT OF THE REQUIREMENTS
FOR
THE DEGREE OF MASTER OF SCIENCE
IN
AEROSPACE ENGINEERING

MAY 2022

Approval of the thesis:

**OPTIMIZATION OF VARIABLE STIFFNESS
CURVED COMPOSITE PANELS UTILIZING NURBS REFERENCE
PATHS**

Submitted by **KAAN ÇİMEN** in partial fulfillment of the requirements for the degree of **Master of Science in Aerospace Engineering, Middle East Technical University** by,

Prof. Dr. Halil Kalıpçılar
Dean, Graduate School of **Natural and Applied Sciences**

Prof. Dr. Serkan Özgen
Head of the Department, **Aerospace Engineering**

Prof. Dr. Altan Kayran
Supervisor, Aerospace Engineering, **METU**

Examining Committee Members:

Prof. Dr. Demirkan Çöker
Aerospace Eng, METU

Prof. Dr. Altan Kayran
Aerospace Eng, METU

Assoc. Prof. Dr. Melin Şahin
Aerospace Eng, METU

Assoc. Prof. Dr. Ercan Gürses
Aerospace Eng, METU

Assoc. Prof. Dr. Barış Sabuncuoğlu
Mechanical Eng., Hacettepe Uni.

Date: 10.05.2022

I hereby declare that all information in this document has been obtained and presented in accordance with academic rules and ethical conduct. I also declare that, as required by these rules and conduct, I have fully cited and referenced all material and results that are not original to this work.

Name Last name : Kaan Çimen

Signature :

ABSTRACT

OPTIMIZATION OF VARIABLE STIFFNESS CURVED COMPOSITE PANELS UTILIZING NURBS REFERENCE PATHS

Çimen, Kaan
Master of Science, Aerospace Engineering
Supervisor: Prof. Dr. Altan Kayran

May 2022, 157 pages

Variable stiffness composite structure concept has been studied since 1972; however, this concept is stepped into a new age after the automated fiber placement manufacturing machines are started to be used in industry. This study presents an optimization method for three-dimensional (3D) variable stiffness composite structures. The main contribution of the current study is the definition of the reference lay-up path by Non-Uniform Rational B Splines (NURBS) in 3D. The methodology is based on defining a reference path by NURBS and optimizing the NURBS parameters by using the Particle Swarm Optimization (PSO) method to minimize the total strain energy and maximize buckling load of the 3D curved composite panel utilizing unconstrained and constrained optimization. The results show that the reference lay-up path defined by NURBS is successfully optimized such that the total strain energy and the buckling load of the final design are minimized.

Keywords: Curved composite panel, fiber angle optimization, fiber path optimization, fiber placement machine, NURBS

ÖZ

NURBS REFERANS YOLLARINI KULLANAN DEĞİŞKEN SERTLİKLİ KAVİSLİ KOMPOZİT PANELLERİN OPTİMİZASYONU

Çimen, Kaan
Yüksek Lisans, Havacılık ve Uzay Mühendisliği
Tez Yöneticisi: Prof. Dr. Altan Kayran

Mayıs 2022, 157 sayfa

Değişken rijitlikli kompozit yapı konsepti 1972 yılından beri çalışılmaktadır, ancak bu konsept, otomatik fiber yerleştirme imalat makinelerinin sanayide kullanılmaya başlanmasıyla yeni bir çağa adım atmıştır. Bu çalışmada, üç boyutlu (3B) değişken rijitlikli kompozit yapılar için optimizasyon yöntemi sunulmaktadır. Mevcut çalışmanın önceki çalışmalardan temel farkı, referans yerleşim yolunun üç boyutlu (3B) düzgün olmayan rasyonel eğriler (NURBS) tarafından tanımlanmasıdır. Metodoloji, NURBS tarafından bir referans yolunun tanımlanmasına ve NURBS parametrelerinin, kısıtsız ve kısıtlı optimizasyon kullanarak toplam gerinim enerjisini ve 3B eğri kompozit panelin burkulma yükünü en aza indirmek için Parçacık Sürü Optimizasyonu (PSO) yöntemini kullanarak optimize etmeye dayanmaktadır. Sonuçlar, NURBS tarafından tanımlanan referans yerleştirme yolunun, nihai tasarımın toplam gerinim enerjisi ve burkulma yükünü en aza indirecek şekilde başarıyla optimize edildiğini göstermektedir.

Anahtar Kelimeler: Eğri kompozit paneller , fiber açısı optimizasyonu, fiber yolu optimizasyonu, fiber yerleştirme makinası, NURBS

To my bellowed family

ACKNOWLEDGMENTS

I would like to express my deepest gratitude to my supervisor Prof. Dr. Altan Kayran, for their guidance, advice, criticism, encouragement, and insight throughout the research.

I would like to thank Hasan İnci for sharing his knowledge and experience about the topic discussed in this thesis. Also, I would like to thank Mert Atasoy for his help and support.

I would like to thank my previous manager also my career and life guide Dr. Burcu Dönmez, for her help and support.

I would like to thank all my friends, whom I can't count names, who always supported me, encouraged me, and cheered me up on this long road until I had finished this thesis.

Finally, I wish to express my deepest feelings to my family. My mother, Arzu, has always supported me and encouraged me on this long road until I have finished this thesis. My father, Fikret, also was one of the main supporters and has always inspired me. Also, my brother Hakan Can serve as a model for me with his high tenacity and attitude of never giving up in hard times.

TABLE OF CONTENTS

ABSTRACT.....	v
ÖZ	vii
ACKNOWLEDGMENTS	x
TABLE OF CONTENTS.....	xi
LIST OF TABLES	xiv
LIST OF FIGURES	xvi
LIST OF ABBREVIATIONS.....	xxi
CHAPTERS	
1 INTRODUCTION	1
1.1 Motivation of the Study.....	3
1.2 Scope of the Study.....	4
2 LITERATURE SURVEY	7
2.1 Methods to Create Variable Stiffness Composites.....	7
2.2 Automated Fiber Placement Machine	19
2.3 Optimization of the VSC Structures.....	26
3 NON-UNIFORM RATIONAL BASIS SPLINES.....	31
3.1 Parametric Representation and Bezier Curves	31
3.2 B Splines	35
3.2.1 Knot Vector.....	37
3.2.2 Basis Functions of B-splines.....	37

3.3	NURBS	42
4	PARTICLE SWARM OPTIMIZATION	47
4.1	Basic PSO Algorithm.....	48
4.2	Constrained Optimization Problems and Penalty Function Approach	54
4.3	Verification of the PSO Code	55
5	MODELLING AND OPTIMIZATION OF VARIABLE STIFFNESS COMPOSITE CURVED PANELS	59
5.1	Creation of Variable Stiffness Composite Structure.....	60
5.1.1	NURBS Path Creation in Rhino	60
5.1.2	NURBS Path Creation in MATLAB	62
5.1.3	Generation of the Geometry and the Finite Element Model	64
5.1.4	Defining Shifted Paths in the Analysis Geometry.....	65
5.2	Optimization Parameters of VSC, Objective Functions and Constraints .	66
5.2.1	PSO Parameters	66
5.2.2	Optimization Variables.....	68
5.2.3	Objective Functions.....	69
5.2.4	Optimization Constraints.....	74
5.3	Optimization Scheme.....	75
5.3.1	MSC. Nastran Input File Manipulation	77
5.3.2	MSC. Nastran Output File Evaluation.....	77
6	RESULTS AND DISCUSSION ON THE ANALYSIS AND OPTIMIZATION RESULTS.....	81
6.1	Verification of the Optimization Algorithm	83
6.1.1	Flat Panel Strain Energy Minimization Verification Case	83

6.1.2	Modelling and Buckling Analysis of an Isotropic Panel with MSC. Patran and MSC. Nastran.....	89
6.2	Flat Panel Optimization.....	91
6.2.1	Strain Energy Minimization of the Flat Panel	92
6.2.2	Failure Index (FI) Minimization of the Flat Panel.....	104
6.3	Curved Panel Optimization	107
6.3.1	Buckling Load Factor (BLF) Maximization of the Curved Panel ..	109
6.3.2	Strain Energy Minimization of the Curved Panel.....	117
6.3.3	Strain Energy Minimization of the Curved Panel with Failure Index (FI) constraint.....	121
6.4	Discussions.....	125
7	CONCLUSION AND FUTURE WORK	129
	REFERENCES	133
	APENDICES.....	139
A.	Example Rhino Step File.....	139
B.	Nastran Input File.....	144
C.	Example of an optimization iteration	148
D.	One Layer Flat Panel Strain Energy Minimization with Fine Mesh.....	155

LIST OF TABLES

Table 4.1 PSO parameters	56
Table 5.1 Contents of the NURBS information card example in the Rhino interface	62
Table 5.2 Parameters of the NURBS curve	63
Table 5.3 PSO parameters used in the optimizations	67
Table 5.4 Explanation of the BLF	74
Table 6.1 Material properties of AS4/855-2, Graphite Epoxy y[34]	82
Table 6.2 Unit consistency table of MSC. Patran	83
Table 6.3 Optimization parameters for the strain energy minimization of the flat panel	83
Table 6.4 Control points of the reference fiber path for the flat panel	85
Table 6.5 Control points of final optimized fiber path for the verification case	87
Table 6.6 Material properties of the isotropic panel.....	90
Table 6.7 Comparison of the buckling stress calculated theoretically and by FEA in MSC. Nastran	90
Table 6.8 Control points of the reference fiber path for the flat panel	93
Table 6.9 Control points of the strain energy optimized fiber path for the one-layer flat panel	94
Table 6.10 Control points of the strain energy optimized fiber path for the four-layer flat panel	97
Table 6.11 Control points of the strain energy optimized fiber path for the four-layer flat panel	102
Table 6.12 Control points of failure index minimized fiber path for the four-layer flat panel	106
Table 6.13 Control points of the reference fiber path for the curved panel	109
Table 6.14 Control points of the BLF optimized fiber path for the four-layer curved panel	111

Table 6.15 Control points of the BLF optimized fiber path for the four-layer curved panel.....	116
Table 6.16 Control points of fiber path for four-layer flat panel with minimum strain energy.....	119
Table 6.17 Control points of the fiber path for four-layer curved panel with minimum strain energy subject to FI constraint.....	123

LIST OF FIGURES

Figure 1.1 Prepreg sheet bobbin and tow bobbin [2]	2
Figure 2.1 Representation of internally dropped ply [4]	8
Figure 2.2 Internally dropped ply, from Langley [4]	8
Figure 2.3 Ply with variable fiber volume fraction [4].....	9
Figure 2.4 Loaded circular plate with a circular hole at the center [12]	10
Figure 2.5 Loaded rectangular plate with a circular hole at the center [13].....	11
Figure 2.6 Spatially varying fiber paths with the fiber angle varying with respect to x coordinate only	13
Figure 2.7 Definition of fiber path angles	13
Figure 2.8 Effect of adding ϕ on the reference path (1) $\phi = 0$, (2) $\phi = 45$ and (3) $\phi = 90$ [4]	14
Figure 2.9 Fiber path definition for $T_0=0^\circ$, $T_1=45^\circ$ and $\phi = 0^\circ$ [10]	15
Figure 2.10 Composite engine fan blade [16]	17
Figure 2.11 Shifted and parallel fiber methods [10].....	18
Figure 2.12 AFP machine head with multiple tows	20
Figure 2.13 AFP machine with storage cabinet (a) cabinet (b) feeding system (c) layup head.....	20
Figure 2.14 Flow chart of the chosen concept.....	21
Figure 2.15 Conceptual design showing the separated parts of an AFP (Automated Fiber Placement) machine	22
Figure 2.16 Differential tow pay illustration [4]	22
Figure 2.17 Cut and restart ability of AFP machines [4]	23
Figure 2.18 Straight, curved, and wrinkled tows.....	23
Figure 2.19 Examples of gapped and overlapped layups	24
Figure 2.20 Layup with 0% coverage parameter.....	25
Figure 2.21 AFP manufacturing of the fuselage section of Airbus A350	26
Figure 2.22 Optimization parameters for MOGA optimization of VSC [22]	29
Figure 3.1 Representation of Bezier Curve in Equation (3.9).....	35

Figure 3.2 Bezier and B-Spline curves with the same control points [25]	36
Figure 3.3 Triangular pattern of basis functions	38
Figure 3.4 Control polyline (dashed line) and convex hull (in gray) of a B-Spline curve [28]	41
Figure 3.5 B-Spline semicircle	42
Figure 3.6 B-spline (polynomial curve) defined in homogeneous coordinates given by blue and its projection on gray plane yields NURBS curve given by red	43
Figure 3.7 Splines with two different P4 control points[24].....	44
Figure 3.8 Splines with two different knot values in possible NURBS envelope[29]	45
Figure 3.9 Splines with different weights for the same control point[24]	45
Figure 3.10 Semicircle Drawn by NURBS, B Spline and, Analytical Calculation	46
Figure 4.1 Geometric illustration of the PSO update scheme.....	51
Figure 4.2 Test problem illustration taken from Güldü [15].....	56
Figure 4.3 Variation of the best value of the objective function with the iteration number	58
Figure 5.1 NURBS layup path with its control points	61
Figure 5.2 Representation of the NURBS in Rhino.....	63
Figure 5.3 MATLAB representation of the NURBS exported from Rhino.....	64
Figure 5.4 An example for the reference fiber path.....	65
Figure 5.5 Shifting of the reference fiber path for covering the entire panel	66
Figure 5.6 Illustration of the method used in finding the fiber angle of finite elements utilizing the NURBS reference path	76
Figure 5.7 Optimization Flow Chart.....	79
Figure 6.1 Flat panel dimensions	84
Figure 6.2 Stacking sequence of the four-layer flat panel	84
Figure 6.3 Boundary conditions and loading for the verification case	85
Figure 6.4 Rhino representation of the reference fiber path	86
Figure 6.5 MATLAB representation of the reference fiber path	86

Figure 6.6 MATLAB representation of the reference fiber path (green) and the final optimized fiber path (purple).....	87
Figure 6.7 Rhino representation of the reference fiber path (yellow) and the final optimized fiber path (black)	87
Figure 6.8 Variation of the strain energy with the iteration number for the four-layer flat panel of the verification case.....	88
Figure 6.9 Flat panel dimensions for the buckling analysis of an isotropic flat panel	89
Figure 6.10 Quarter panel boundary conditions for the buckling analysis.....	90
Figure 6.11 Loading and boundary conditions of the flat panel.....	91
Figure 6.12 Reference NURBS path for flat panel created by Rhino	92
Figure 6.13 Flat panel reference path created by MATLAB.....	92
Figure 6.14 Strain energy optimized fiber path for the one-layer flat panel; Matlab representation	93
Figure 6.15 Strain energy optimized fiber path for the one-layer flat panel; Rhino representation	94
Figure 6.16 Strain energy versus the iteration number for the one-layer flat panel strain energy minimization problem.....	95
Figure 6.17 Setodeeh et al.'s work for fiber angle optimization with cellular automata [42].....	95
Figure 6.18 Strain energy optimized fiber path for the four-layer flat panel	96
Figure 6.19 Strain energy optimized fiber path for the four-layer flat panel; Rhino representation	97
Figure 6.20 Strain energy versus the iteration number for the four-layer flat panel strain energy minimization problem.....	98
Figure 6.21 Strain energy versus the iteration number for the four-layer flat panel strain energy minimization problem solved with (T_0, T_1) fiber path definition method	100
Figure 6.22 Strain energy optimized fiber path for the four-layer flat panel; solved with (T_0, T_1) fiber path definition method.....	100

Figure 6.23 Strain energy optimized fiber path for the four-layer flat panel subject to FI constraint	101
Figure 6.24 Rhino representation of strain energy optimized fiber path (yellow) and its opposite signed path (black) for the four-layer flat panel subject to FI constraint	102
Figure 6.25 FI plot of the flat panel with the initial reference path under the given load and boundary conditions	103
Figure 6.26 FI plot of the flat panel with the optimized fiber path under the given load and boundary conditions	103
Figure 6.27 Strain energy versus the iteration number for the four-layer flat panel strain energy minimization problem with FI constraint.....	104
Figure 6.28 Failure index minimized fiber path for the four-layer flat panel; Matlab representation	105
Figure 6.29 Failure index minimized fiber path for the four-layer flat panel; Rhino representation	105
Figure 6.30 Strain energy versus the iteration number for the four-layer flat panel	106
Figure 6.31 Curved panel dimensions (mm).....	107
Figure 6.32 Reference NURBS path for the curved panel created by Rhino	108
Figure 6.33 MSC. Patran model of the curved panel for the BLF maximization case study	110
Figure 6.34 BLF optimized fiber path for the four-layer curved panel	110
Figure 6.35 Variation of the BLF with the iteration number for the BLF maximization of the curved panel	112
Figure 6.36 First buckling mode shape of the curved panel with the initial reference fiber path	113
Figure 6.37 First buckling mode shape of the curved panel with the optimized fiber path.....	113
Figure 6.38 MSC. Patran model of the curved panel for the BLF maximization case study	114

Figure 6.39 BLF optimized fiber path for the four-layer curved panel.....	115
Figure 6.40 Variation of the BLF with the iteration number for the BLF maximization of the curved panel	117
Figure 6.41 MSC. Patran model of the curved panel for the strain energy maximization case study.....	118
Figure 6.42 Fiber paths for the curved panel; reference fiber path and the fiber path with minimum strain energy.....	119
Figure 6.43 Variation of the strain energy with the iteration number for the curved panel strain energy minimization case study	120
Figure 6.44 MSC. Patran model of the curved panel for the strain energy maximization case study constrained with FI	121
Figure 6.45 Rhino representation of the fiber paths for the four-layer curved panel ; reference fiber path and the fiber path with minimum strain energy	122
Figure 6.46 FI plot of the curved panel with the initial reference path under the given load and boundary conditions	124
Figure 6.47 FI plot of the optimized curved panel under the given load and boundary conditions	124
Figure 6.48 Variation of the strain energy with the iteration number for the strain energy minimization of the curved panel with FI constraint.....	125
Figure 6.49 Short cantilever design with different meshes(a) Uniformly distributed loaded short cantilever beam; (b)46 x16 mesh; (c) 91 x31 mesh; (d) 301x101 mesh [42]	126

LIST OF ABBREVIATIONS

AFP: Automated Fiber Placement

BLF: Buckling Load Factor

FI: Failure Index

FEA: Finite Element Analysis

FEM: Finite Element Model

NURBS: Non-Uniform Rational Bezier Splines

PSO: Particle Swarm Optimization

VSC: Variable Stiffness Composite

CHAPTER 1

INTRODUCTION

Composite means “made up of distinct parts or elements.” In engineering, composite material is used for two or more materials league together to form a new material that has powerful material properties [1]. One special type of composite named prepreg is made from strong straight fibers placed within a polymeric matrix. Prepregs are either in the form of sheet bobbins or tow bobbins, as shown in Figure 1.1. Prepregs are widely used in engineering to manufacture composite structures. In the aerospace industry, structures are desired to be lightweight, and they should be able to operate under heavy loading conditions. These design constraints cannot be met by metals easily; however composite materials have a high strength-to-weight ratio. This property makes composite materials one of the best choices to design and manufacture aerospace structures. Another advantageous property of the composite structures, especially prepregs, is the ability to tailor composite material to provide optimum resistance to different load cases. Thin layers of laid up prepreg, which consists of fiber and resin mixtures, are named as ply. By arranging the number of plies and/or arranging the layup angle sequence of the plies, composite structures can be made stronger against the loading conditions. Although these arrangements can be done by traditional manufacturing methods and they give good results, the development of Automated Fiber Placement (AFP) machine changed the design of composites aerospace structures by introducing more design parameters to obtain the desired structural properties.



Figure 1.1 Prepreg sheet bobbin and tow bobbin [2]

AFP enables to modify the in-plane layup path which cannot be obtained utilizing straight fiber path. By using AFP, in plane variations of the fiber direction can be achieved. This variation causes composite layer to have variable stiffness in its plane. By optimizing the fiber path definition, variable stiffness composite (VSC) structures become more efficient. To carry out the optimization, the path of the fiber should be defined mathematically. This path can be defined with a smooth antisymmetric function with respect to one of the axis of the composite structure to be optimized and it passes through the origin of the cartesian coordinate frame [3]. This method is efficient and easy to use for defining a path on a flat surface [4]. To manufacture curved surfaces with variable stiffness, either the layup path should be defined in three dimensions by splines, or the curved surfaces would be manufactured by bending the straight panels. The mathematical equation of the path depends on several variables and these variables should be optimized to achieve the optimized variable stiffness composite structure. To define the path in three dimensions, Non-Uniform Rational B Splines (NURBS) with control points, knots and weights as the design variables can be used. Various optimization methods can be used for optimizing the path. There are gradient based optimization and gradientless optimization methods. However, gradientless methods like genetic algorithm or

particle swarm optimization are easier to use for composite structures' optimization. Because they do not need the gradient information [5].

1.1 Motivation of the Study

This thesis aims to study the effectiveness of NURBS based fiber path definition to construct variable stiffness composite structures in 3D. Previous studies have shown that variable stiffness composite (VSC) structures are superior to the constant stiffness straight fiber path composite structures since the variable stiffness concept allows the definition of more design variables to tailor the stiffness of the composite structure with respect to the loads applied. Variable stiffness concept is a relatively new topic because of the manufacturing techniques are developed in the last decades. Most of the studies about variable stiffness composites are performed on two-dimensional plate-like structures.

In the thesis contrary to the previous studies on VSC structures, a 3D path definition is made on a curved surface and the fiber path defined by NURBS is optimized according to the selected objective functions. As for the objective functions, minimization of total strain energy optimization and maximization of buckling load factors are selected. Furthermore, unconstrained and constrained optimization studies are performed with these objective functions. In most of the studies encountered in the literature, are done on flat surfaces and paths are defined in 2D. However, in this study the goal is to define a 3D NURBS path on a 3D panel and optimize the fiber path according to the objective function by obeying the constraints.

The concentration of this work is on developing a structural optimization methodology for the definition of the fiber path on curved composite panels. For this purpose, to define the reference path on a curve surface, NURBS based Rhinoceros software [6] is used. Optimization process involves structural modelling, structural analysis, and design variable optimization steps. To create the finite element model (FEM), MSC. Patran is used, and as the finite element solver MSC. Nastran is used.

Optimization of the NURBS parameters, modelling the VSC structure and finite element analysis of the model is automatized via a code developed in MATLAB. With the developed tool, reference fiber path can be defined and optimized directly on the curved panel as a spline.

1.2 Scope of the Study

This thesis is organized as seven chapters.

Chapter 1 is the introduction chapter which introduces the variable stiffness concept, and the motivation of the study is explained.

Chapter 2 includes the literature survey on the variable stiffness concept and optimization studies conducted on variable stiffness composites. In this chapter the methods to create variable stiffness composites are explained, alternative fiber path definitions are discussed. Automated Fiber Placement (AFP) concept is explained, and the flow chart of the AFP manufacturing process is presented. Lastly, analysis of variable stiffness composites structures, and their optimization are reviewed.

Chapter 3 focuses on the fiber path definition method. The theory and background information about the NURBS is given. Formulation of the NURBS curve is explained in detail.

Chapter 4 is about the optimization method; Particle Swarm Optimization (PSO). The penalty approach to solve the constrained optimization problem with the PSO is explained. Verification of the PSO code and the penalty approach are done for a generic optimization problem.

Chapter 5 gives the details of the optimization process and the algorithm. Creation of VSC panels and fiber path definition method on a curved panel are explained. The optimization parameters, constraints and objective functions used are defined and the optimization scheme is given. Details of the generation of the finite element model, coupling of the finite element solver MSC. Nastran and the PSO algorithm via the interface code developed in MATLAB are given.

Chapter 6 gives the optimization results of different geometries and load cases. Based on the numerical results, conclusions are drawn. Initially, flat panel optimization results for strain energy minimization and failure index minimization are presented. Then, unconstrained, and constrained strain energy minimization and buckling load maximization of curved panel has been performed and results are presented. In strain energy minimization of flat panel, the analysis is done for one layered panel and four layered panel. Following to that four layered panels are used for failure index minimization of flat panel. Lastly, unconstrained, and constrained strain energy minimization and buckling load factor maximization of curved panels are examined .

Chapter 7 is the conclusion of the thesis study and gives information about further discussions on the whole study. It is the summary chapter of the study and the potential further studies about the topic are also discussed in this chapter.

CHAPTER 2

LITERATURE SURVEY

2.1 Methods to Create Variable Stiffness Composites

The composite laminates used in the industry consist of stacked plies. Traditionally, each ply has a constant fiber orientation angle throughout the layer. The ply has straight fibers stacked in different angles, typically 0, 90, +/-45 degrees, to construct the laminate [7], and each ply has specific material properties and thickness. The mechanical strength of the ply in the fiber direction is very high. In the traditional method, plies with constant fiber angles are stacked up in different angles to handle various loading conditions. For multi-axial load conditions, intended for the composite structure to be stronger in the high stress areas, variable stiffness composite (VSC) concept is proposed in the literature. Variation of the stiffness can be achieved by various ways. Dropping plies in the laminate, variation of the fiber volume fraction in a ply or changing the fiber orientation within a layer are some of these approaches in creating variable stiffness composites. However, creating variable stiffness composite is not limited to these approaches [4].

DiNardo [8] worked on the internally dropped plies in his thesis. The representation of dropped ply can be seen in Figure 2.1 and Figure 2.2. In the study, variation of the stiffness provided by the dropped plies are examined for plates loaded in compression. In this method, in addition to the change of elastic properties, an eccentricity in loading is introduced and it is concluded that changes in the elastic properties have reduced the buckling loads [8]. This reduction is caused by the mid-plane change, and it is not related to the introduced eccentricity of the loading [4].

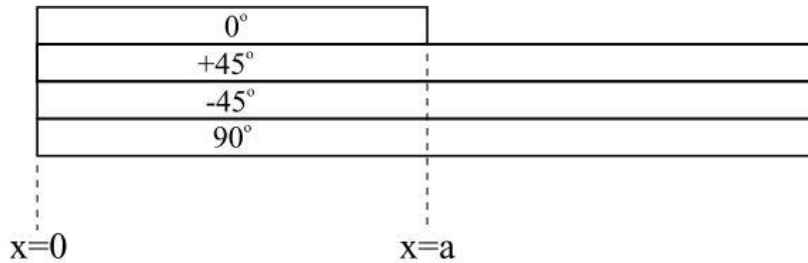


Figure 2.1 Representation of internally dropped ply [4]

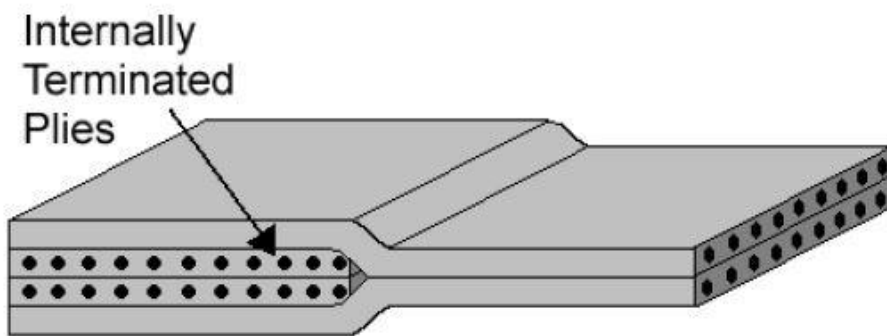


Figure 2.2 Internally dropped ply, from Langley [4]

As an example for providing variable stiffness in the ply by changing the volume fraction, the study conducted by Leissa and Martin [9] can be given. In this study, volume fraction of the straight and parallel fibers is increased continuously towards the one end of the ply as seen in Figure 2.3 [3]. The buckling and vibration response of a rectangular ply, which has variable fiber density is examined in this study. Because the fiber volume fraction varies from one edge to other edge of the ply as seen in Figure 2.3, the material is considered as nonhomogeneous. Variation of fiber volume fraction causes the stiffness properties and constants of governing elasticity equations to vary to vary[10]. This variation makes the problem hard to solve

analytically; thus, Ritz method is used to solve the in-plane elasticity problem. It is seen that in some cases, there are 38 % increase in the critical buckling load and 21% improvement in the fundamental frequency of vibration [10]. However, in some cases deterioration of both parameters is seen [9] .

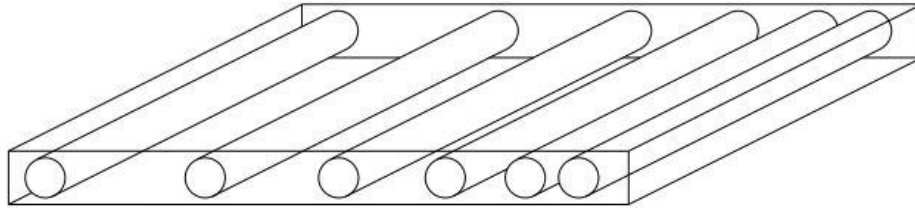


Figure 2.3 Ply with variable fiber volume fraction [4]

The third method to manufacture variable stiffness composite structures is spatially varying the orientation of fibers in a layer of the composite structure. By continuously placing the composite prepreg tows over the surface following a curved reference path, VSC structures can be manufactured. To manufacture variable stiffness composite by this method, layup process must be very sensitive; thus, automatized. Cooper [11] in 1972 proposed a computer-aided laying system for analogue fiber lay-up. This is the very first study for VSC with computer based automatized lay-up system.

Hoff and Muser [12] worked on the design problem of a circular plate with a circular hole loaded uniaxially, as seen in in Figure 2.4. They performed the closed form solution of the stress concentration factor of the circular plate with the circular hole. According to their study, arranging the fiber layup around the hole can result in significant reduction in the stress concentration factor.

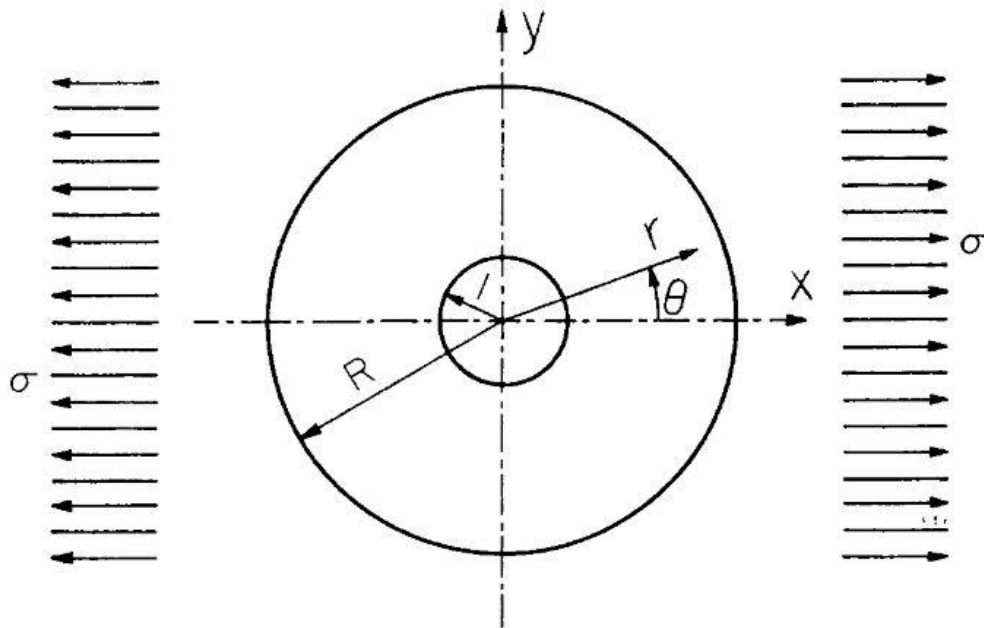


Figure 2.4 Loaded circular plate with a circular hole at the center [12]

Although there are some studies about increasing the performance of composite structures by tailoring the ply, curvilinear fiber format is first proposed by Hyer and Charette in 1989 [13]. They claim that aligning the fibers parallel to each other in straight lines is not the best way to use fiber reinforced composites [13]. In their study, unidirectionally loaded plate with a hole problem seen in Figure 2.5 is examined. In the hole in a plate problem, there is a discontinuity in the plate which causes stress concentration. To handle this discontinuity, it is proposed that curvilinear continuous fibers can be passed around the hole to eliminate discontinuity and decrease the stress concentration.

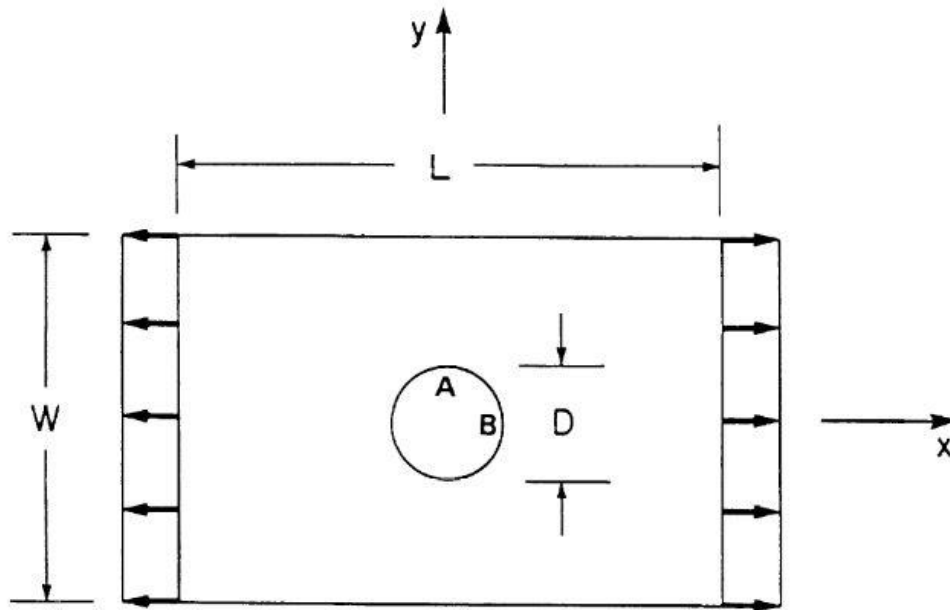


Figure 2.5 Loaded rectangular plate with a circular hole at the center [13]

In their study, 16 layered quarter plate with 18 elements is used. To make comparison quasi-isotropic ply $[\pm 45 / 0 / 90]_s$ sequence is examined in terms of tensile load capacity and buckling response and they are taken as datum. While constructing the variable stiffness laminate top and bottom two plies ($\pm 45^\circ$ plies) are used to enhance the structure against unwanted shear failure. Middle 12 plies are used in a curvilinear fashion to optimize composite plate in terms of loading capacity and the buckling response. This study is one of the very first studies on the VSC. It is discussed that manufacturing of curvilinear plies is considered as a drawback. However, besides the practical manufacturing related considerations, theoretically it is seen that loading capacity has risen in curvilinear stacking compared to the quasi-isotropic stacking [13].

Following the study of Hyer and Charette, Hyer and Lee [14] studied on the improvement of the buckling response of a compressively loaded plate with a hole by using continuous fiber placement. In this study, they have used a gradient search method to maximize the buckling load factor by optimizing the fiber orientation

angles in the ply [14]. They found out that by optimizing the fiber path, it is possible to distribute load from the hole to the edges of the plate. The results show that buckling load factor increased 2.96 times compared to the quasi -isotropic layup taken as datum [14].

Spatially varying fiber angle concept for manufacturing VSC is studied in several research. However, until Gürdal and Olmedo's work [3], there were not any solid path definition technique to introduce the layup paths mathematically. In this study, they defined the continuous lay-up path that varies only with respect to one of the coordinates. This is because of the practical limitations in manufacturing. In such a definition, the lay-up path passes through the origin of the cartesian coordinate frame and defined as a smooth antisymmetric function of the x coordinate [3]. This path definition has minimum number of variables for the layup path in a rectangular panel [15]. Spatial variation of the layup path also changes the mechanical properties of the ply. This is because prepregs are fiber reinforced composites and their material properties are different in the fiber direction and in the transverse direction. In the Figure 2.6 spatially varying fiber path is depicted.

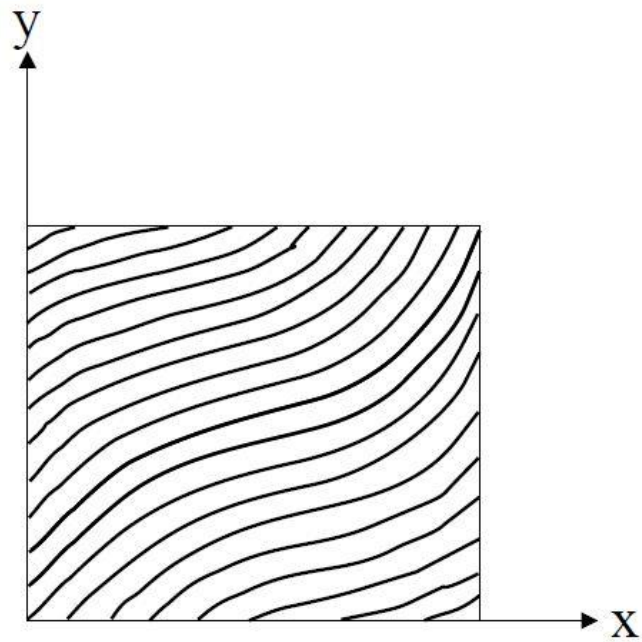


Figure 2.6 Spatially varying fiber paths with the fiber angle varying with respect to x coordinate only

In this method, the fiber path angle (θ) is defined by three parameters. T_1 is the angle of the fiber at a characteristic distance away from the center of the panel and T_0 is the angle of the fiber path at the center of the panel and, ϕ is the variation angle at the center of the panel giving the rotation of the tow placement axis (see Figure 2.7).

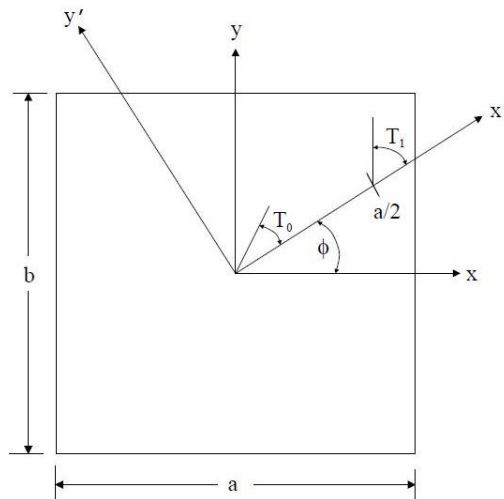


Figure 2.7 Definition of fiber path angles

A linear variation of the fiber orientation along the x coordinate is obtained if the fiber orientation is defined by Equation.(2.1) [3].

$$\theta(x) = \frac{2(T_1 - T_0)}{a}x + T_0 \quad (2.1)$$

The fiber angle starts with T_0 at the panel's center and reaches the angle T_1 at the panel's edge. The variation angle ϕ is assumed to be zero. The most basic function of variation of the y coordinate with respect to the x is given by Eqns.(2.2) and (2.3).

$$y = \frac{a}{2(T_1 - T_0)} \left\{ -\ln \left[\cos \left(T_0 + \frac{2(T_1 - T_0)x}{a} \right) \right] + \ln [\cos(T_0)] \right\} \quad (2.2)$$

$$0 \leq x < a/2$$

$$y = \frac{a}{2(T_1 - T_0)} \left\{ \ln \left[\cos \left(T_1 + \frac{2(T_1 - T_0)x}{a} \right) \right] - \ln [\cos(T_1)] \right\} \quad (2.3)$$

$$-a/2 \leq x < 0$$

In Figure 2.8 the effect of the rotation angle ϕ on the composite laminate can be seen.

In Figure 2.9 a fiber path for $T_0=0^\circ$, $T_1=45^\circ$ and $\phi = 0^\circ$ shown

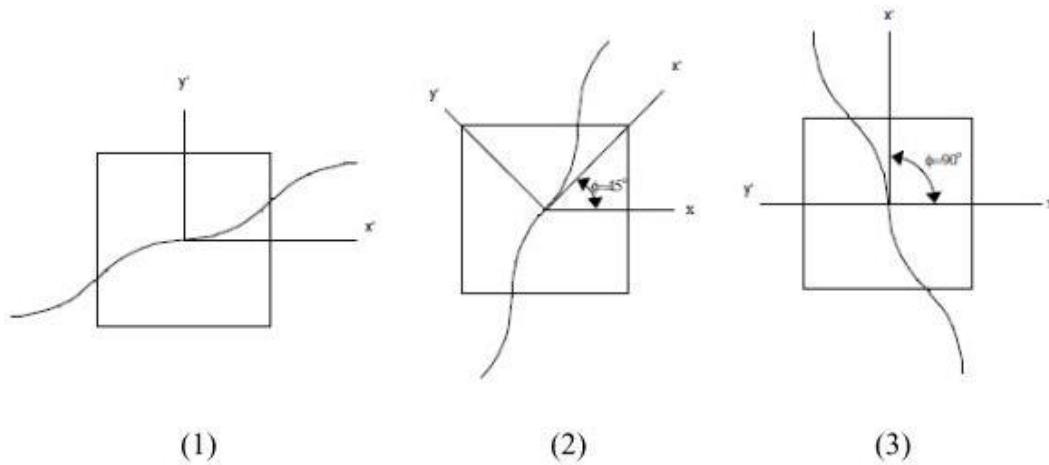


Figure 2.8 Effect of adding ϕ on the reference path (1) $\phi = 0$, (2) $\phi = 45$ and (3) $\phi = 90$ [4]

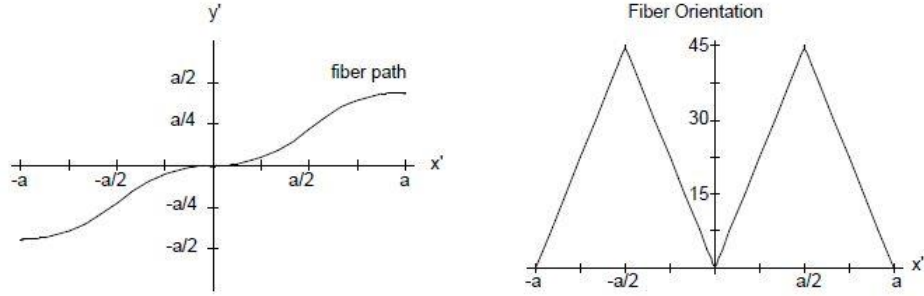


Figure 2.9 Fiber path definition for $T_0=0^\circ$, $T_1=45^\circ$ and $\phi = 0^\circ$ [10]

In more general case the, when there is rotation of axis such that $\phi \neq 0$, the fiber path angle (θ) and the y coordinate of the fiber path with respect to the x are defined by Equation (2.4), Equation (2.5) and Equation (2.6).

$$y'(x') = \begin{cases} \frac{a}{2(T_0 - T_1)} \left\{ \ln [\cos T_0] - 2 \ln [\cos T_1] + \ln \left[\cos \left(-T_0 + 2T_1 + \frac{2(T_1 - T_0)}{a} x' \right) \right] \right\} \\ \quad \text{for } -a \leq x' \leq -\frac{a}{2} \\ \frac{a}{2(T_0 - T_1)} \left\{ -\ln [\cos T_1] + \ln \left[\cos \left(T_1 + \frac{2(T_1 - T_0)}{a} x' \right) \right] \right\} \\ \quad \text{for } -\frac{a}{2} \leq x' \leq 0 \\ \frac{a}{2(T_0 - T_1)} \left\{ -\ln [\cos T_0] + \ln \left[\cos \left(T_0 + \frac{2(T_1 - T_0)}{a} x' \right) \right] \right\} \\ \quad \text{for } 0 \leq x' \leq \frac{a}{2} \\ \frac{a}{2(T_1 - T_0)} \left\{ \ln [\cos T_0] - 2 \ln [\cos T_1] + \ln \left[\cos \left(-T_0 + 2T_1 + \frac{2(T_1 - T_0)}{a} x' \right) \right] \right\} \\ \quad \text{for } \frac{a}{2} \leq x' \leq a \end{cases} \quad (2.4)$$

$$\theta(x') = \begin{cases} \phi + \frac{2}{a}(T_1 - T_0)x' + T_0 - 2(T_0 - T_1), & \text{for } -a \leq x' \leq -\frac{a}{2} \\ \phi + \frac{2}{a}(T_0 - T_1)x' + T_0, & \text{for } -\frac{a}{2} \leq x' \leq 0 \\ \phi + \frac{2}{a}(T_1 - T_0)x' + T_0, & \text{for } 0 \leq x' \leq \frac{a}{2} \\ \phi + \frac{2}{a}(T_0 - T_1)x' + T_0 - 2(T_0 - T_1), & \text{for } a/2 \leq x' \leq a \end{cases} \quad (2.5)$$

$$x' = x \cos(\phi) + y \sin(\phi) \quad (2.6)$$

The formulation to define fiber path with a smooth antisymmetric function of x , is very efficient and easy to use for defining the fiber path on a flat surface [4]. Nagendra et al. [16] worked on a different method to define the fiber path on surfaces. In this work, the focus is optimizing the fiber paths which can easily be manufactured by AFP [16]. To define the fiber path, Nonuniform Rational B Splines (NURBS) is used. It should be noted that NURBS has superior control capability of the spline and flexibility since it is used in commercial design tools [17]. In the study, a plate with a central hole and an engine blade in Figure 2.10 are used as geometries. The design objective is to optimize the buckling loads of the variable stiffness composite structures utilizing fiber paths which are defined by NURBS. The NURBS parameters are optimized to find best fiber path against buckling. By utilizing the NURBS, the best fiber path that is manufacturable by the AFP machine with active manufacturing constraints is determined. The manufacturing constraints come from the limits of the 7-axis AFP machine developed by Cincinnati Milacron Inc. they have used.

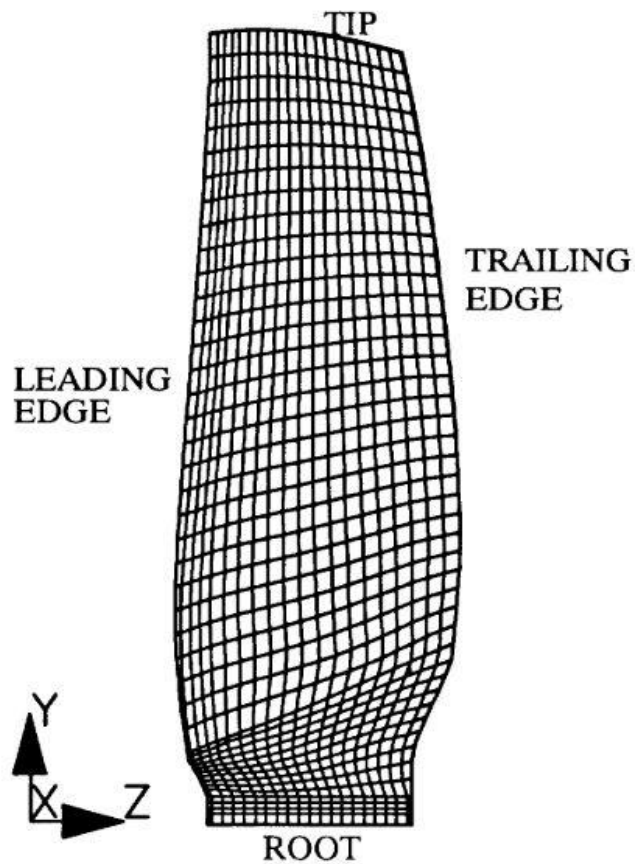


Figure 2.10 Composite engine fan blade [16]

NURBS curves are splines defined on either on flat surfaces or curved surfaces. This is main advantage when manufacturing constraints are considered. Because the multi-axis layup machines work in 3D space and defining the fiber layup path in three dimensions is advantageous in terms of sensitivity and accuracy of the layup. Another way of defining the fiber path is in 2D and after optimizing the fiber path defined in 2D, the real 3D shape is manufactured. The laminate optimized in 2D is placed on a mold to give the wanted 3D shape. However, with NURBS one can define 3D fiber path, optimize it to design a manufacturable structure in 3D.

After the reference fiber path is defined, AFP machine covers the whole geometry using this fiber path definition. Waldhart proposed two methods to manufacture variable stiffness composite structures [4]. The first method is the shifted reference path method in which the reference path is shifted along one of the axis; it could be x or y (see Figure 2.11). In Waldhart’s study the shift axis is taken as the y direction of global coordinate axis as shown in Figure 2.11. In this method, the distance between two shifted paths differs according to the position as seen in Figure 2.11(a). The other method is the parallel fiber method. In this method, new layup paths, which are parallel to the reference path, are defined. In this method the distance between two paths perpendicular to the path itself does not change by the position, as seen in Figure 2.11 (b). In Figure 2.11, the thicker solid lines are the fiber path of the center of the prepreg tow and thinner dashed lines are the edges of the prepreg material.

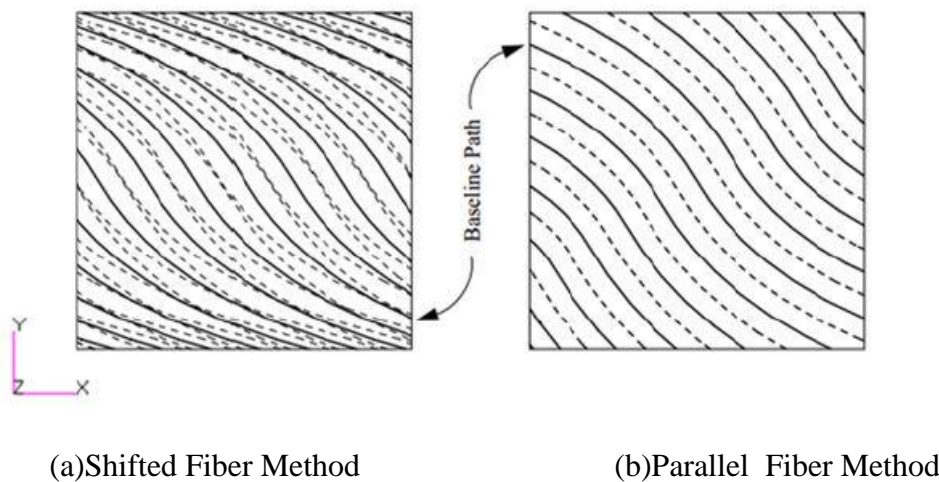


Figure 2.11 Shifted and parallel fiber methods [10]

When these two methods are compared, the shifted fiber method is more effective in terms of the redistributing the loads. This causes more improvement in the buckling loads [18]. When the manufacturability is compared, since in parallel method the shape of the layup path changes, there can be problems associated with manufacturability [15], and the minimum turning radius constraint of the prepreg tows may not be satisfied.

2.2 Automated Fiber Placement Machine

With the advent in composite technology and increasing usage of composite materials, automation becomes more and more necessary in manufacturing of composite products. Automated Fiber Placement Machines (AFP) are designed for this purpose increasing the speed and quality of the composite layup process. The most time consuming and expensive part of composite production is the layup process. Automation of this process increases the production speed and the quality as well as allowing more complex geometries to be produced. The automation in production is achieved by Automated Fiber Placement machines (AFP).

In the industry, AFP machines first went into action in 1980s. AFP appeared commercially as the combination of automated tape laying (ATL) and filament winding [19]. AFP is basically a composite part manufacturing technique by using six or seven axes CNC controlled machines. These machines increase the speed of production, enable high volume production, increase reliability, and in the long-term cost effectiveness because of the reduction of waste [7].

Modern AFP machine heads (Figure 2.12) can lay up to 32 prepreg tows collaterally in a controlled manner. The CNC control enables the tows to follow up a defined path [6]. The capabilities of the machine head allow it to cover all surfaces of the geometry [19]. They use prepreg tows with varying widths from 1/8" to 1" [15]. The layup material is not only the thermoset prepreg tow, but also thermoplastic composites can also be used. Some AFP machines can store the material in a special cabinet and feed the prepreg tow from this cabinet (Figure 2.13). However, in some AFP machines, material is loaded to the AFP machine head and machine feeds the prepreg tow from its head as seen in Figure 2.12. There are two different head designs, one is mounted on a gantry and can have 6 axis movement and there are also robot heads that are cable of laying up to manufacture more complex shapes.



Figure 2.12 AFP machine head with multiple tows

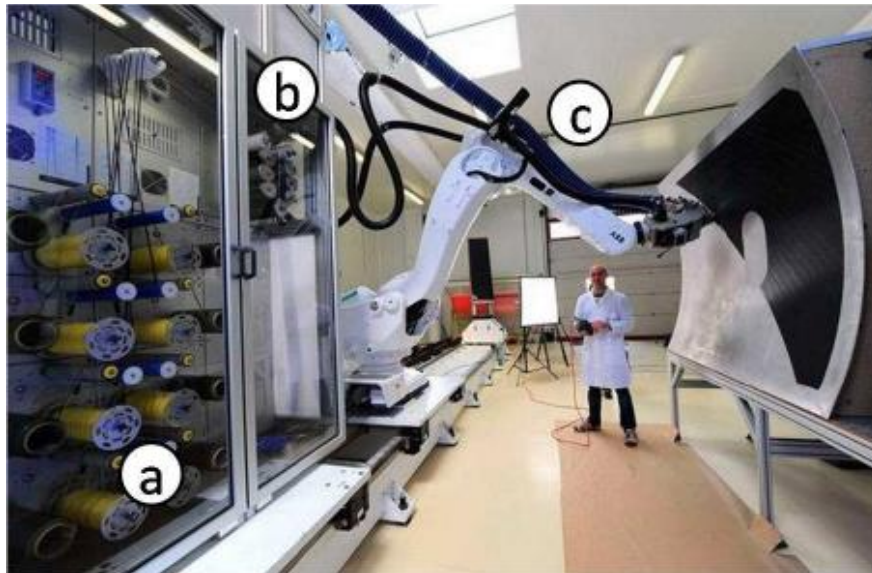


Figure 2.13 AFP machine with storage cabinet (a) cabinet (b) feeding system (c) layup head

There are several processes that an automated fiber placement machine should be capable of no matter how the machine is designed. These processes are given in Figure 2.14.

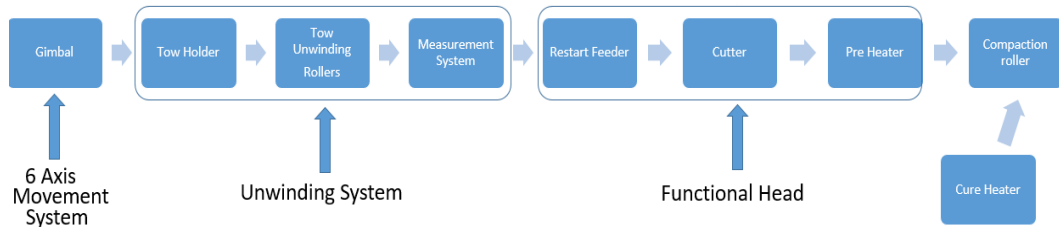


Figure 2.14 Flow chart of the chosen concept

An AFP machine should be able to hold the material that will be used for lay-up. Composite material should be unwound, and this process should be done by applying tension to the composite in a certain range. Measurement system should be used to keep the tension in this acceptable range such that the tension will not harm the material. After the unwinding operation, the material enters the functional head. Functional head should be capable of four main functions; restart feed, cut mechanism, heating and compaction system. These functions are necessary for the lay-up process. When the composite material is cut to start a new ply (lay-up), due to the tension material tries to go back to the tow holder; hence to prevent the material leaving the functional head, a mechanism should hold the material just after the cutting operation. Moreover, after the cutting operation, the material should be fed to the compaction roller for the start of the next lay-up which is done by the restart feed mechanism. In addition, the material should be laid-up with a certain pressure applied against the surface. This pressure is obtained by compressing the material between a roller, called the compaction roller, and the surface area. Finally, heating system is used to cure the thermoset/thermoplastic material after the lay-up. A conceptual design of an AFP machine head is illustrated in Figure 2.15.

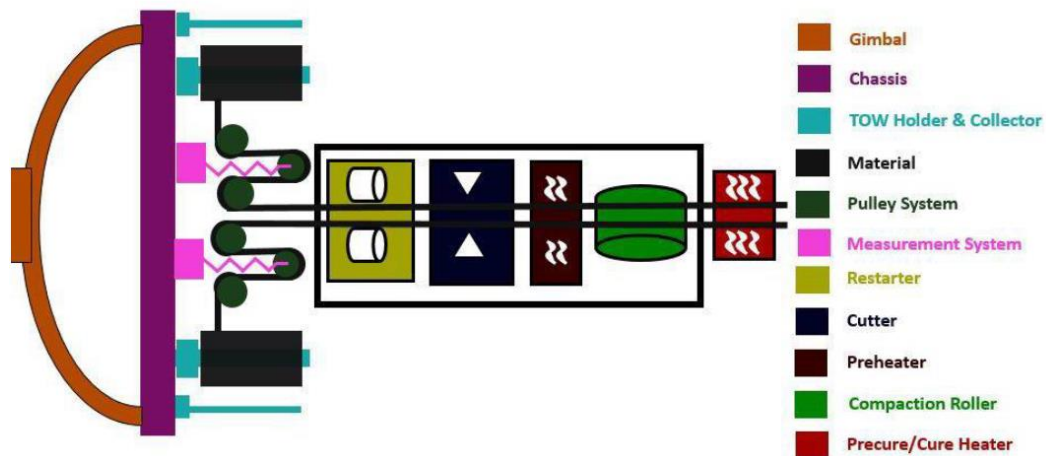


Figure 2.15 Conceptual design showing the separated parts of an AFP (Automated Fiber Placement) machine

There are several critical capabilities and constraints in AFP processes. First one is called as the tow pay. Tow pay is the difference of the tow feed speed in radial layups. It should be noted that tows are laid up on the mold surface and when the surface has a curvature, the inner tow feed speed must be slower than the outer tow feed speed. As shown in Figure 2.16, for radial paths, tow path A's tow feed speed must be higher than the tow path B's tow feed speed. This is controlled by the machine automatically [4].

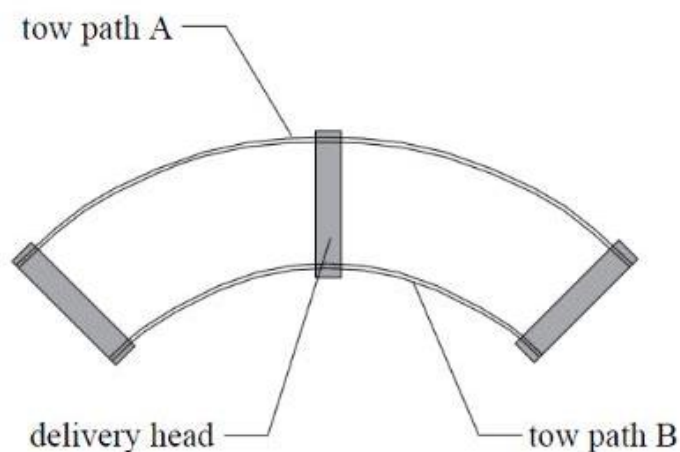


Figure 2.16 Differential tow pay illustration [4]

In AFP machines, machine head must have the capability of cutting and restarting each tow to enable layup on complex surfaces with holes and edges. Figure 2.17 illustrates the cut and restart capability of AFP machines.

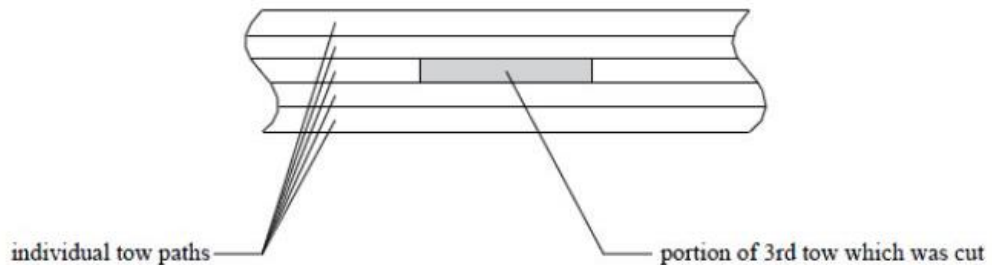


Figure 2.17 Cut and restart ability of AFP machines [4]

When laying up the tows on a curved path, there could be some wrinkles due to the forced in-plane deformation [15]. The reason for this is that tow's inner radius is smaller than the tow's outer radius when laying up tows on curved paths. Hence, there is a minimum turning radius constraint for AFP machines. In Figure 2.18 examples of straight, curved, and wrinkled tow are represented. The wrinkling lowers the laminate quality and can cause early ply failures [15].

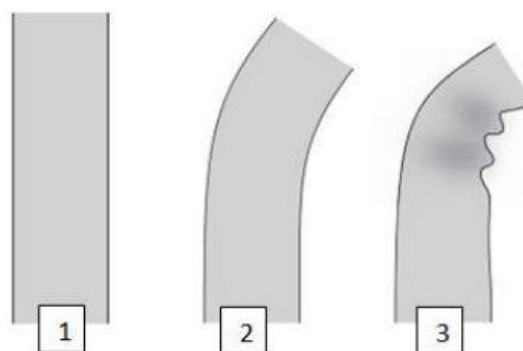


Figure 2.18 Straight, curved, and wrinkled tows

In automatic fiber placement, due to the non-straight fiber paths fiber angle variations occur. These variations cause gaps and overlaps on the ply course, as shown in Figure 2.19. These gaps and overlaps change the thickness of the composite structure spatially. If the gaps and overlaps are considered when designing and optimizing the VSC structure, there would be thickness differences in the manufactured structure [14].

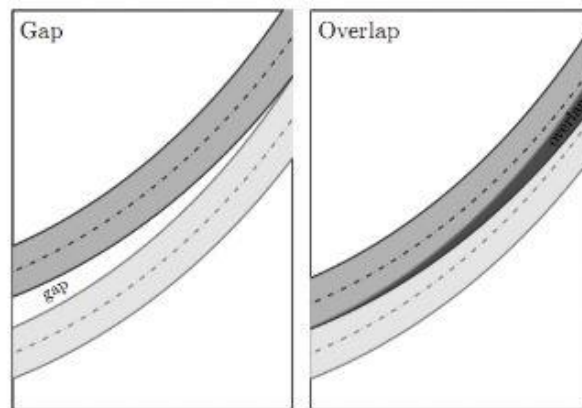


Figure 2.19 Examples of gapped and overlapped layups

Another constraint related with the gap and overlap issue is the coverage parameter. When the coverage parameter changes from 0% to 100%, the gaps between the tow courses get close and overlaps start to appear. This coverage parameter affects the strength of the structure. If the coverage parameter is 0%, the structure is at its weakest state, however if the coverage parameter is 100% this causes low surface quality. In Figure 2.20, a composite laminate with 0% coverage is shown. It should be noted that if the coverage parameter is high, although the surface quality decreases the overlap regions could act as like stiffeners and this can increase the strength of the composite structure.



Figure 2.20 Layup with 0% coverage parameter

Minimum cut length is another constraint in the AFP layup process. It is the minimum tow length that must be laid down on the surface that the AFP machine is able to cut the tow properly and continue the lay down process. Due to the minimum cut length constraint at the corners of the parts the tow laid down more than the corner's length. The excessive parts of the tow are then trimmed. Minimum cut length constraint varies according to the fiber placement head, and in the literature, minimum cut length is seen to be between 63 -152 mm. [15].

In recent years, demand for composite structures in the industry has rapidly increased. From military applications to communication antennas, from automotive to marine structures composites are widely used. In such applications, especially in military and aerospace structures, there are many parts which are manufactured by the AFP process. This process became a standard manufacturing process for aerospace companies like Airbus, Boeing Lockheed Martin etc. In Figure 2.21, fuselage section of Airbus A350 which is manufactured by the AFP is given.



Figure 2.21 AFP manufacturing of the fuselage section of Airbus A350

2.3 Optimization of the VSC Structures

The first studies on the variable stiffness composite structures focused on different manufacturing methods instead of structural optimization and analysis of VSC structures. The optimization of AFP manufactured VSC structures is mainly studied in the last 20 years. In most of the studies, there are significant improvements for different geometries achieved by using different optimization techniques.

In 2008, Tatting and Gürdal [18] worked on rectangular variable stiffness composite panels to optimize the buckling and in-plane responses of two distinct cases of stiffness variation. In the first case stiffness varies along the direction of loading. In this case, small improvements in the buckling load of some panels have been obtained. This improvement is due to the redistribution of transverse stresses over the panel. The improvement in the buckling load is determined to be about 19%. In the second case study, variation of stiffness is perpendicular to the loading direction and in this case 80% increase has been obtained in the normalized critical buckling load [18].

In 2012, Inci [7] studied variable stiffness rectangular flat plates. Different techniques have been used for optimization in his study. In the thesis study,

Nastran's gradient-based optimization solver and genetic algorithm are used for discrete fiber angle optimization. In addition, for continuous fiber layup path optimization genetic algorithm is used. Two different cases are studied; one is a cantilevered plate and the other one is a quarter of a rectangular panel with a central hole. For different loading conditions strain energy minimization and maximization of first buckling load are studied. For discrete optimization, theoretically good results are obtained; however, they are practically not applicable since in every element a different fiber angle is defined. The practical/manufacturable case is the continuous fiber layup case for this study. In the continuous fiber path case with the curvature constraint imposed, 30% of increase in the first buckling load is obtained compared to the zero-degree straight fiber path.

Following this study, Güldü [15] has worked on the optimization of cylindrical shell. In this study, particle swarm optimization technique is used to optimize the buckling load factor of cylindrical shells. In his study, minimum turning radius and gaps and overlaps are also taken into account. The exceptional result in the study is obtained in the case of axially variable stiffness cylinder compared to the baseline constant stiffness cylinder. In this case, 37 % increase in the specific buckling load factor is achieved, and it is concluded that stiffness variation proved to be beneficial for the structural performance of variable stiffness composite cylinders [15].

It is validated by an experimental study that performance increases in the variable stiffness composite is a crystal-clear fact. In 2021 Matsuzaki et al. [20] worked on the optimization of variable stiffness quarter composite panel with a central hole. They worked on open hole tension model, and they have verified the analysis results by testing the manufactured prototypes. They have used multi-objective optimization using fracture criterion and mean curvature as objective functions. It is shown by the experiments that strength of the plate with a hole is increased by 34.4% [20].

In 2019 Hao et al. [21] has tried to optimize VSC structures by using isogeometric analysis. They developed a multistage design method to overcome the non-convexity of the design space. First, they optimized the stiffness of the composite plate by

gradient based optimization, then by using evolutionary algorithm fiber angles are optimized, and lastly fiber path design is constructed. Manufacturing constraints are used as constraint for the objective function. To design the stiffness and to find out the optimum spatial distribution of lamination parameters, they used B Splines surfaces. This method is used because the strong convex-hull property of the B Splines overcome the nonconvexity. By using the lamination parameters obtained, realistic fiber paths that obey the manufacturing constraint are then constructed. To do that uniformly, distributed grid is constructed on a rectangular plate and the corresponding fiber angles from the lamination parameters obtained before are determined by the evolutionary algorithm. In the study fully simply supported boundary conditions are used on a rectangular plate and maximum buckling load of the structure is increased by 30%.

Lately in 2022 Coskun and Turkmen [22] has worked on Multi-Objective Genetic Algorithm (MOGA) based optimization of VSC structures. The objective of the study is to maximize the buckling load and the stiffness. Also, in the study minimum allowable curvature is used as constraint. In this study, fiber path is defined using parametric Bezier curves on flat rectangular panels by three parameters. These parameters affect the shape of the curve and by optimizing these three parameters, best objective value is sought for. These parameters are the segment (n) parameter that divide the structure as many segments as the parameter value, angle of each segment (θ) with respect to the selected axis and the segment width multiplier (c) used for changing the width of each segment (Figure 2.22). Optimization results show that buckling load is increased by 103% while 44% decrease in equivalent stiffness is obtained compared to the quasi-isotropic laminate. Although the increment in the buckling load is very high, they stressed out that the buckling performance is highly dependent on the boundary conditions. In the study, 103% buckling load increase is achieved for simply supported plates and it is mentioned that clamped plates give least gain due to the additional constraints on the edges.

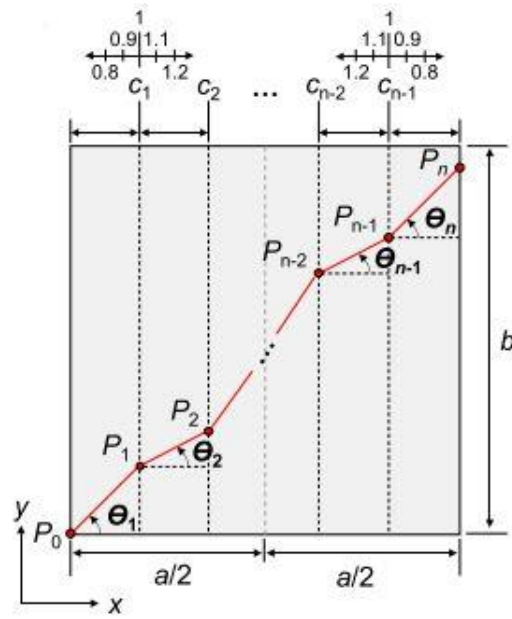


Figure 2.22 Optimization parameters for MOGA optimization of VSC [22]

Previous studies showed that VSC structures are superior to the constant stiffness straight fiber path composite structures. The development of AFP machines enabled to manufacture the of VSC structures. However, in most studies, optimization of VSC structures is done on flat surfaces, and paths are defined in 2D. This study aims to show the effectiveness of NURBS based fiber path definition in constructing variable stiffness composite structures in 3D. Therefore, in this study, a structural optimization methodology for defining the fiber path on curved composite panels utilizing the control points of NURBS as design variables is developed.

CHAPTER 3

NON-UNIFORM RATIONAL BASIS SPLINES

The Non-Uniform Rational B Splines (NURBS) are generated from Bezier curves developed by Pierre Bezier in late 1960s. Bezier Curve is a special case of NURBS. The pioneering work of Bezier constitute a basis for B Splines and the NURBS [23]. NURBS are very powerful to represent curves and surfaces. They have great flexibility and precision to represent conic curves and surfaces. They can also represent straight lines, flat planes, precise circles, and spheres as well as intricate piecewise sculptured surfaces [23]. Hence, the exact geometry can be represented very successfully in all kinds of computer aided design programs [17].

NURBS has a very deep mathematical background. Therefore, an introduction to B Splines and NURBS is given in this Chapter.

3.1 Parametric Representation and Bezier Curves

There are two common methods to represent curves and surfaces mathematically in geometric modelling. They are parametric function or implicit equation representations.

Implicit equations are in the form of $f(x,y,z)=0$. For instance, implicit equation for a unit sphere is given by Equation (3.1).

$$f(x, y) = x^2 + y^2 + z^2 - 1 = 0 \quad (3.1)$$

In parametric form, each of the coordinates of a point on the curve is represented separately as an explicit function of independent parameters as shown in Equation (3.2).

$$C(u, v) = x(u, v) + y(u, v) + z(u, v) = 0 \quad a < u, v < b \quad (3.2)$$

Accordingly, $C(u, v)$ is vector-valued function of the independent variables, u , and v and parameters u and v are limited in an arbitrary interval “a” and “b”. In general, the limits of the interval are usually normalized.

One quarter of the unit sphere can be parametrically written as follows.

$$\begin{aligned} x(u, v) &= \sin(u) \cos(v) \\ y(u, v) &= \sin(u) \sin(v) \\ z(u, v) &= \cos(u) \end{aligned} \quad (3.3)$$

$$0 \leq u \leq \frac{\pi}{2}$$

$$0 \leq v \leq 2\pi$$

Two parameters are needed to describe a surface whereas if we want to represent a planar shape one parameter is enough. By holding u fixed and varying v , latitudinal lines are generated, for longitudinal lines vice versa is valid. However, in the parametric form there are some difficulties like determining a point on the surface and there can be some other parametric anomalies. Therefore, “Power Basis” form given by Equation (3.4) is used to overcome these problems [24]. In Equation (3.4), an n^{th} degree curve defined with “Power Basis” form is given. In the Power Basis form, a well-known function class, polynomials, are used and by their help curves can be represented better.

$$C(u) = (x(u), y(u), z(u)) = \sum_{i=0}^n a_i u^i \quad 0 \leq u \leq 1 \quad (3.4)$$

In Equation (3.4), coefficients are the coefficients of polynomials of each coordinate axis and given by Equation (3.5).

$$x(u) = \sum_{i=0}^n x_i u^i \quad y(u) = \sum_{i=0}^n y_i u^i \quad z(u) = \sum_{i=0}^n z_i u^i \quad (3.5)$$

Index “i” represents the degree of the polynomials and during the calculation it goes up to the polynomial degree of n of the “Power Basis” form. Bezier curve is mathematically same as the power basis form. Polynomials are used to represent their coordinate functions. However, Bezier form is better than the power basis. Bezier form is more useful for geometric modelling because they can represent geometric information much better. Power basis polynomials are processed algebraically not geometrically, and power basis method has higher rounding errors [23], [24]. Bezier curve is defined by Equation (3.6),

$$\mathbf{C}(u) = \sum_{i=0}^n B_{i,n}(u) \mathbf{P}_i \quad 0 \leq u \leq 1 \quad (3.6)$$

where $B_{i,n}$ is the Bernstein basis polynomial defined by Equation (3.7).

$$B_{i,n}(u) = \frac{n!}{i!(n-i)!} u^i (1-u)^{n-i} \quad (3.7)$$

Index “n” represents the degree of the polynomial and $i \leq n$. In Equation (3.6) \mathbf{P}_i values are the control points of the curve. Control points are main parameters that govern the shape of the Bezier curve. They are represented by the coordinates in three-dimensional space. It should be noted that Equation (3.6) can also be represented as Equation (3.8).

$$\mathbf{C}(u) = \sum_0^n B_{i,n}(u) (x_i, y_i, z_i) \quad 0 \leq u \leq 1 \quad (3.8)$$

For a value of the parameter u, Equation (3.8) returns the x, y, and z coordinates of a particular point on the Bezier curve corresponding to the parameter value u. As the

parameter u varies between 0 and 1, the collection of points whose x, y, z coordinates are calculated by Equation (3.8) forms the Bezier curve. Bezier Curve defined in Equation (3.6) is constructed by the $(n-1)^{\text{th}}$ degree interpolation between the control points, respectively. The degree of the curve (n) is one less than the number of control points.

In the Equation (3.6), Bezier curve defined as a function of the independent parameter, u . The parameter u is defined in the interval $[0,1]$. This means that when the parameter $u=0$, consequently $C(u)=C(0)$ and Equation (3.6) must give the coordinates of the starting point. Accordingly, when $u=1$, consequently $C(u)=C(1)$ and Equation (3.6) must give the coordinates of the end point of the curve. In addition, the values of the parameter u between “0” and “1” must be on the Bezier curve.

As an example, a 3rd degree Bezier Curve with control points $P_0[1,1]$, $P_1[2,3]$, $P_2[4,3]$, $P_3[3,1]$ is constructed via Equation (3.9).

$$B_{0,3}(u) = \frac{3!}{0!(3-0)!} u^0(1-u)^{3-0} = (1-u)^3 \quad (3.9a)$$

$$B_{1,3}(u) = \frac{3!}{1!(3-1)!} u^1(1-u)^{3-1} = 3u(1-u)^2 \quad (3.9b)$$

$$B_{2,3}(u) = \frac{3!}{2!(3-2)!} u^2(1-u)^{3-2} = 3u^2(1-u) \quad (3.9c)$$

$$B_{3,3}(u) = \frac{3!}{3!(3-1)!} u^3(1-u)^{3-3} = u^3 \quad (3.9d)$$

$$C(u) = (1-u)^3[1,1] + 3u(1-u)^2 [2,3] + 3u^2(1-u)[4,3] + u^3[3,1] \quad (3.9e)$$

$$x(u) = (1-u)^3 * 1 + 3u(1-u)^2 * 2 + 3u^2(1-u) * 4 + u^3 * 3 \quad (3.9f)$$

$$y(u) = (1-u)^3 * 1 + 3u(1-u)^2 * 3 + 3u^2(1-u) * 3 + u^3 \quad (3.9g)$$

* 31

In Equation (3.9e), when $u=0$ the $C(u)=C(0)=[1,1]$ is the coordinate of the starting point and first control point of the curve in the two-dimensional coordinate space.

The same case is valid for end point of the curve. For $u=1$ that $C(u)=C(1)=[3,1]$ and this is the end point also the coordinate of the last control in the two-dimensional space.

Figure 3.1 represents the Bezier curve drawn according to Equation (3.9e).

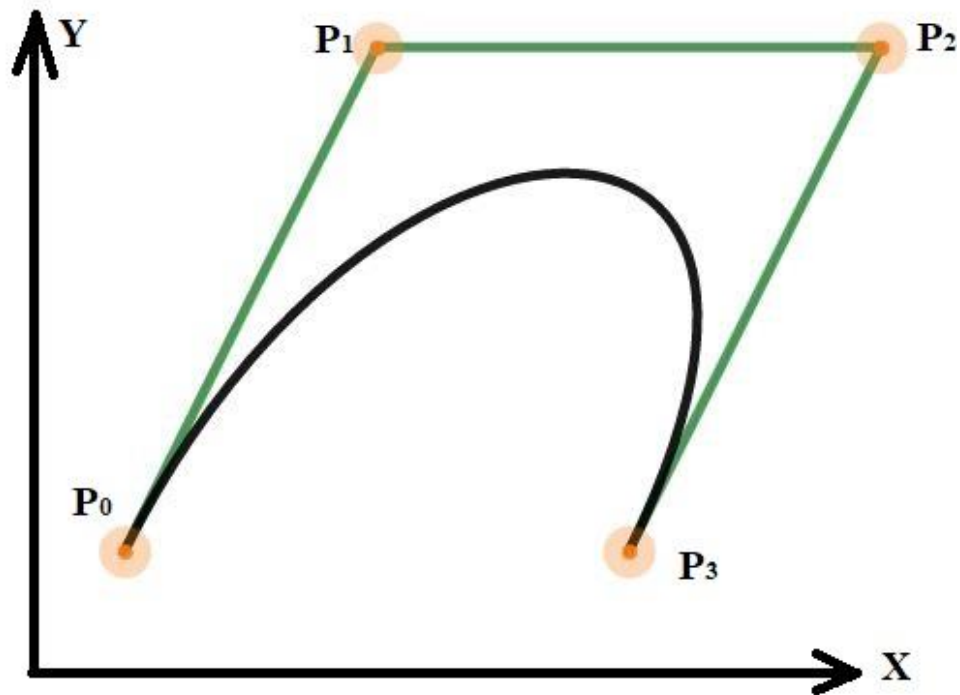


Figure 3.1 Representation of Bezier Curve in Equation (3.9)

3.2 B Splines

Bernstein basis has some disadvantages in terms of the ability to make local changes on the shape of the curve. One disadvantage is that the order of the Bernstein polynomials can be changed only by decreasing or increasing the number of control points. When there is high number of controls points, the degree of the curve increases but this is very inefficient. Other disadvantage is that control points have a dominant effect on the overall shape of the curve. Polynomial is not defined in a piecewise manner; hence modification of the local points affects the whole curve. In

Figure 3.2 difference between a Bezier curve and B-Spline curve with same control points is presented.

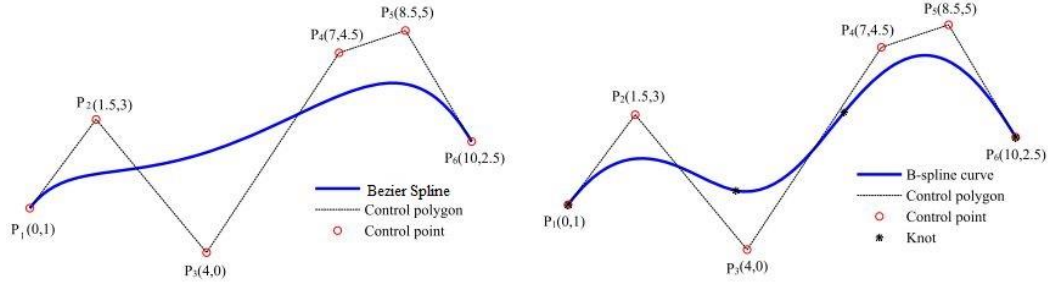


Figure 3.2 Bezier and B-Spline curves with the same control points [25]

In Basis Splines (B-Splines), curves are defined by piecewise polynomials such that the disadvantages of Bezier curves can be overcome. The curve is divided into pieces by the knot values which are defined in the knot vector. In B-Splines definition, knot vector is used to construct the B-Spline's Basis functions. Knot vector and Basis functions are explained in the following sections.

A p^{th} degree B-Spline is defined by Equation (3.10),

$$C(u) = \sum_{i=0}^m N_{i,p}(u) P_i \quad a \leq u \leq b \quad (3.10)$$

where P_i are the control points and $N_{i,p}(u)$ are p^{th} degree B Spline basis functions defined on the non-periodic knot vector limited by “a” and “b” given in Equation (3.11). A knot vector (U) has multiplicity of knot values at each end and the multiplicity value is equal to the degree of the B-spline basis function (p), plus one ($p+1$). Knot vector has $m+1$ knot values, and m is the last index of the knot vector which is equal to the length of the knot vector minus 1.

$$U = \{u_0, \dots, u_m\} = \underbrace{\{a, \dots, a\}}_{p+1}, u_{p+1}, \dots, u_{m-p-1}, \underbrace{\{b, \dots, b\}}_{p+1} \quad (3.11)$$

3.2.1 Knot Vector

Knot vector divides the parametric space into the pieces, referred to as knot spans. Knot vector $U=\{u_0, \dots, u_m\}$ is a non-decreasing sequence of parameters which control where and how the control points affect the curve. The knot vector divides the parametric space in the interval. To control the curve in a piecewise fashion, as the knot value increases throughout the knot vector and enters a new knot span, a new control point gets active, and it enables to control the shape of the curve locally.

The number of knots is always equal to the number of control points (n) plus degree of the curve (p) and plus one ($n+p+1$). There are evenly spaced knot vectors called uniform knot vectors and there are non-uniform knot vectors. Non-uniform knot vectors are spaced unevenly, and one knot value can repeat itself. If there are $p+1$ “a” and “b” which are the end points of a knot vector, the knot vector is named as open knot vector, otherwise knot vector is named as periodic. As mentioned, a knot vector has multiplicity of knot values at each end (first and last values of the interval) and the multiplicity value is equal to the degree of the B-spline basis function and plus one ($p+1$). Lastly, unless otherwise specified $a=0$ and $b=1$ is used for the end points of the knot span. Otherwise, end points “a” and “b” of the knot vector can be normalized [23].

3.2.2 Basis Functions of B-splines

To calculate the Basis Functions of B-splines, Cox-de Boor [26,27] recursion formula is used. In Equation (3.12), the formulation for the B spline basis functions is given.

$$N_{i,0}(u) = \begin{cases} 1, & u_i \leq u < u_{i+1} \\ 0, & \text{otherwise} \end{cases} \quad (3.12.a)$$

$$N_{i,p}(u) = \frac{(u - u_i)}{u_{i+p} - u_i} N_{i,p-1}(u) + \frac{(u_{i+p+1} - u)}{u_{i+p+1} - u_{i+1}} N_{i+1,p-1}(u) \quad (3.12.b)$$

From Equation (3.12a) second condition is valid; hence the first two basis functions become equal to zero.

$$N_{0,0}(u) = 0, N_{1,0}(u) = 0 \quad (3.13.a)$$

For $i=2$ and $i=3$ basis functions are calculated by Equation (3.13).

$$N_{2,0}(u) = \begin{cases} 1, & 0 \leq u \leq 0.5 \\ 0, & \text{otherwise} \end{cases} \quad (3.13.b)$$

$$N_{3,0}(u) = \begin{cases} 1, & 0.5 \leq u \leq 1 \\ 0, & \text{otherwise} \end{cases} \quad (3.13.c)$$

For $i=4$, $u_4=1$ and $u_{4+1}=u_5=1$ and for $i=5$ $u_5=1$ and $u_{5+1}=u_6=1$. From Equation (3.12a) second condition is valid and the last two basis functions becomes equal to zero.

$$N_{4,0}(u) = 0, N_{5,0}(u) = 0 \quad (3.13.d)$$

For $p=1$, there are 5 (7-2) basis functions, and they are calculated by Equation (3.14).

$$N_{0,1}(u) = \frac{(u - u_0)}{u_1 - u_0} N_{0,0}(u) + \frac{(u_2 - u)}{u_2 - u_1} N_{1,0}(u) = 0 \quad (3.14.a)$$

$$\begin{aligned} N_{1,1}(u) &= \frac{(u - u_1)}{u_2 - u_1} N_{1,0}(u) + \frac{(u_3 - u)}{u_3 - u_2} N_{2,0}(u) = \frac{0,5 - u}{0,5} N_{2,0}(u) \quad (3.14.b) \\ &= (1 - 2u)N_{2,0}(u) = \begin{cases} 1 - 2u, & 0 \leq u < 0.5 \\ 0, & \text{otherwise} \end{cases} \end{aligned}$$

$$\begin{aligned} N_{2,1}(u) &= \frac{(u - u_2)}{u_3 - u_2} N_{2,0}(u) + \frac{(u_4 - u)}{u_4 - u_3} N_{3,0}(u) \quad (3.14.c) \\ &= \frac{u}{0,5} N_{2,0}(u) + \frac{1 - u}{1 - 0,5} N_{3,0}(u) \\ &= \begin{cases} 2u, & 0 \leq u < 0.5 \\ 2 - 2u & 0.5 \leq u < 1 \\ 0, & \text{otherwise} \end{cases} \end{aligned}$$

$$\begin{aligned} N_{3,1}(u) &= \frac{(u - u_3)}{u_4 - u_3} N_{3,0}(u) + \frac{(u_5 - u)}{u_5 - u_4} N_{4,0}(u) \quad (3.14.d) \\ &= \frac{u - 0,5}{1 - 0,5} N_{3,0}(u) + \frac{1 - u}{1 - 1} N_{4,0}(u) \\ &= \begin{cases} 2u - 1, & 0.5 \leq u \leq 1 \\ 0, & \text{otherwise} \end{cases} \end{aligned}$$

$$N_{4,1}(u) = \frac{(u - u_4)}{u_5 - u_4} N_{4,0}(u) + \frac{(u_6 - u)}{u_6 - u_5} N_{5,0}(u) = 0 \quad (3.14.e)$$

For $p=2$, there are 4 basis functions, and they are calculated by Equation (3.15).

$$\begin{aligned} N_{0,2}(u) &= \frac{(u - u_0)}{u_2 - u_0} N_{0,1}(u) + \frac{(u_3 - u)}{u_3 - u_1} N_{1,1}(u) & (3.15.a) \\ &= \begin{cases} (1 - 2u)^2, & 0 \leq u < 0.5 \\ 0, & \text{otherwise} \end{cases} \end{aligned}$$

$$\begin{aligned} N_{1,2}(u) &= \frac{(u - u_1)}{u_3 - u_1} N_{1,1}(u) + \frac{(u_4 - u)}{u_4 - u_2} N_{2,1}(u) & (3.15.b) \\ &= 2u \begin{cases} 1 - 2u, & 0 \leq u < 0.5 \\ 0, & \text{otherwise} \end{cases} \\ &\quad + (1 - u) \begin{cases} 2u, & 0 \leq u < 0.5 \\ 2 - 2u & 0.5 \leq u < 1 \\ 0, & \text{otherwise} \end{cases} \\ &= \begin{cases} 4u - 6u^2, & 0 \leq u < 0.5 \\ 2(1 - u)^2 & 0.5 \leq u < 1 \\ 0, & \text{otherwise} \end{cases} \end{aligned}$$

$$\begin{aligned} N_{2,2}(u) &= \frac{(u - u_2)}{u_4 - u_2} N_{2,1}(u) + \frac{(u_5 - u)}{u_5 - u_3} N_{3,1}(u) & (3.15.c) \\ &= \begin{cases} 2u^2, & 0 \leq u < 0.5 \\ -6u^2 + 8u - 2 & 0.5 \leq u < 1 \\ 0, & \text{otherwise} \end{cases} \end{aligned}$$

$$\begin{aligned} N_{3,2}(u) &= \frac{(u - u_3)}{u_5 - u_3} N_{3,1}(u) + \frac{(u_6 - u)}{u_6 - u_4} N_{4,1}(u) & (3.15.d) \\ &= \begin{cases} (2u - 1)^2, & 0.5 \leq u < 1 \\ 0, & \text{otherwise} \end{cases} \end{aligned}$$

Once all the basis functions are calculated, Equation (3.10) is used to determine the equation of the B-spline. To do that the control points must also be defined.

$$\mathbf{C}(u) = \sum_{i=0}^m N_{i,p}(u) \mathbf{P}_i = \sum_{i=0}^m N_{i,p}(u) \begin{bmatrix} x_i \\ y_i \\ z_i \end{bmatrix} \quad a \leq u \leq b \quad (3.16)$$

B splines have some important properties which are summarized below [23], [24]:

- If m in the definition is equal to p (degree), this is a Bezier curve.
- $C(u)$ is piecewise polynomial since its basis functions $N_{i,p}(u)$ are piecewise polynomials.
- The degree p , length of knot vector $m+1$ and number of control points (n) satisfy the relation $m+1=p+n+1 \implies m=p+n$.
- Starting point and end points of the spline are the first and the last control points, respectively. However, except for the straight lines other control points serve for creating the convex hull of the curve and generally they are not on the curve.
- B spline has strong convex hull property which means that the B-spline curve is contained in the convex hull of its control polyline, as shown in Figure 3.4.

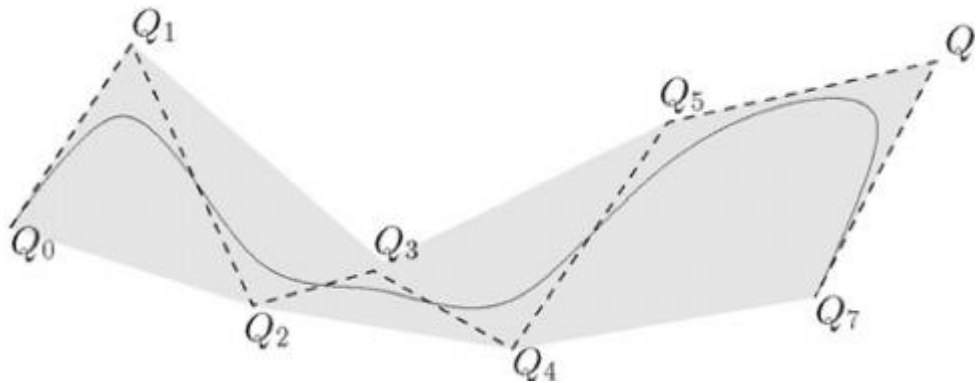


Figure 3.4 Control polyline (dashed line) and convex hull (in gray) of a B-Spline curve [28]

For the given knot vector $u=[0 \ 0 \ 0 \ 0.5 \ 1 \ 1 \ 1]$ and control points $P=[(-1,0), (-1,1), (1,1), (1,0)]$, a semicircle B spline is drawn in Figure 3.5.

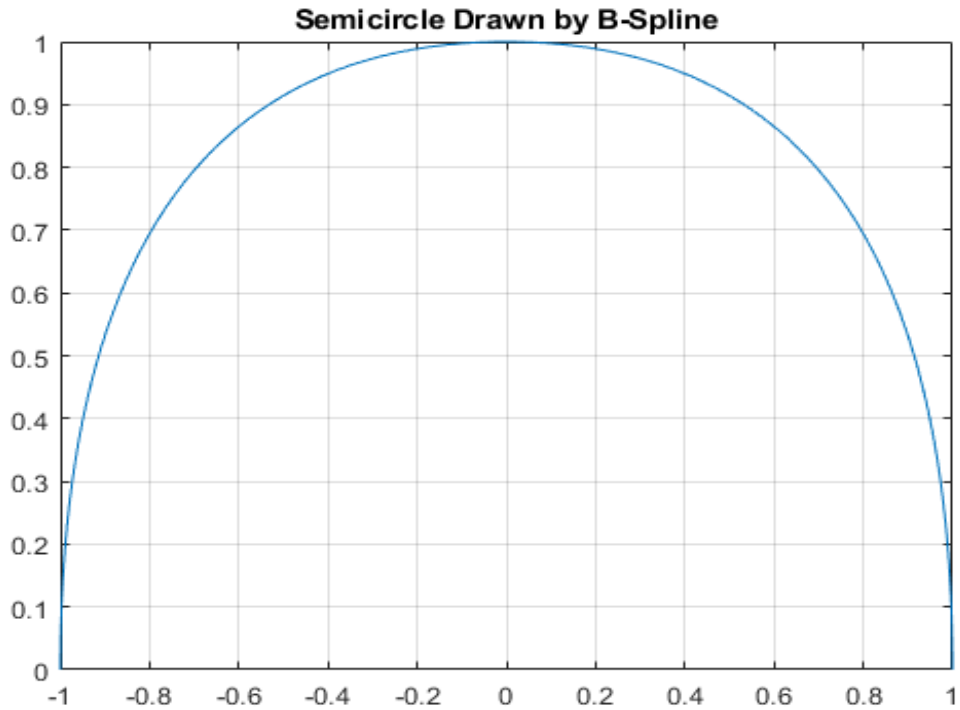


Figure 3.5 B-Spline semicircle

3.3 NURBS

B-splines are the non-rational (polynomial) curves, and their basis functions are non-rational (polynomial). However, conical shapes can be represented in an exact manner by rational curves [17]. Therefore, non-uniform rational B-splines (NURBS) with rational basis functions are introduced. The weights defined for each control point (w_i) make the basis functions rational. Weights provide more control on the shape of the curve without increasing the number of control points. Therefore, exact representation of shapes is accomplished. In many computer aided design (CAD) applications and data transfer format such as in IGES, STEP, etc. NURBS have been used as a standard since 1983.

Mathematically, NURBS are the projection of polynomial B-spline curves defined in the four-dimensional homogenous coordinate space (projective space) onto the three-dimensional physical space as shown in Figure 3.6. NURBS are defined with

three parameters [23]. They are the weight (w_i), knots (u), and control points (P_i) which are used to construct the NURBS control polygon. NURBS curve ($C(u)$) is defined by Equation (3.17),

$$C(u) = \frac{\sum_{i=0}^m N_{i,p}(u)w_i P_i}{\sum_{i=0}^m N_{i,p}(u)w_i} \quad a < u < b \quad (3.17)$$

where “a” and “b” are the limit values of the knot vector and $N_{i,p}(u)$ is the i^{th} basis function and “a” and “b” are taken as 0 and 1 unless otherwise specified [24]. The rational part in Equation (3.17) can be written as,

$$R_{i,p} = \frac{N_{i,p}(u)w_i}{\sum_{i=0}^m N_{i,p}(u)w_i} \quad (3.18)$$

Hence, the NURBS formulation can be rewritten as,

$$C(u) = \sum_{i=0}^m R_{i,p}(u)P_i \quad (3.19)$$

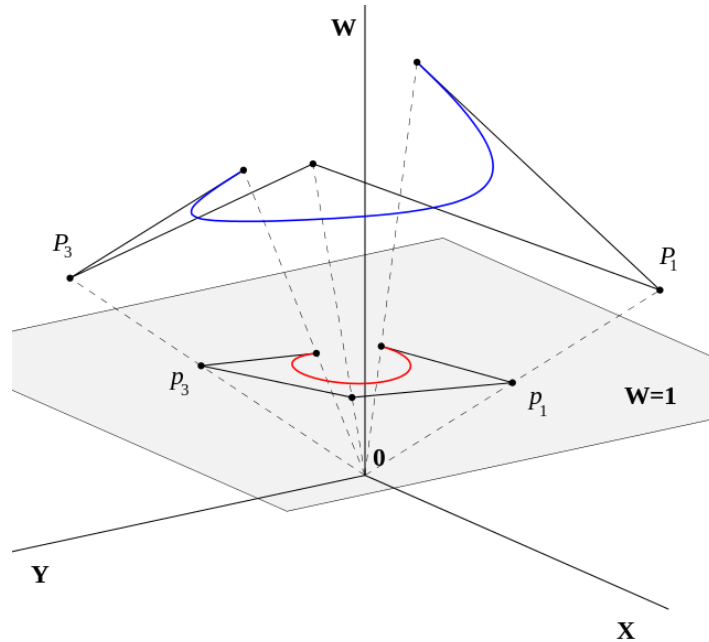


Figure 3.6 B-spline (polynomial curve) defined in homogeneous coordinates given by blue and its projection on gray plane yields NURBS curve given by red

The most dominant parameter to control the shape of the NURBS is the control points as shown in Figure 3.7. Weight and the knots can also change the shape of the NURBS as shown in Figure 3.8 and Figure 3.9. By modifying the knot vector significant shape changes can be achieved [29]. However, their effect on the shape control of NURBS is more limited than the effect of the control points.

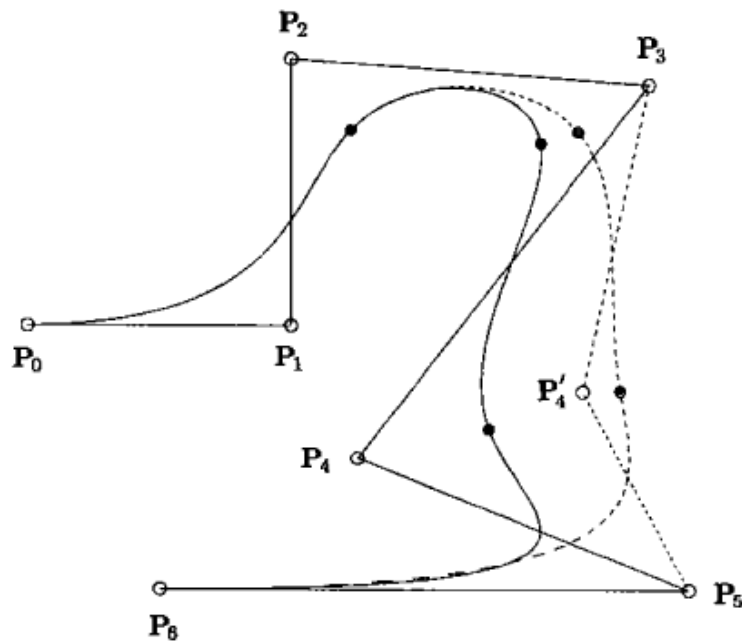


Figure 3.7 Splines with two different P4 control points[24]

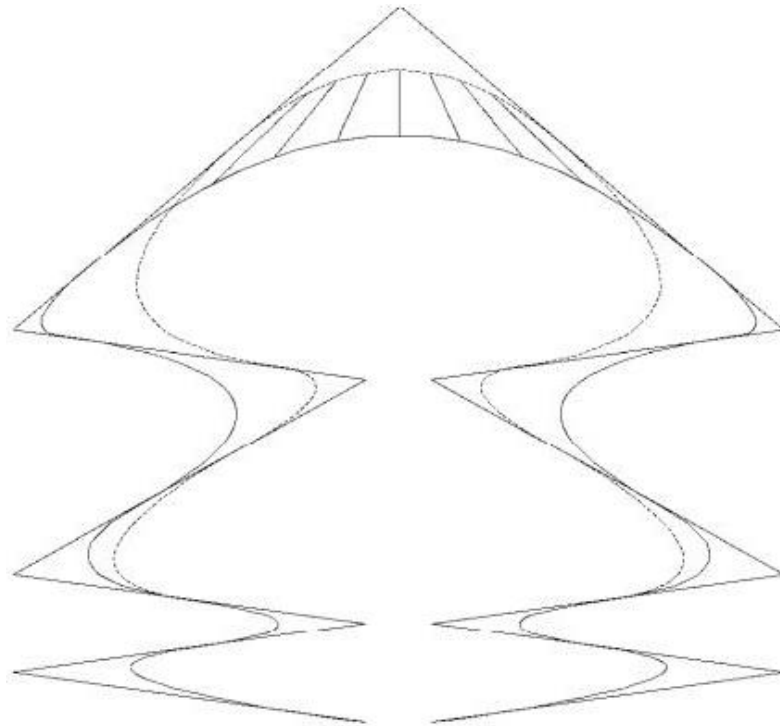


Figure 3.8 Splines with two different knot values in possible NURBS envelope[29]

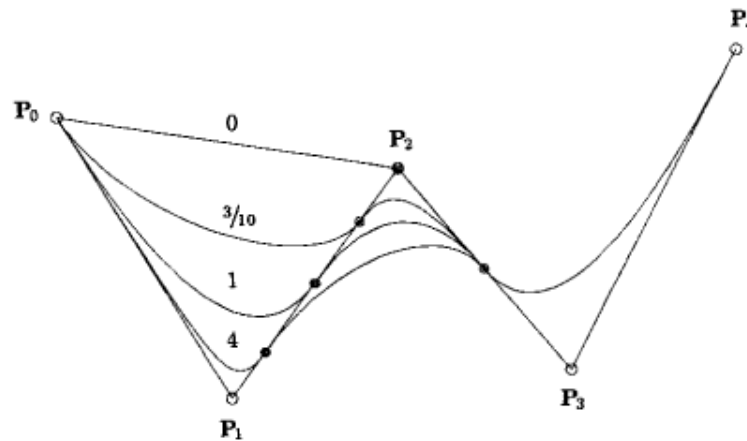


Figure 3.9 Splines with different weights for the same control point[24]

For a given knot vector $u=[0 \ 0 \ 0 \ 0.5 \ 1 \ 1 \ 1]$, control points $P=[(-1,0), (-1,1), (1,1), (1,0)]$ and weights $w=[1 \ \frac{1}{2} \ \frac{1}{2} \ 1]$, Figure 3.10 shows the resultant semicircle. To plot the semicircle thousand parameter values in the range of $[0,1]$ is calculated. To

make a comparison, in Figure 3.9 B-Spline and NURBS with same control points and knot vector are plotted.

In Figure 3.10, the data points of analytically calculated semi-circle are shown with black circles, green line behind the black circles is the semi-circle created by NURBS and the pink line is the semi-circle created by B-spline. Figure 3.10 shows that NURBS is much better in approximating the analytical semi-circle. This is because of the ability of NURBS in representing the conical shapes more closely than the B-splines by its definition.

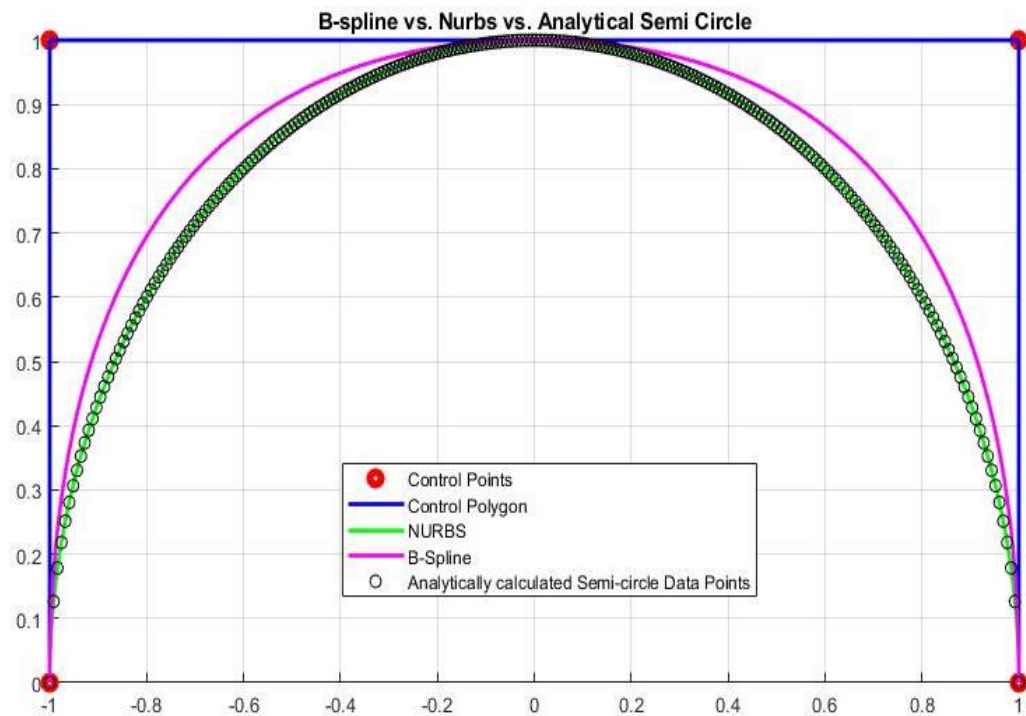


Figure 3.10 Semicircle Drawn by NURBS, B Spline and, Analytical Calculation

CHAPTER 4

PARTICLE SWARM OPTIMIZATION

There are various optimization methods in the literature. One of the primary considerations when choosing an optimization method is to determine the needs of the problem and choose a suitable method for it. Because each iteration has a process time cost, and this cost needs to be minimized. The variable type, type of search space, objective function, and other problem parameters are the factors for choosing a suitable optimization method.

In many studies on developing optimization techniques, simulations have been carried out by modeling the animal population problem-solving strategies and group intelligence. These simulations have shown that the behavior of a group of animal's ways of problem-solving can be used as a metaheuristic optimization method. Such kind of optimization techniques is named as Swarm Intelligence [30].

In this thesis, Particle Swarm Optimization (PSO) method is used to optimize the objective function of the optimization problems. PSO is a metaheuristic global optimization method that can also be defined as a population-based stochastic search algorithm [31]. It is used for complex non-linear optimization problems [5]. The method was developed by Eberhart and Kennedy [32] in 1995; the animals' social behavior inspired them. They see that birds, fish, and ant flocks can find food or the best migration route by each flock member sharing their knowledge with the other individuals in the flock. The animals are in a big search space, and members do not know the best way to go; however, if any member can find a better way to follow, it shares this information with others to follow this path. To find the best way, individual's knowledge, and groups knowledge reshared iteratively on the road. The group knowledge and individual knowledge act in harmony to find the best way [5].

PSO is studied on continuous variable problems, and its performance is comparable to another metaheuristic method, the Genetic Algorithm. PSO has been applied successfully to a wide variety of problems. In structural optimization, it is used for shape optimization, sizing optimization, and topology optimization. It is also used in the training of neural networks for the identification of Parkinson's disease, image recognition, etc. There are also various other implementations in different subjects like electrical engineering and biomedical engineering [5].

PSO has the following advantages and disadvantages[5]:

- Insensitive to scaling of design variables
- Simple implementation
- Derivative free
- Has very few algorithms parameters
- A very efficient global search algorithm
- However, local search ability is very weak

4.1 Basic PSO Algorithm

In particle swarm optimization, there are “n” number of candidate solutions, called as particles, in real valued “d” dimensional search space “X”. Equation (4.1) is a generic optimization statement.

$$\min_{x \in X} f(x) \quad (4.1)$$

where;

$$X = [x_1^{min}, x_1^{max}] \dots [x_d^{min}, x_d^{max}] \subset \mathbb{R}^d \quad (4.2)$$

In Equation (4.2), x_i is the current position of particles in the search space “X” and x_i^{max} and x_i^{min} are the boundaries of the search space in the i^{th} coordinate direction of the search space.

Particles search for the best solution in the search space X by iteratively changing their position. Two information determine the new position of each particle. First, each particle keeps its best position information up to the current iteration in its memory during the iteration. Each particle tries to change its position towards there. At the same time, the swarm keeps track of the best position determined by any particle in the swarm. All particles are also influenced by the swarm's best position information and try to change their position towards this potential best position. This two information simultaneously affect the new position of each particle. Let A denote the particles and assume that there are n number of particles in a swarm P , as described by Equation (4.3).

$$P = \{A_1, A_2, \dots, A_n\} \quad (4.3)$$

For the iteration number t , each particle A_i is defined with four vectors given by Equation (4.4),.

$$A_i = \langle \mathbf{x}_i^{(t)}, \mathbf{v}_i^{(t)}, \mathbf{p}_i^{(t)}, \mathbf{p}_{gi}^{(t)} \rangle \quad i \in I \quad (4.4)$$

where $I = \{1, 2, \dots, n\}$ is the set of indices of the particles. The first vector $\mathbf{x}_i^{(t)}$ is the position vector of the i^{th} particle defined in Equation (4.5). This vector gives the position of the i^{th} particle in iteration t with all its components in the d dimensional space.

$$\mathbf{x}_i^{(t)} = (x_{i1}^{(t)}, x_{i2}^{(t)}, \dots, x_{id}^{(t)}) \in X \quad (4.5)$$

The second vector $\mathbf{v}_i^{(t)}$ is the velocity vector of the i^{th} particle defined in Equation (4.6). This vector gives the velocity of the i^{th} particle in iteration t with all its components in the d dimensional space. The velocity vector is responsible for the motion of the particles in the search space.

$$\mathbf{v}_i^{(t)} = (v_{i1}^{(t)}, v_{i2}^{(t)}, \dots, v_{id}^{(t)}) \quad (4.6)$$

Velocity of a particle also has limits. The user defined value $v^{(\max)}$ is equal to the difference of boundaries of the search space along the j^{th} coordinate direction. This

limitation is done for disabling the arbitrary growth of the velocities and disabling the violation of the boundaries of the search space. The boundaries of the search space along the j^{th} coordinate direction is defined as x_j^{max} and x_j^{min} , respectively. For the generic optimization problem defined in Equation (4.1) and its boundaries, the maximum velocity would be set as in Equation (4.7) and Equation (4.8) with μ being a user defined coefficient. The coefficient μ is used because in case of extremely large number of minimizers or very narrow regions of attraction around them, smaller velocities can offer better search accuracy [30].

$$v_j^{(\text{max})} = \mu_j(x_j^{\text{max}} - x_j^{\text{min}}) \quad j \in D \text{ and } \mu_j \in (0,1) \quad (4.7)$$

$$v_j^{(\text{min})} = -v_j^{(\text{max})} \quad (4.8)$$

In Equation (4.7), $D=\{1,2,\dots,d\}$ is the set of the coordinate directions.

The third vector $\mathbf{p}_i^{(t)}$ is the best position vector of the i^{th} particle in Equation (4.9). This vector gives the best position of the i^{th} particle ever visited in the search space X until the t^{th} iteration. For the generic problem defined by Equations (4.1) and (4.2), it is the position with the minimum objective value that is reached during the travel of the i^{th} particle in the search space.

$$\mathbf{p}_i^{(t)} = (p_{i1}^{(t)}, p_{i2}^{(t)}, \dots, p_{id}^{(t)}) \in X \quad (4.9)$$

Although each particle knows its best position ever visited in search space; solely, this is not enough to find the best objective function solution, because there is a risk of getting stuck in the local best position. Therefore, in addition to particles' discovery in the search space, there is an implicit communication mechanism that all members in the swarm exchange information with others and try to move through the best solution found ever by any particle in the swarm. This is the global best value vector in Equation (4.10).

$$\mathbf{p}_{gj}^{(t)} = (p_{g1}^{(t)}, p_{g2}^{(t)}, \dots, p_{gd}^{(t)}) \quad (4.10)$$

The basic concept of PSO is to direct each particle toward its best position $\mathbf{p}_i^{(t)}$ and the swarm's best position $\mathbf{p}_{gj}^{(t)}$, with a random acceleration in each iteration.

Equation (4.11) and Equation (4.12) are the governing equations of the PSO algorithm for $(t+1)^{\text{th}}$ iteration.

$$v_{i,j}^{(t+1)} = w * v_{i,j}^{(t)} + c_1 r_1 (p_{i,j}^{(t)} - x_{i,j}^{(t)}) + c_2 r_2 (p_{gj}^{(t)} - x_{i,j}^{(t)}) \quad (4.11)$$

$$x_{i,j}^{(t+1)} = x_{i,j}^{(t)} + v_{i,j}^{(t+1)} \quad (4.12)$$

Equation (4.11) is the update equation of the velocity of the i^{th} particle in the j^{th} coordinate direction for the $(t+1)^{\text{th}}$ iteration, and Equation (4.12) is the update equation of the position of the i^{th} particle in the j^{th} coordinate direction for the $(t+1)^{\text{th}}$ iteration.

Figure 4.1 shows the geometric illustration of the PSO update scheme in a two-dimensional search space.

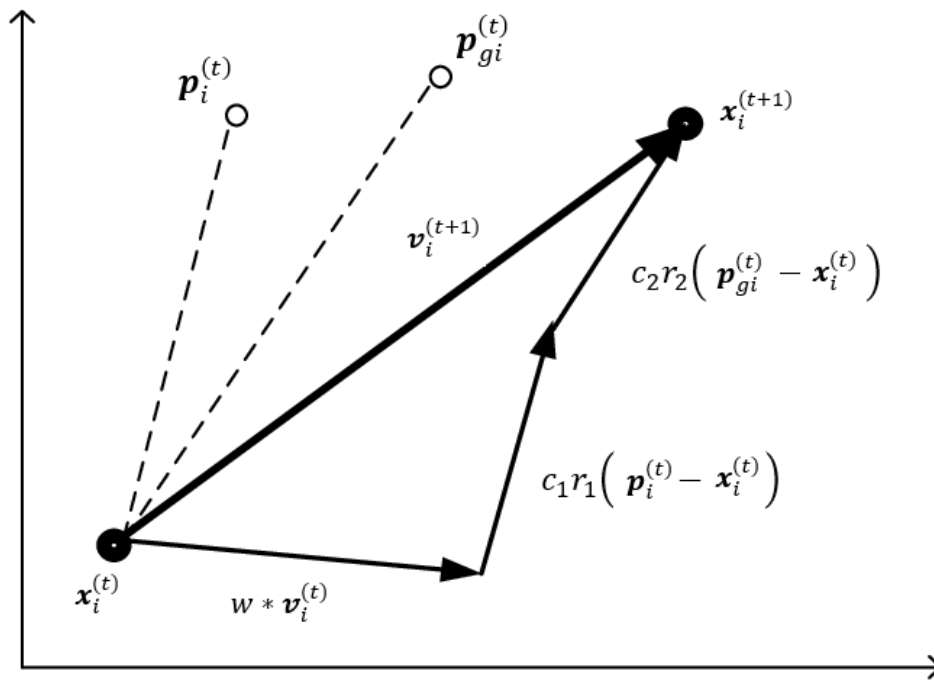


Figure 4.1 Geometric illustration of the PSO update scheme

Terms of the equations (Equation (4.11) and Equation (4.12)) are explained below.

- $x_{i,j}^{(t)}$: Particle's current location
- $x_{i,j}^{(t+1)}$: Particle's modified location
- $v_{i,j}^{(t)}$: Particle's current velocity
- $v_{i,j}^{(t+1)}$: Particle's modified velocity
- $c_1 r_1 (p_{i,j}^{(t)} - x_{i,j}^{(t)})$: Personal (cognitive) velocity influence
- $c_2 r_2 (p_{gj}^{(t)} - x_{i,j}^{(t)})$: Social velocity influence

The multiplier parameters of particle's current velocity, personal (cognitive) velocity influence and social velocity influence terms of the update Equation (4.11) and Equation (4.12) are given below.

- c_1, c_2 - cognitive and social parameters, respectively
- r_1, r_2 - random numbers from uniform distribution between 0 and 1.
- w - inertia weight factor for the velocity

The first difference term $(p_{i,j}^{(t)} - x_{i,j}^{(t)})$ in Equation (4.11) is cognitive term because it contains only the particle's own information. The c_1 is a stochastic parameter named as "cognitive parameter" because it is a multiplier of the cognitive difference term. The second difference term $(p_{gj}^{(t)} - x_{i,j}^{(t)})$ in Equation (4.11) is social term because it contains information from other particles. The c_2 is a stochastic parameter named as the "social parameter" because it is a multiplier of the social difference term [30].

Velocity is limited by the limits of the search space in Equation (4.7) and Equation (4.8). Although this limitation is effective to hinder divergence, it is proven that limiting the velocity is insufficient to produce convergent behavior of the particles [30]. Gradual decrease of the velocity term is needed to converge a point in the search space. This is achieved by introducing an inertia weight factor (w) to the velocity update equation (Equation (4.11)) [30].

The selection of the PSO parameters is critical to have a good convergence rate and optimization performance [15]. Social and cognitive parameters c_1, c_2 in Equation (4.11) usually take values around 1.5 and 2.5 to ensure not to overfly the target and to make the algorithm stable [15], [30]. Parsopoulos recommends taking them as 1.5 [30]. However, 1.5-2.5 range is good to set as the value for these parameters.

Furthermore, the weight factor “ w ” should be appropriately set to decrease the previous velocity effect during iterations [30]. This value can be a fixed value between (0,1); however, it is preferred to decrease the weight factor between two values by using a reduction factor (α). This is done as described in Equation (4.13) for having better optimization performance. In the equation the limits of the weight factor can be taken as $w_{min} = 0$ and $w_{max} = 1$. The reduction factor α can be taken as $\alpha = 0.99$ [15], [30].

$$w = \begin{cases} w_{min} , & w < w_{min} \\ w_{max} * \alpha & \end{cases} \quad (4.13)$$

The convergence criterion used in this thesis is that the distance of all particles to the best objective valued particle must be less than the set value. The user determines the set value at the beginning of the optimization process as an input parameter. Such a convergence criterion ensures that if the number of particles is set wisely, almost all search space is scanned, and getting stuck in the local optimum is prevented.

Steps of the PSO optimization algorithm are given below.

1. Create a ‘population/swarm’ of agents (called particles) uniformly distributed over search space X.
2. Initialize particles’ positions and velocities.
3. Evaluate each particle’s position according to the objective function.
4. If a particle’s current position is better than its previous best position, update it.
5. Determine the best particle (according to the particle’s previous best positions).
6. Update particles’ velocities according to Equation (4.11).

7. Move particles to their new positions according to Equation (4.12)
8. Go to step 3 until the stopping criterion is satisfied.

4.2 Constrained Optimization Problems and Penalty Function Approach

In optimization problems, there may be constraints that the design variables must satisfy. Constraints limit the values that design variables can take; therefore, constraints limit the search space to a feasible region [30]. This type of optimization problem is named as constrained optimization problem. PSO method does not handle the constraints by itself. However, the constraints can be satisfied by using the penalty function approach [15].

Constrained optimization problems are defined as follows.

$$\begin{aligned} & \min_{\mathbf{x} \in X} f(\mathbf{x}) & (4.14) \\ & \text{subject to } C_i(\mathbf{x}) \leq 0 \quad i = 1, 2, \dots, k \end{aligned}$$

where, $C_i(\mathbf{x}) \leq 0$ are the constraints of the optimization problem that the solutions during the iterations must satisfy. If any of these solutions do not satisfy the constraint, this solution counts as infeasible. Optimization continues until an optimum feasible solution that satisfies the constraints is found. Constraints can be equality and inequality constraints, and they put limits on the optimization problem.

In optimization problems, penalty functions are widely used to penalize the solutions that are not in the feasible region. Utilizing the penalty function method, optimization iterations are not allowed to continue in the infeasible region. Using the penalty function method infeasible solutions are determined and they are penalized such that it is ensured that these solutions cannot be selected as the best solution for the particle and the swarm up to the current iteration. For constrained optimization problems, Equation (4.14) is modified to include the penalty function as given in Equation (4.15),

$$\min_{\mathbf{x} \in X} f(\mathbf{x}) + P(\mathbf{x}) \quad (4.15)$$

where the penalty function is defined in Equation (4.16).

$$P(\mathbf{x}) = \begin{cases} \gamma > 0, & \text{if at least for one } i \ C_i(\mathbf{x}) > 0 \\ 0, & \text{otherwise} \end{cases} \quad (4.16)$$

As defined in Equation (4.16), the penalty function is usually a number that is sufficiently high or low to penalize the infeasible solution. Thus, infeasible solutions are precluded from being selected as the particle's or swarm's best solution during the iterations. In the use of penalty functions, it is recommended to incorporate weight functions to change the penalty's weight to understand the degree of violation or how far away the solution is from the feasible region [30]. Via the weight functions, time varying penalty functions, or penalty functions that get more strict or looser, can be defined.

$$\min_{\mathbf{x} \in X} f(\mathbf{x}) + h(t)H(\mathbf{x}) \quad (4.17)$$

Equation (4.17) represents an optimization problem with a weighted penalty function $h(t)H(\mathbf{x})$. In Equation (4.17) $H(\mathbf{x})$ is the penalty function and $h(t)$ is a weight function that can be changed during the iterations for the purpose of controlling the impact of the penalty function.

4.3 Verification of the PSO Code

In this thesis, to optimize the layup angle of variable stiffness composite structures, PSO is used as an optimizer. The basics of the PSO are given above, and definitions of the variables and functions that are used are explained in detail. This part of the chapter is for verification of the written optimization code by using a simple test problem which is taken from Güldü [15].

The test problem is illustrated in Figure 4.3. The objective is to minimize the function defined. The test problem (Equation (4.18)) has two variables X_1 and X_2 which are limited by the constraint in Equation (4.19). The search space of the variables is limited by Equation (4.20).

$$f(X_1, X_2) = 0.25 * X_1^4 - 3 * X_1^3 + 11 * X_1^2 - 13 * X_1 + 0.25 * X_2^4 \quad (4.18)$$

$$- 3 * X_2^3 + 11 * X_2^2 - 13 * X_2$$

$$g(X_1, X_2) = 4 - X_1 - X_2 \leq 0 \quad (4.19)$$

$$0 < X_1, X_2 < 6 \quad (4.20)$$

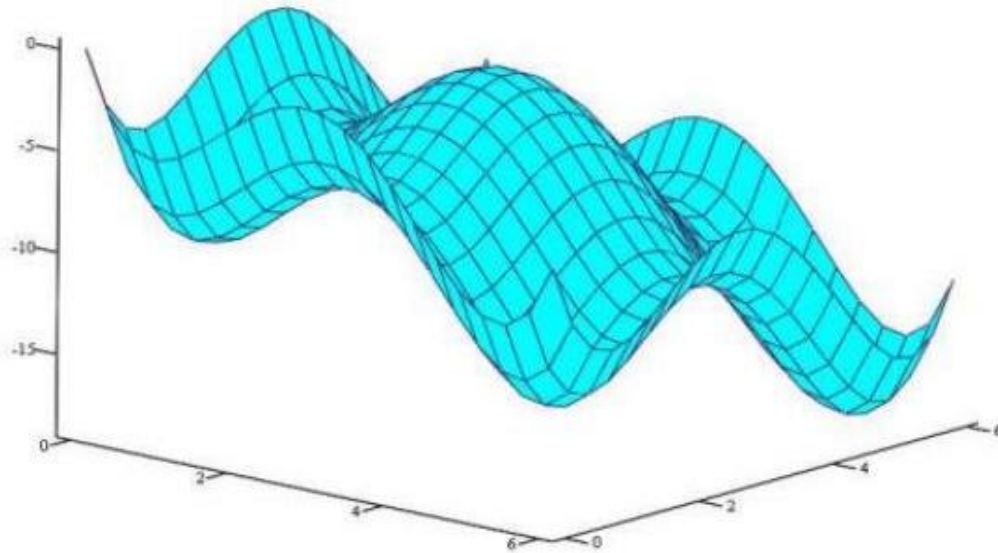


Figure 4.2 Test problem illustration taken from Güldü [15]

The PSO parameters are given in Table 4.1.

Table 4.1 PSO parameters

PSO Parameters		Value
c_1	cognitive parameter	1.5
c_2	social parameter	2.0
w_{max}	inertia weight factor	1
μ	user defined velocity clamping coefficient	0.1
α	reduction factor	0.99
γ	penalty value	10^{28}

In Equation (4.21) penalty function is added to the objective function, and the penalty condition is defined by Equation (4.22). Hence, the constrained optimization problem is converted into an unconstrained optimization problem.

$$F(X_1, X_2, \gamma) = f(X_1, X_2) + P(X_1, X_2, \gamma) \quad (4.21)$$

$$P(X_1, X_2, \gamma) = \begin{cases} 0, & \text{if } g(X_1, X_2) = 4 - X_1 - X_2 \leq 0 \\ \gamma, & \text{otherwise} \end{cases} \quad (4.22)$$

The exact solution of the problem can be determined using calculus. For a function that has two variables $z = f(x, y)$ the potential minimum and maximum points can be found by taking the derivatives with respect to each variable and finding the roots of the equations as shown in Equation (4.23).

$$f_x(a, b) = 0 \text{ and } f_y(a, b) = 0 \quad (4.23)$$

where f_x and f_y are the first derivatives of the function $f(x, y)$ with respect to x and y . Then, D-test is applied as follows.

$$D = f_{xx}(a, b) * f_{yy}(a, b) - [f_{xy}(a, b)]^2 \quad (4.24)$$

- If $D > 0$, then $f(x, y)$ has a maximum if $f_{xx}(a, b) < 0$ and a minimum if $f_{xx}(a, b) > 0$
- If $D < 0$, then $f(x, y)$ has neither a maximum or minimum
- If $D = 0$, then the test fails

By applying this method, the exact result is found, and it is given in Table 4.2.

The problem has been solved by the developed PSO code, and the results of PSO code and the exact values are compared in Table 4.2. Variation of the best objective function value with the iterations during the optimization is shown in Figure 4.3.

Table 4.2 Comparison of the optimization results obtained by the PSO and exact solution

	Exact solution	Current PSO solution
X_1	5.33	5.33
X_2	5.33	5.32
Objective Value	-18.568	-18.568

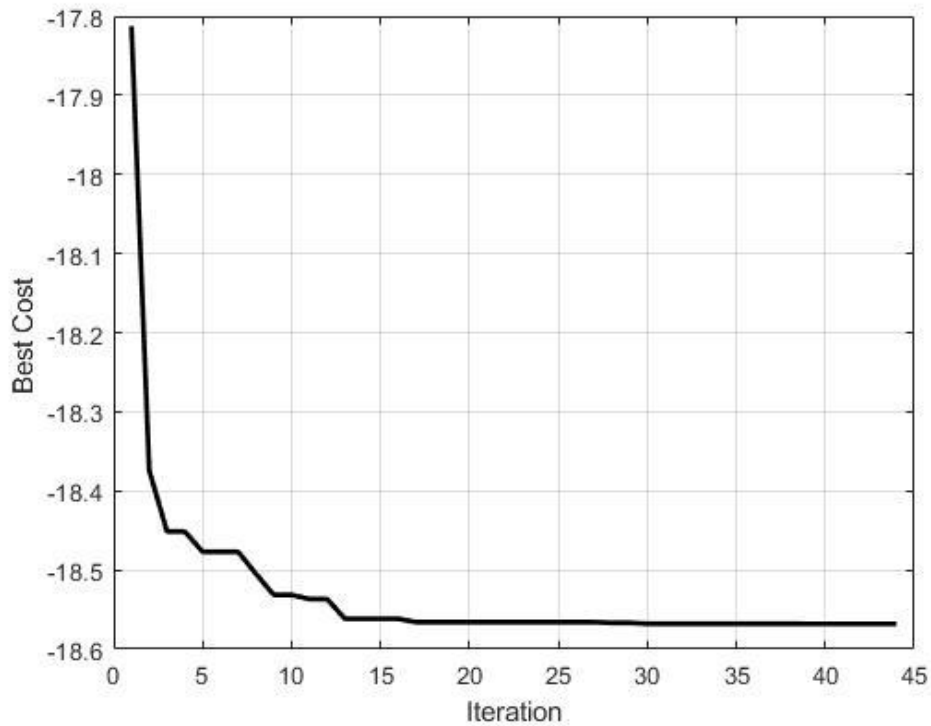


Figure 4.3 Variation of the best value of the objective function with the iteration number

As shown in Table 4.2, optimum values of the variables X_1 and X_2 are very close to the exact values, and the objective function value is identical to the exact value of the objective function at the optimum point. This example shows that the PSO algorithm developed works fine and can be used for further optimization of the fiber angle in variable stiffness composite structures.

CHAPTER 5

MODELLING AND OPTIMIZATION OF VARIABLE STIFFNESS COMPOSITE CURVED PANELS

Optimizing the response of variable stiffness composite structures to different loading conditions is a highly complex task; because it is impossible to analytically solve the response of a structure having spatially varying fiber orientations to a loading. Such an optimization study requires the definition of a layup path and iterative finite element analysis. In every iteration, a new path must be defined and introduced to the analysis model, and the analysis results should be processed to get a better result in each iteration. In this thesis study, different software and theoretical methods are used to achieve this, and a practical method is developed.

In this chapter, path creation technique utilizing NURBS, discussed in chapter 3, and the Particle Swarm Optimization (PSO), discussed in chapter 4, are combined to come up with a methodology for the optimization of variable stiffness composite curved panels.

One of the main differences of the present method from most of the studies performed in the literature is defining a NURBS based reference layup path on a curved 3D surface. Unlike the 2D fiber path definition methods used in the literature, defining the fiber path in 3D makes a difference. Defining a 3D path on a 3D surface is the most direct way to analyze the structure and optimize the path. Especially, NURBS is a straightforward way to define the path if the curvature is multi-directional.

In the present study, the design variables are selected from the parameters used in the definition of the NURBS reference fiber path and they are optimized via the PSO algorithm. Both unconstrained and constrained optimization problems are defined

and with different objective functions, and optimum solutions for the reference paths defined in terms of NURBS parameters are determined.

In the thesis study, flat panels, and curved panels, which are manufactured utilizing variable stiffness concept, are investigated. To define an initial NURBS path, Rhino [6] software is used. MATLAB is used for constructing the NURBS paths mathematically, running the PSO algorithm, and coupling the MSC. Nastran FEA software, which is used as the solver, with the PSO algorithm.

5.1 Creation of Variable Stiffness Composite Structure

To create variable stiffness composite structures, continuous paths are defined in AFP machines. There are different methods to do that as mentioned before. However, in this study NURBS are used for the layup path definition. By using the NURBS based computer aided design software Rhino, an initial random NURBS path is created. Then, an initial NURBS is created in MATLAB environment. To create the NURBS in MATLAB, NURBS toolbox developed by D.M. Spink [33] is used. Furthermore, some new functions are added according to the aim of this study. Specifically, NURBS curvature calculation and NURBS plotting functions are added to the toolbox. The reason for creating the initial NURBS in Rhino environment is that in Rhino software the curved panel geometry can also be modelled, and a reference NURBS layup path can easily be defined. Rhino software also generates a table which gives the NURBS parameters.

5.1.1 NURBS Path Creation in Rhino

Rhino is a commercial computer aided design and computer graphics software. It uses NURBS to model complex shapes. One of the advantages of the program is that it allows the users to visually see and change the shape of spline. The position of control points is also visualized, and via the commands one can easily change the knots and the weights. As an example, a curved panel and a NURBS layup path with

control points are shown in Figure 5.1. Table 5.1 gives the contents of an example information card of the NURBS definition in the relevant interface in Rhino. Following the creation of the NURBS curve, it can be exported as a step file. To construct the NURBS curve, the step file includes the control point, knot, the weight information, and other necessary information such as the degree of the curve. An example step file content exported from Rhino is given in Appendix A. Since the standard of step file is "ISO 10303 the STEP Standard for Product Data Exchange" to extract the information about the NURBS, this standard is used. The initial NURBS curve is created in Rhino, and the information about the NURBS parameters is transferred by extracting the NURBS curve information as a step file.

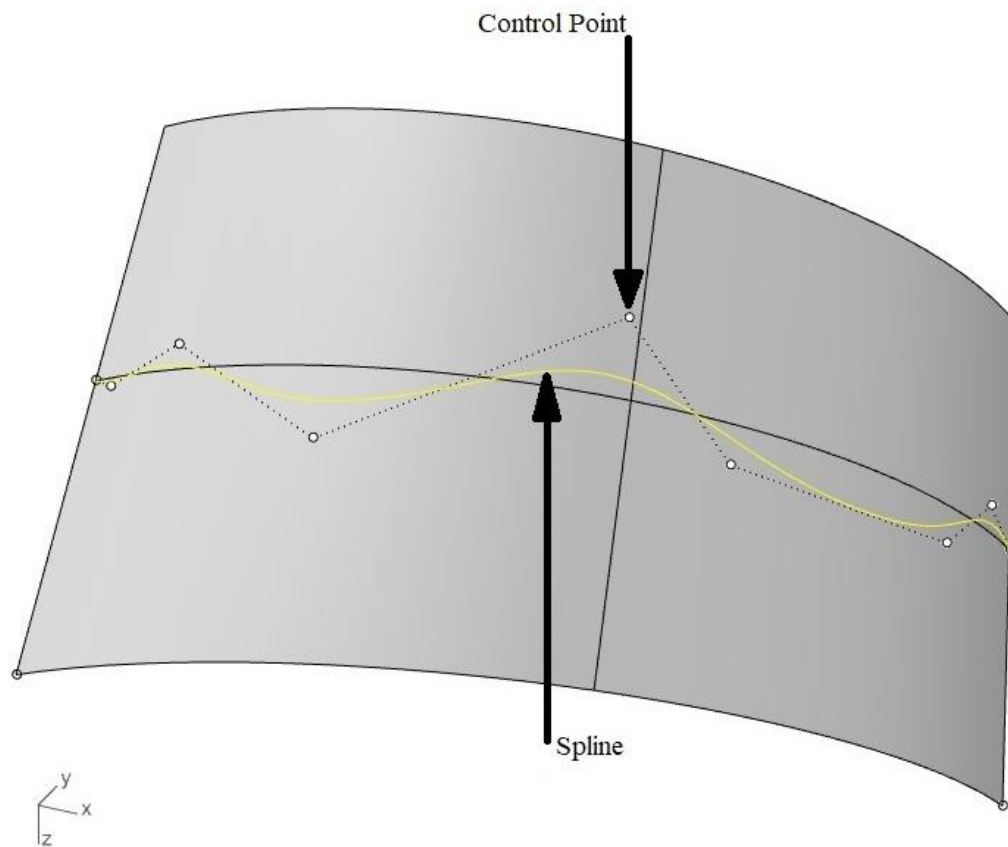


Figure 5.1 NURBS layup path with its control points

Table 5.1 Contents of the NURBS information card example in the Rhino interface

Curve type	Open NURBS curve
Starting point	(-800,0,500)
Ending point	(800,0,500)
Degree of curve	3
Control points type	Non-rational
Number of control points	9
Knot type	Non-uniform
Knot domain	(0,1886.8)

5.1.2 NURBS Path Creation in MATLAB

In this thesis, NURBS toolbox for MATLAB developed by Spink [33] is used to construct the NURBS curves in MATLAB environment. Firstly, the extracted step file is opened by MATLAB, and by using the information from ISO 10303, the related lines, and keywords for the parameters are determined. From the step file, NURBS parameters which are the degree of the curve, size of the knot vector, knot vector, weights, and coordinates of control points are extracted using the MATLAB command “regexp”. Then, the NURBS structure array is created and each NURBS parameter is stored in this structure array. Basis functions are constructed utilizing Equation (3.12). Constructed basis functions, extracted control points and weights are implemented in Equation (3.17). An example NURBS curve created in Rhino is shown in Figure 5.2 and the parameters of the NURBS curve are given in Table 5.2. MATLAB representation of the NURBS curve is given in Figure 5.3.

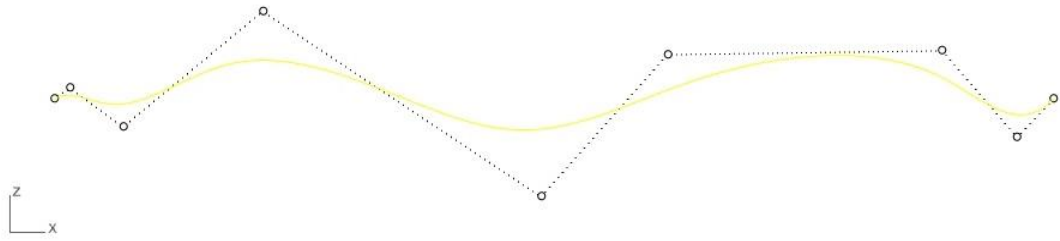


Figure 5.2 Representation of the NURBS in Rhino

Table 5.2 Parameters of the NURBS curve

Control Points												
X	-800.0	-774.8	-689.8	-466.24	-20.59	181.4	621.4	741.5	80			
	0	6	4			5	3	1	0			
Y	0	25.31	100.3	231.25	298.8	274.9	138.1	47.80	0			
			7		5	0	9					
Z	500	517.3	455.8	637.63	346.2	569.6	575.7	439.7	50			
		1	0		9	1	8	9	0			
Knots												
0	0	0	0	0.07	0.2	0.43	0.76	0.89	1	1	1	1
					0							
Weights												
1	1	1	1	1	1	1	1	1	1	1	1	1

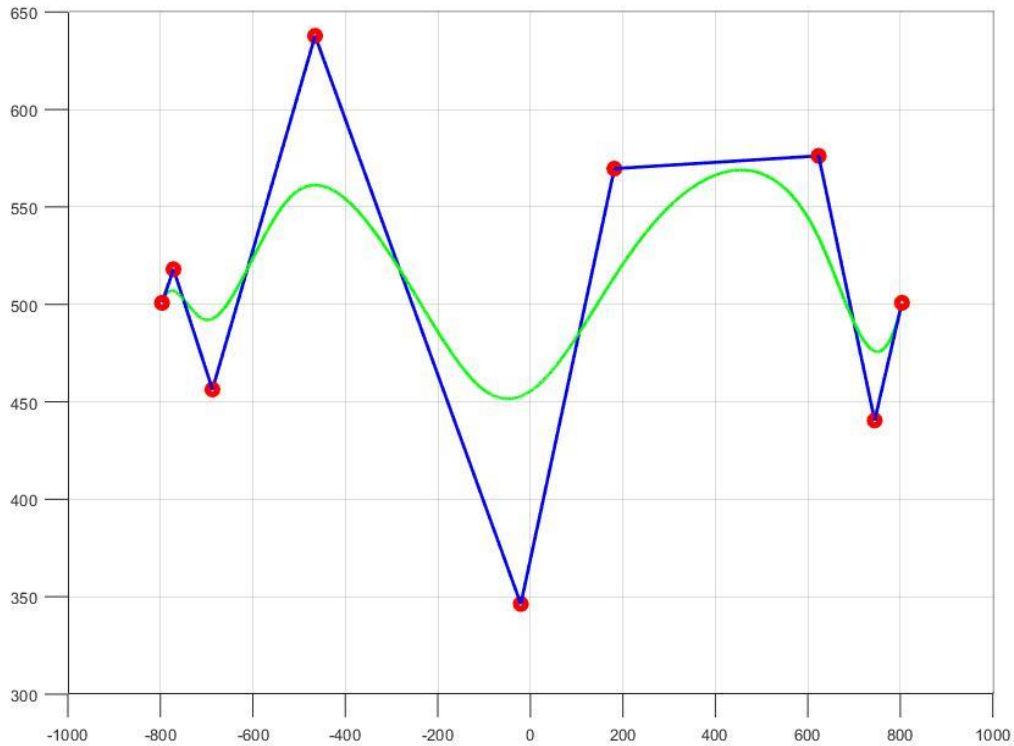


Figure 5.3 MATLAB representation of the NURBS exported from Rhino

5.1.3 Generation of the Geometry and the Finite Element Model

In the thesis study, on the finite element modeling side, MSC. Patran [34] and MSC. Nastran [35] are used. MSC. Patran is the pre-post processor of MSC. Nastran and it is used to create the geometry and the finite element model. The analysis geometries are created in the MSC. Patran environment. Two different analysis geometries are used in the study. First one is a flat panel and the second one is a curved panel. The material properties of the plies of composite panels are defined as 2D orthotropic materials, and the composite laminate is created from this ply material. The panels are defined as laminated shell structures. The load and boundary conditions are defined in the preprocessor MSC. Patran. The solver type is selected depending on the problem.

5.1.4 Defining Shifted Paths in the Analysis Geometry

In the manufacturing of variable stiffness composite structures, reference fiber path method is commonly used in the literature. To cover the entire body, shifted and parallel fiber paths are generally used, as discussed before. In the present study, shifted fiber path method is used and the reference fiber path is shifted until the entire body is covered. An example for the reference fiber path is shown in Figure 5.4. Figure 5.5 shows the shifting of the reference fiber path for covering the entire panel. In this example, reference fiber path is shifted along the z direction of the global coordinate system shown in the lower left corner of Figure 5.5. It should be noted that this study deals with fiber path optimization, not tow path optimization. In tow placement, since tows have a finite width, gaps or overlaps may occur during the shifted path manufacturing technique, as opposed to manufacturing utilizing the parallel tow path placement method.

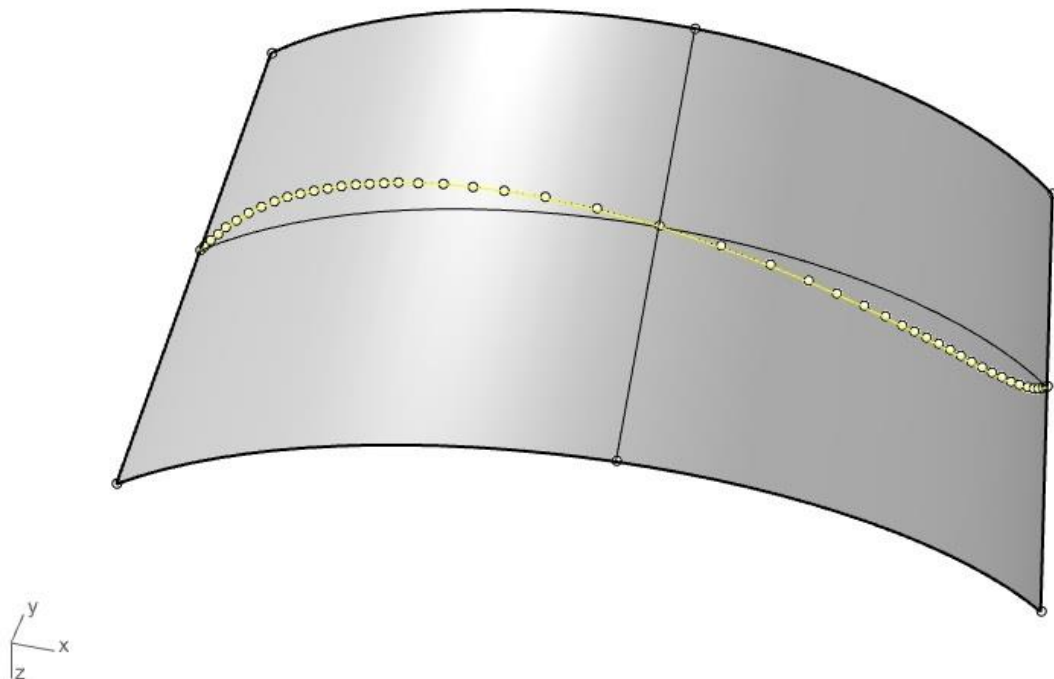


Figure 5.4 An example for the reference fiber path

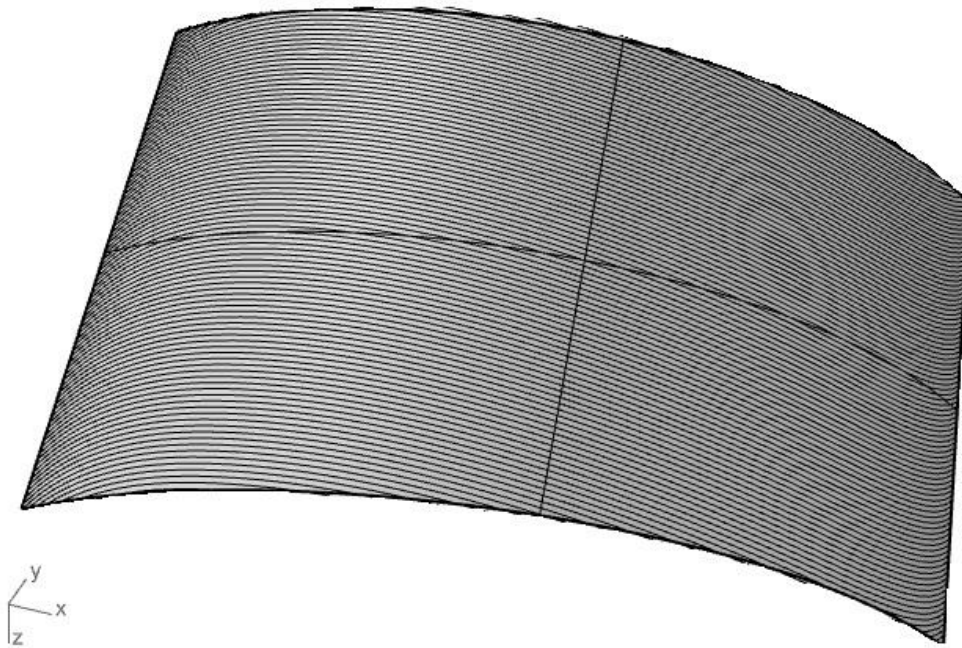


Figure 5.5 Shifting of the reference fiber path for covering the entire panel

5.2 Optimization Parameters of VSC, Objective Functions and Constraints

In the optimization of variable stiffness composite structures, finite element solution is required at each iteration of the optimization since fiber paths vary over the structure and fiber angles of each ply change from one finite element to another. In the iteration process of particle swarm optimization, at each iteration the value of the objective function solution is compared with the previous solutions and the particles move towards the better solution until they reach the optimum design.

5.2.1 PSO Parameters

Selection of the optimization parameters is very important for the success of the optimization. Parameters affect the performance of the optimization algorithm in finding the global optimum as well as the convergence speed in reaching the global optimum. The parameters of PSO used in the current study is presented in Table 5.1.

Table 5.3 PSO parameters used in the optimizations

PSO Parameter	PSO Parameter Value [5], [30]
c_1	1.5
c_2	2.0
w_{max}	1
μ	0.1
α	0.99
γ	10^{28}
# of particles	25

Besides the parameters in the basic PSO algorithm, for convergence a tolerance parameter is also defined. Convergence parameter is used to terminate the optimization iterations once the specified criterion is met. For convergence to the global optimum, tolerance values are used. Until all particles converge within the specified tolerance, the algorithm continues to search the space for the optimum solution to prevent getting stuck at a local optimum.

In the literature for c_1 (cognitive parameter) and c_2 (social parameter) it is suggested to be around 1.5 to 2.5 [5], [30]. If the c_2 (social parameter) is bigger than c_1 , it is stated that optimization is affected by the group. In contrast, for a case that c_1 is bigger than c_2 particles are affected by their own experience more [5] [36]. In this study c_1 is selected as 1.5 and c_2 is selected as 2.0. In the literature it is stated that, if c_2 is much bigger than c_1 there is a risk for particles to run prematurely to the optima [5]. However, selecting c_2 bigger than c_1 speeds up the optimization and decreases computation time. In this study defining a convergence tolerance leads the algorithm to scan the search space even if a global optimum is found, disabling particles from running prematurely to the optima and decreasing the computation time.

Population size is the number of particles n in the swarm. A big swarm generates larger parts of the search space to be covered per iteration. A big population may reduce the number of iterations needed to obtain a good optimization result. In

contrast, huge amounts of particles rise the computational complexity per iteration and are more time-consuming. In the literature, empirical studies show that number of particles should be in an interval of 20 to 60 [5]. In this study, the number of particles selected as 25. Because different number of particles are tried, and it is seen that there is no need to choose a big swarm.

In the algorithm, μ user defined velocity clamping coefficient is 0.1. As it is stated in Chapter 4 the coefficient μ is used because smaller velocities can offer better search accuracy [30]. The α reduction factor is used as 0.99 as it is proposed in a similar study of Güldü [15]. For the γ penalty value 10^{28} is selected as a very big value to penalize the infeasible solution.

5.2.2 Optimization Variables

An optimization variable is a symbolic object that enables one to create expressions for the objective function and the problem constraints in terms of the variable. Objective function value changes as the optimization variables change. In this study, according to the defined objective function NURBS layup path is optimized. It should be noted that any one of the NURBS parameters can be used as an optimization variable to optimize the layup path. These parameters are control points, knot vectors, and weights. In this study, control points are used as optimization variables.

5.2.2.1 Control Points

Control points are the main parameters that specify the characteristics of the NURBS curve. The change of the control points affects the shape of the curve significantly. Boundaries of the control points are limited to the geometry of the panel. Coordinate values of the edges of the panel specify the limits. Control points specify the control polygon of the NURBS, hence when the positions of these points change, this has a significant effect of the shape of the spline. An example of the effect of the control

points on the shape of the spline was given in Figure 3.4. It should be noted that in the current study, since shifted fiber path method is used in the manufacturing of variable stiffness composite panels, only one of the coordinates (x or y) of the NURBS is altered by the optimization algorithm.

5.2.2.2 Knot Vectors

Knot vector is one of the other design parameters of NURBS. Changing the knot vector also affects the shape of the NURBS, as shown in Figure 3.6. However, when changing the elements of the knot vector, the elements of the knot vector should be positioned in the knot vector in an increasing order. This condition can tighten each the search span of each element during the optimization process. Because the position of the design variable is updated during the optimization, the search space of each knot value changes. When the knot vector is updated, knot vector elements should be positioned in an increasing order. Knot vector must be updated in an order from the first value to last value one by one.

5.2.3 Objective Functions

Objective functions measure the merit of the different designs [35].[35].. There can be many design alternatives obtained by changing the design variables; however, to understand which one is the one that designer wants is decided by the objective function. In optimization problems, objective function value is either minimized or maximized by changing the design variables. Depending on the minimization or a maximization process, objective function is named as cost function or profit function, respectively. By changing the design variables, objective function values must be changed, otherwise the design variable would not have a meaning [36].[36].. In this study, three different objective functions are used. Total strain energy of the composite structure subject to a load and boundary condition set is one of the objective functions that is used in the optimization problem. In this case, the goal is

to minimize the total strain energy of the composite panel utilizing the optimized reference fiber path according to which the whole panel is covered with composite material. Hence, without changing the thickness of the composite panel, optimum stiffness distribution is achieved through the variable stiffness concept. The second objective function used in the thesis study is the failure index of the composite calculated according to one of the well-established composite failure theories. In this case, the goal is to maximize the failure index by altering the reference fiber path via the changes imposed on the NURBS parameters through the optimization process. The third objective function is the buckling load factor of the composite panel. In this case, the goal is to maximize the buckling load factor of the composite panel via the optimization of variable stiffness composite panel.

5.2.3.1 Strain energy as the objective function

Strain energy is the energy that material stores internally throughout its volume when it is deformed by an external loading [38]. In the following a general strain energy expression is derived for anisotropic materials. The generalized stress strain relation is given in Equation (5.1), where σ_i is the contracted form of the stress tensor and ε_i is the contracted form of the strain tensor and C_{ij} are elements of the elastic coefficient matrix for anisotropic materials

The inverse of the stiffness matrix C in Equation (5.1) is the compliance matrix “S” and Equation (5.2) gives the strain-stress relation.

$$\begin{bmatrix} \sigma_1 = \sigma_{xx} \\ \sigma_2 = \sigma_{yy} \\ \sigma_3 = \sigma_{zz} \\ \sigma_4 = \sigma_{yz} \\ \sigma_5 = \sigma_{xz} \\ \sigma_6 = \sigma_{xy} \end{bmatrix} = \begin{bmatrix} C_{11} & C_{12} & C_{13} & C_{14} & C_{15} & C_{16} \\ C_{21} & C_{22} & C_{23} & C_{24} & C_{25} & C_{26} \\ C_{31} & C_{32} & C_{33} & C_{34} & C_{35} & C_{36} \\ C_{41} & C_{42} & C_{43} & C_{44} & C_{45} & C_{46} \\ C_{51} & C_{52} & C_{53} & C_{54} & C_{55} & C_{56} \\ C_{61} & C_{62} & C_{63} & C_{64} & C_{65} & C_{66} \end{bmatrix} * \begin{bmatrix} \varepsilon_1 = \varepsilon_{xx} \\ \varepsilon_2 = \varepsilon_{yy} \\ \varepsilon_3 = \varepsilon_{zz} \\ \varepsilon_4 = \varepsilon_{yz} \\ \varepsilon_5 = \varepsilon_{xz} \\ \varepsilon_6 = \varepsilon_{xy} \end{bmatrix} \quad (5.1)$$

$$\begin{bmatrix} \varepsilon_1 = \varepsilon_{xx} \\ \varepsilon_2 = \varepsilon_{yy} \\ \varepsilon_3 = \varepsilon_{zz} \\ \varepsilon_4 = \varepsilon_{yz} \\ \varepsilon_5 = \varepsilon_{xz} \\ \varepsilon_6 = \varepsilon_{xy} \end{bmatrix} = \begin{bmatrix} S_{11} & S_{12} & S_{13} & S_{14} & S_{15} & S_{16} \\ S_{21} & S_{22} & S_{23} & S_{24} & S_{25} & S_{26} \\ S_{31} & S_{32} & S_{33} & S_{34} & S_{35} & S_{36} \\ S_{41} & S_{42} & S_{43} & S_{44} & S_{45} & S_{46} \\ S_{51} & S_{52} & S_{53} & S_{54} & S_{55} & S_{56} \\ S_{61} & S_{62} & S_{63} & S_{64} & S_{65} & S_{66} \end{bmatrix} * \begin{bmatrix} \sigma_1 = \sigma_{xx} \\ \sigma_2 = \sigma_{yy} \\ \sigma_3 = \sigma_{zz} \\ \sigma_4 = \sigma_{yz} \\ \sigma_5 = \sigma_{xz} \\ \sigma_6 = \sigma_{xy} \end{bmatrix} \quad (5.2)$$

Strain energy density (u) is expressed by Equation (5.3).

$$u = \int_0^{\varepsilon_{ij}} \sigma_i d\varepsilon_i \quad (5.3)$$

Utilizing the stress-strain relationship, one can express the total strain energy in an elastic body as in Equation (5.4).

$$U = \int_V u dV = \frac{1}{2} \int_V \sigma_i \varepsilon_i dV = \frac{1}{2} \int_V S_{ij} \sigma_i \sigma_j dV \quad (5.4)$$

For a specified external loading, in order to minimize the total strain energy in an elastic body, compliance matrix, hence the compliance of the body, must be minimized or the stiffness of the body must be maximized since the elastic coefficient matrix is the inverse of the compliance matrix.

5.2.3.2 Failure criterion as the objective function

A successful structural design requires safe and efficient use of material. Therefore, theories are developed to comment of the structural integrity of the design and to decide on if the design is safe or not [39]. For composite structures, different failure theories are developed. Some of the well-established failure theories are the maximum strain, maximum stress, Tsai-Hill, Hoffman, and Tsai-Wu failure theories.

Finite element software MSC. Nastran calculates the stresses in every layer of each element in the fiber, transverse to the fiber and shear directions. These stresses can then be employed in a failure criterion to calculate the failure indices to predict failure in each layer. Furthermore, MSC. Nastran can supply the failure index of each

element for different failure theories. In this thesis, the failure index definition of the Tsai-Wu failure criterion is used as one of the objective functions. In this criterion, if the failure index reaches a value of 1.0 or higher, failure is assumed to occur. Hence, the failure index must be lower than 1.0 to have a safe design [39].

The Tsai-Wu failure theory is based on the total strain energy failure theory and applied to the laminae under plane stress [40].[40].. Tsai-Wu failure theory lets the failure strengths vary in tension and compression. The failure can happen due to a mixture of failure modes [39]. It is necessary to supply failure strengths in both compression and tension for the fiber and the transverse directions and the shear failure strength to the theory [15].[15].. The formulation of the criterion is presented in Equations (5.5)-(5.12).

$$F_1 = \left(\frac{1}{X_t}\right) - \left(\frac{1}{X_c}\right) \quad (5.5)$$

$$F_2 = \left(\frac{1}{Y_t}\right) - \left(\frac{1}{Y_c}\right) \quad (5.6)$$

$$F_{11} = \left(\frac{1}{X_t}\right) * \left(\frac{1}{X_c}\right) \quad (5.7)$$

$$F_{22} = \left(\frac{1}{Y_t}\right) * \left(\frac{1}{Y_c}\right) \quad (5.8)$$

$$F_6 = \left(\frac{1}{S^2}\right) \quad (5.9)$$

$$F_{12} = -0.5(F_1 * F_2)^{0.5} \quad (5.10)$$

$$FI = \sigma_1 * F_1 + \sigma_2 * F_2 + \sigma_1^2 * F_{11} + \sigma_2^2 * F_{22} + \sigma_3^2 * F_6 + 2F_{12} * \sigma_1 * \sigma_2 \quad (5.11)$$

$$FI < 1 \quad (5.12)$$

In Equations (5.5)-(5.12),

- X_t, X_c are the ultimate tensile and compression strength in material direction 1
- Y_t, Y_c are the ultimate tensile and compression strength in material direction 2
- S is the shear strength of the material in the 1-2 direction
- FI is the failure index

With the Tsai-Wu failure criterion, different tensile and compressive strengths can be addressed, and all possible interactions are accounted for.

5.2.3.3 Buckling load factor as the objective function

One of the objective functions used in this thesis is the buckling load factor (BLF). Buckling load factor is described as a safety factor against buckling, and it is calculated by taking the ratio of the buckling load to the applied load. In this study, BLF is calculated by the finite element solver, MSC. Nastran directly using the Sol 105 solution option. Table 5.2 gives the explanation of the BLF values [15],[15]..

Table 5.4 Explanation of the BLF

BLF	Buckling Status	Remark
$1 < \text{BLF}$	Buckling not predicted	The applied loads are less than the critical loads.
$0 < \text{BLF} < 1$	Buckling predicted	The applied loads exceed the critical loads.
$\text{BLF} = 1$	Buckling predicted	The applied loads are exactly equal to the critical loads.
$\text{BLF} = -1$	Buckling not predicted	The model is in tension and buckling is not expected.
$-1 < \text{BLF} < 0$	Buckling not predicted	Buckling is predicted if you reverse all loads.
$\text{BLF} < -1$	Buckling not predicted	Buckling is not expected even if you reverse all loads

5.2.4 Optimization Constraints

In this study, different constraints are used to limit the search space for feasible solutions. Minimum turning radius constraint and the failure criterion constraint are used as the constraints. When particles of a solution violate this constraint, the penalty function penalizes the objective function during iterations. If the constraint is violated, the penalty function ensures that the solution is infeasible.

The minimum turning radius constraint concept is discussed in Chapter 2. This constraint is used to prevent the wrinkles in the tow due to the forced in-plane deformation. Minimum turning radius changes from one AFP machine to another; therefore, in this study, it is not defined as a constant but left to the user as an input.

The second constraint is the failure index criterion. In this study, failure index is used both as an objective function and constraint in different case studies. Failure index is also used as a constraint in some of the case studies to see its effect on the optimized solution.

5.3 Optimization Scheme

The optimization process consists of several steps. Input file manipulation of the finite element solver MSC. Nastran, extracting data from the output file of the finite element solver, setting the optimization parameters and calculation of the objective function are the main steps of the optimization. This sub-section describes the process in detail and provides a flowchart of the optimization process. As mentioned earlier, the input reference path is prepared in Rhino, and then the data is transferred to MATLAB. Furthermore, input file of the finite element model is prepared using the pre-processor MSC. Patran.

For starting the optimization, the PSO parameters are set in the MATLAB script or entered as MATLAB input. MATLAB uses some information from MSC. Nastran input file as an input for the optimization. According to the optimization process, some design variables are changed and entered the MSC. Nastran input file. This process is described below. In the MSC. Nastran input file, there are element and grid information. This information is vital in finding the center points of the finite elements required for assigning the fiber orientation angle to the elements. Coordinates of the element centers are found from the grid information. Coordinates of the elements' centers are compared with the coordinates of the reference NURBS path and the closest NURBS coordinates to the coordinates of the element center are determined and they are used to calculate fiber angles at the element centers. Figure 5.6 shows an illustration of the method used in finding the fiber angle of finite elements utilizing the NURBS reference path. It should be noted that NURBS is defined at predefined number of parametric coordinates. In this study, coordinates along the NURBS path are calculated at 10^6 parametric values between 0-1. Hence,

according to the coordinate axis established in Figure 5.6, the x-coordinate of the element center perpendicular to the shifting direction y (x if the shifting direction is y or y if the shifting direction is x) may not coincide exactly with an x-coordinate in the NURBS defined at 10^6 parametric values. However, since 10^6 number of coordinates are used in the definition of NURBS, NURBS x-coordinates, which are very close to the x-coordinates of the element centers, can be determined. Having determined the x-coordinates of the NURBS at the element centers, fiber angles at the element centers are determined utilizing the tangent information at the NURBS coordinate corresponding to the element center. Relevant field, for the fiber angles of the plies, of the input file of the finite element program MSC. Nastran is then updated. In the shifted path method, fiber angles of elements at different y-coordinates are same if they have the same x-coordinates.

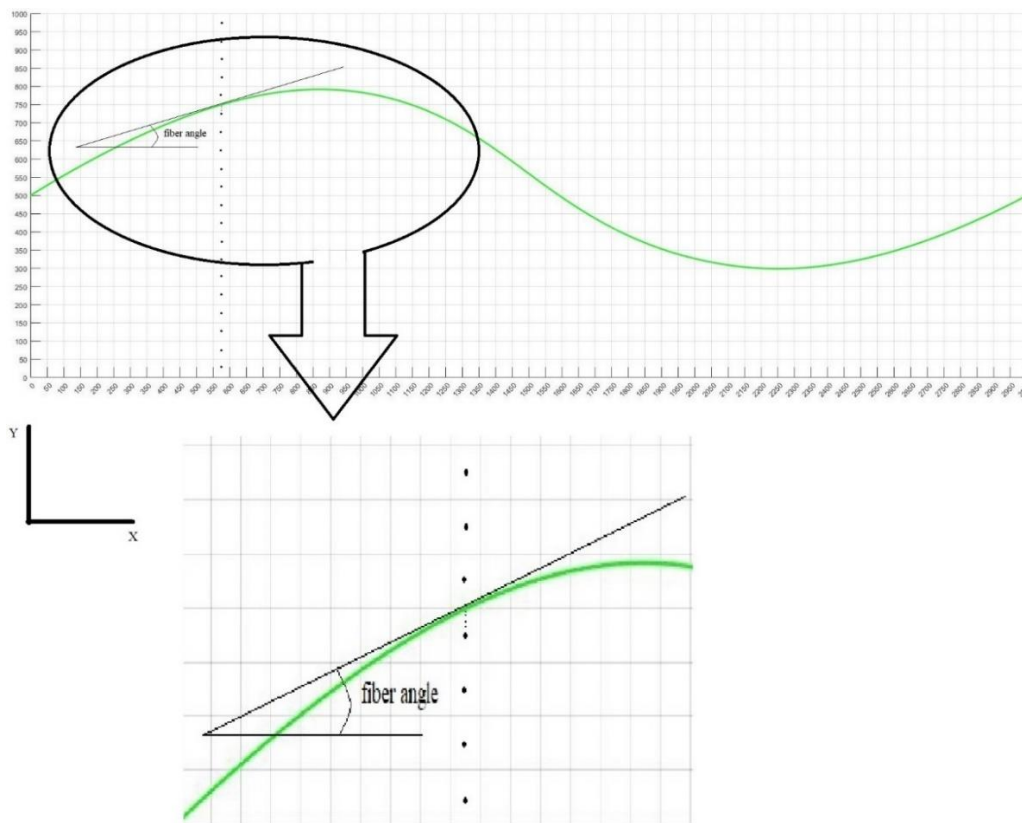


Figure 5.6 Illustration of the method used in finding the fiber angle of finite elements utilizing the NURBS reference path

5.3.1 MSC. Nastran Input File Manipulation

Input file of MSC. Nastran has element property information written for all elements line by line. The cards that describe the composite structure are the PCOMP cards in Nastran terminology and the number of element property cards is equal to the number of elements in the geometry. In the input file of Nastran, each card occupies certain number of lines with different fields which can be edited for modification purposes. Element property cards include information on the number of plies in each element, the ply thickness, and the fiber angle information of each ply in an element. While optimizing the layup path, the fields of the lines storing the fiber angles are modified according to the changes that occur in the NURBS based reference fiber path during the optimization process. Definition of the PCOMP card used for element property information in MSC. Nastran is given in Appendix B.

5.3.2 MSC. Nastran Output File Evaluation

When the layup path is described in the MSC. Nastran input file, MATLAB calls MSC. Nastran to analyze the created subcase. Following a finite element analysis, MSC. Nastran produces an output file from which the value of the objective function can be extracted. In the present study, the strain energy of the structure, buckling load factor, and failure index information all are provided in the output file, and they are used as the objective functions in different case studies.

Rhino is not used in the optimization process after the first iteration, because it is only used to create a reference path. In the course of optimization, PSO changes the optimization variables, and new NURBS layup paths are created in the MATLAB environment. Every time a new reference fiber path is generated throughout the optimization process, fiber angles of each finite element are updated in the MSC. Nastran input file. Finite element analysis is performed utilizing the updated fiber angle information and corresponding objective function value is extracted. The process continues until the termination condition of the optimization process is

satisfied. In this study, the termination condition is the convergence tolerance. Until positions of all particles converge within the specified tolerance, the algorithm continues to search the space for the best solution. The flowchart of the optimization process is presented in Figure 5.7. In Appendix C, an example of explanation and results of the optimization process is given.

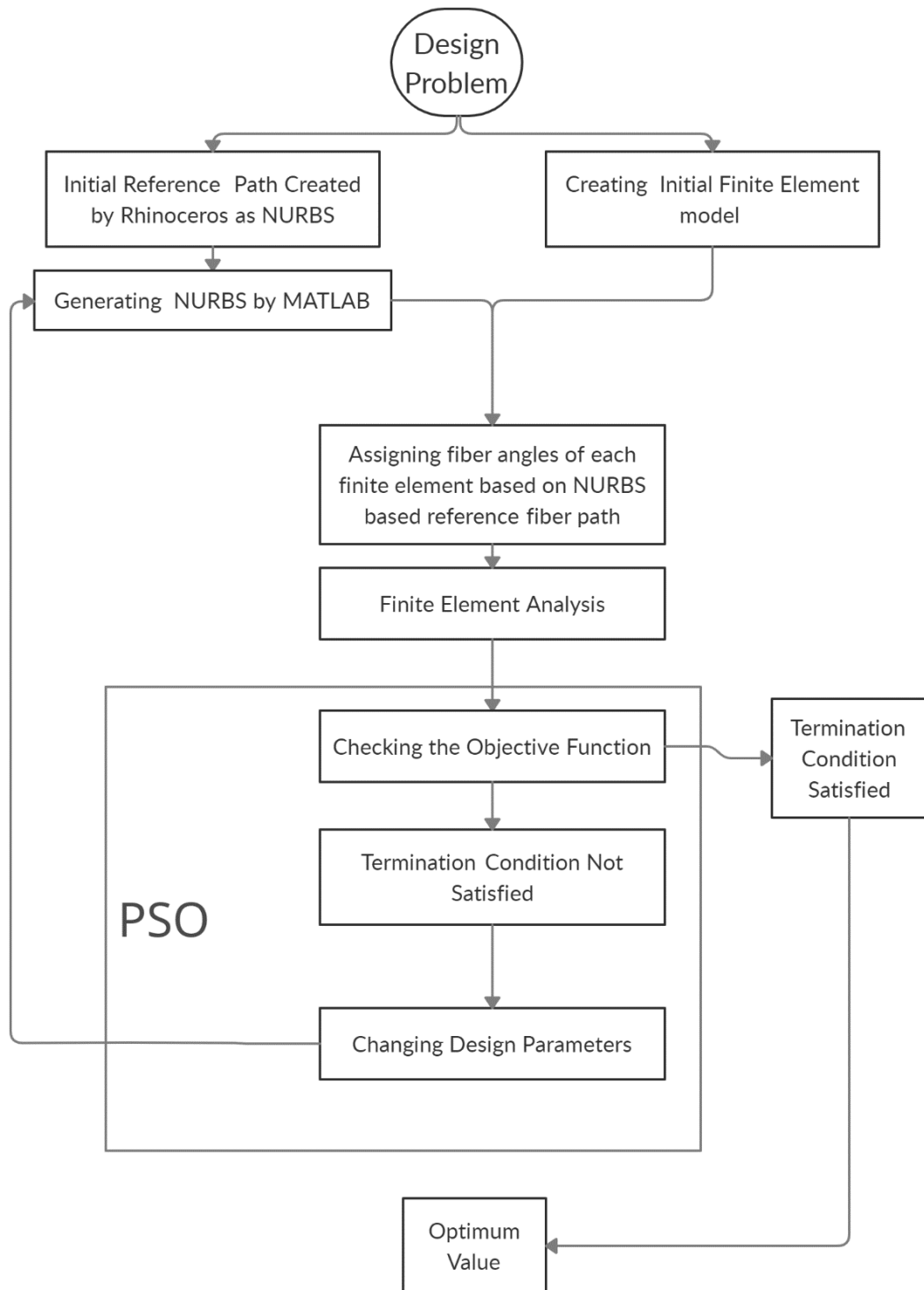


Figure 5.7 Optimization Flow Chart

CHAPTER 6

RESULTS AND DISCUSSION ON THE ANALYSIS AND OPTIMIZATION RESULTS

In the literature, many studies are performed on the optimization of variable stiffness composite structures [4], [10], [18], [40]–[42]. In these studies, significant improvements in the mechanical strength of the composite structures are achieved. In most of the studies, as the layup path definition, smooth antisymmetric function of x is used, as proposed by Gürdal and Olmedo in 1993 [3]. In this method layup path is defined on the x - y plane and the equation of the path is defined with respect to this coordinate frame. However, it is stated that this layup path definition method is efficient for flat surfaces [4]. The NURBS is used in computer-aided design software to generate 3D shapes. Three dimensional shapes consist of curves and surfaces created by NURBS. Therefore, for three dimensional shapes such as curved panels, the layup path can be defined by NURBS, as described in Chapters 3 and 5. NURBS path definition is also used in the VSC optimization study [16]. In this part of the study, optimization results of the VSC flat and curved panels are presented. For this, the method described in the Chapter 5 is used.

In this chapter firstly, strain energy minimization of a flat panel is performed to verify the algorithm and buckling analysis of an isotropic panel is done to show that the theoretical results and finite element analysis results are consistent.

In the second part, four cases are studied. In this part, geometry is a flat panel and the cases studied are listed below.

- One layered flat panel strain energy minimization
- Four layered flat panel strain energy minimization
- Four layered flat panel strain energy minimization constrained with failure index

- Flat panel failure index minimization

In the third part, a VSC curved panel is optimized. Three cases are studied and they are listed below.

- Four layered curved panel BLF maximization
- Four layered curved panel strain energy minimization
- Four layered curved panel strain energy minimization constrained with failure index

The material properties of the composite material AS4/855-2, Graphite-Epoxy used in the panels are taken from Güldü's work [15] and presented in Table 6.1.

Table 6.1 Material properties of AS4/855-2, Graphite Epoxy y[34]

Material Property	Value
E_1	134 GPa
E_2	16.75 GPa
G_{12}	5.8625 GPa
ν_{12}	0.3
X_t	2070 MPa
X_c	1160 MPa
Y_t	132.7 MPa
Y_c	199.8 MPa
S	117.1 MPa

As discussed before, finite element models are created by using MSC. Patran and MSC. Nastran is used as the finite element solver. The consistent units used in the finite element analysis are given in Table 6.2.

Table 6.2 Unit consistency table of MSC. Patran

Length	Force	Elastic Modulus	Mass Density	Acceleration	Displacement	Stress
mm	N	MPa	ton/Mg	mm/s ²	mm	MPa

For the optimization cases in this chapter, the PSO parameters given in Table 6.3 are used. Optimization variables are the control points, and the convergence criterion is defined as 10 mm for all cases.

Table 6.3 Optimization parameters for the strain energy minimization of the flat panel

PSO Parameter Name	<i>PSO Parameter Value</i>
c_1	1.5
c_2	2.0
w_{max}	1
μ	0.1
A	0.99
γ	10 ²⁸
<i># of particles</i>	25
<i>Convergence tolerance</i>	10 mm

6.1 Verification of the Optimization Algorithm

6.1.1 Flat Panel Strain Energy Minimization Verification Case

In this section, verification of the optimization algorithm is performed for a flat panel shown in Figure 6.1. Flat panel has a length of 3000 mm and a height of 1000 mm. Ply material properties of the composite flat panel are given in Table 6.1. The flat

panel consists of 4 layers with a ply thickness of 0.183 mm. The stacking sequence is shown in Figure 6.2 for the 4-layer panel. Boundary conditions and loading is presented in Figure 6.3. The panel is clamped from its center node and uniformly compressed by a distributed load of 200 kN/m from the two short edges. For the finite element analysis, 736 elements (46x16) are used. It is expected that with the referred boundary and loading conditions, the fiber path must converge to a straight line for maximum stiffness, hence minimum strain energy.

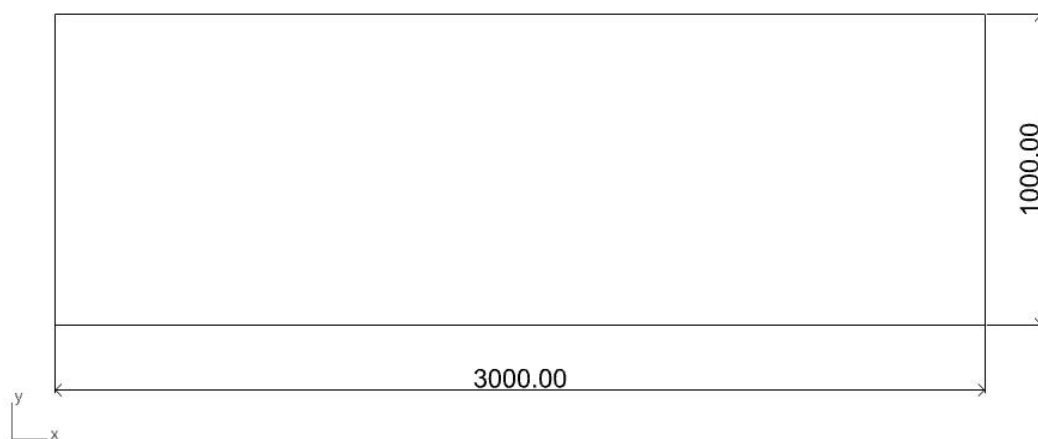


Figure 6.1 Flat panel dimensions

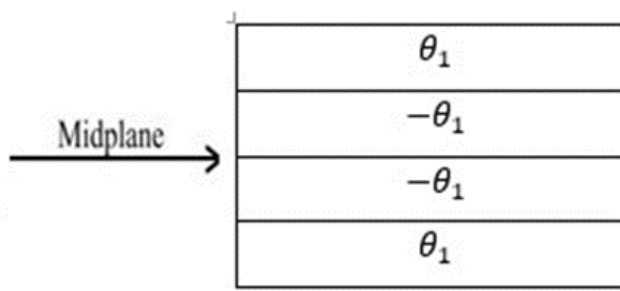


Figure 6.2 Stacking sequence of the four-layer flat panel

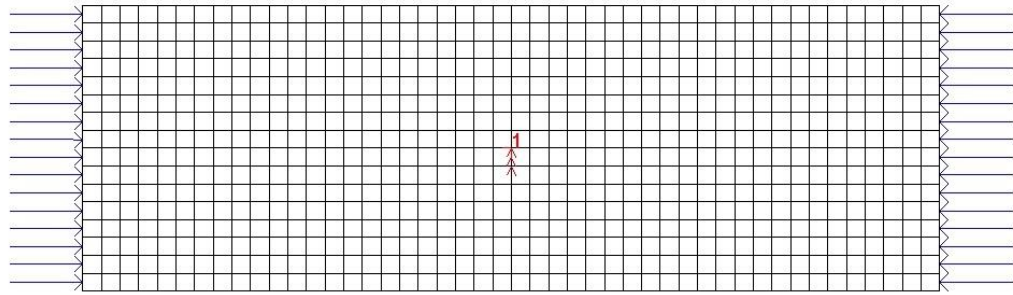


Figure 6.3 Boundary conditions and loading for the verification case

For the PSO of the reference fiber path, first a reference fiber path is created in Rhino environment. The reference fiber path is given in Figure 6.4. Control points of the NURBS curve are given in Table 6.4. Knot vector and weights are given below.

$$U=[0\ 0\ 0\ 0\ 0.25\ 0.5\ 0.75\ 1\ 1\ 1] \quad w=1.0$$

The reference fiber path is also created again in the MATLAB as shown in Figure 6.5 by importing the NURBS curve properties from the created step file from the Rhino model.

Table 6.4 Control points of the reference fiber path for the flat panel

Control points	x	0	515.48	1113.67	1519.77	1966.08	2549.32	3000
	y	500	791.23	841.07	535.29	272.80	282.77	500

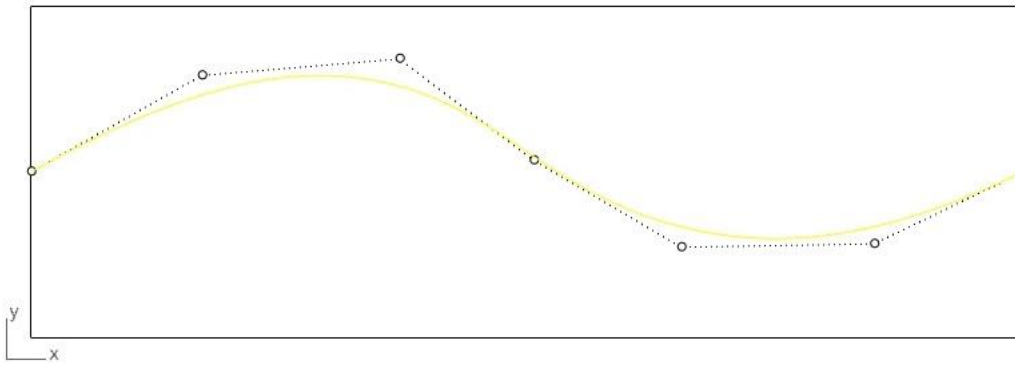


Figure 6.4 Rhino representation of the reference fiber path

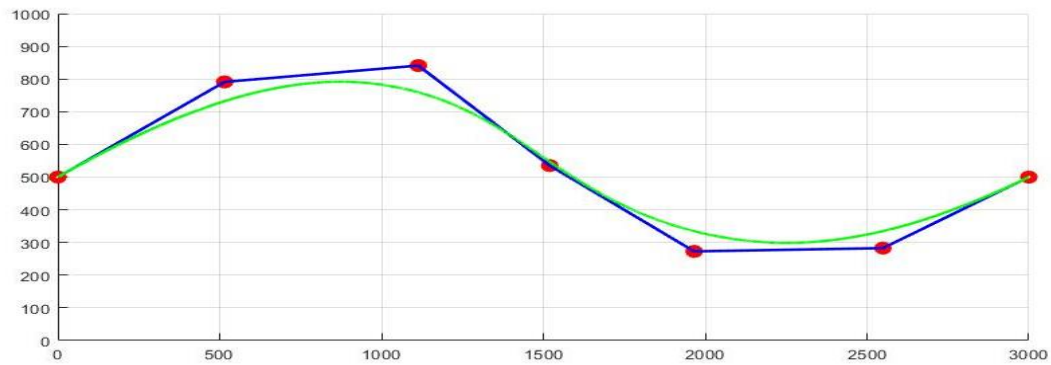


Figure 6.5 MATLAB representation of the reference fiber path

For the PSO, control points are the optimization variables and convergence tolerance is set as 10 mm. All optimization parameters are given in Table 6.3.

For the four-layer verification case, the optimized path is given in Figure 6.6 as the purple line and the initial reference path is presented in the same figure as the green line. Optimized reference fiber path is shown on the flat panel in Rhino in Figure 6.7 and control points given in Table 6.5. As it is expected, the optimized path converges to a straight line.

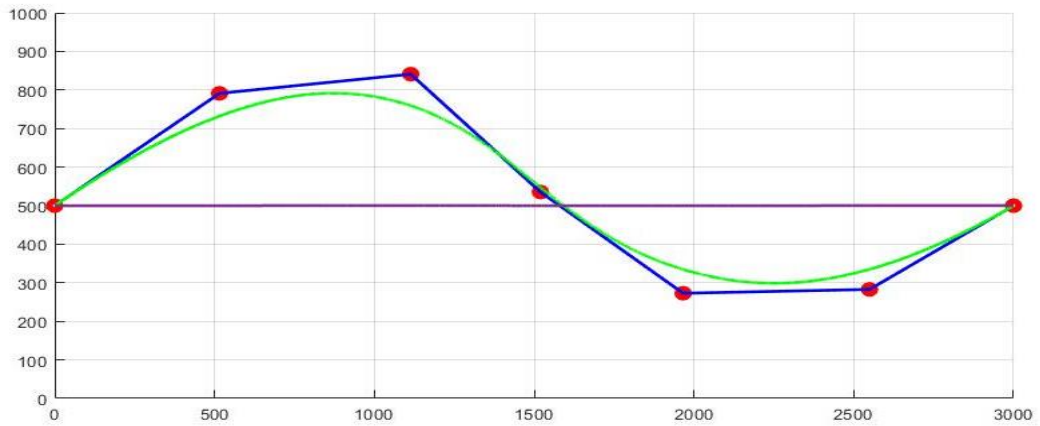


Figure 6.6 MATLAB representation of the reference fiber path (green) and the final optimized fiber path (purple)

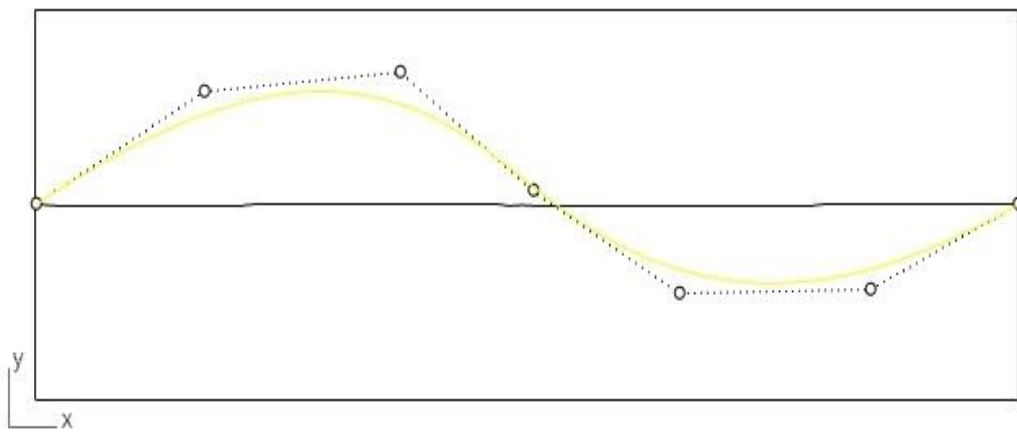


Figure 6.7 Rhino representation of the reference fiber path (yellow) and the final optimized fiber path (black)

Table 6.5 Control points of final optimized fiber path for the verification case

Control points	x	0	515.48	1113.67	1519.77	1966.08	2549.32	3000
	y	500	499.67	500.69	499.69	499.65	500.17	500

Before starting the optimization, a population with 25 particles are created by the algorithm. These particles consist of control point coordinates. One of these particles

has the control point information of initial reference path created with Rhino, other 24 is created randomly. The strain energy is reduced by 46.25 % compared to the strain energy of the best particle that is created in the first population. The strain energy of the flat panel with the reference fiber path of best particle of the initial population was 284.54 GJ and the strain energy of the flat panel with the optimized fiber path is 152.92 GJ. Figure 6.8 gives the variation of the strain energy with the iteration number for the four-layer flat panel of the verification case. The reason for why the optimization iterations continue after the optimum result is reached is the specified convergence criterion. The optimization algorithm stops after all the particles convergence within the tolerance limit given in Table 6.3.

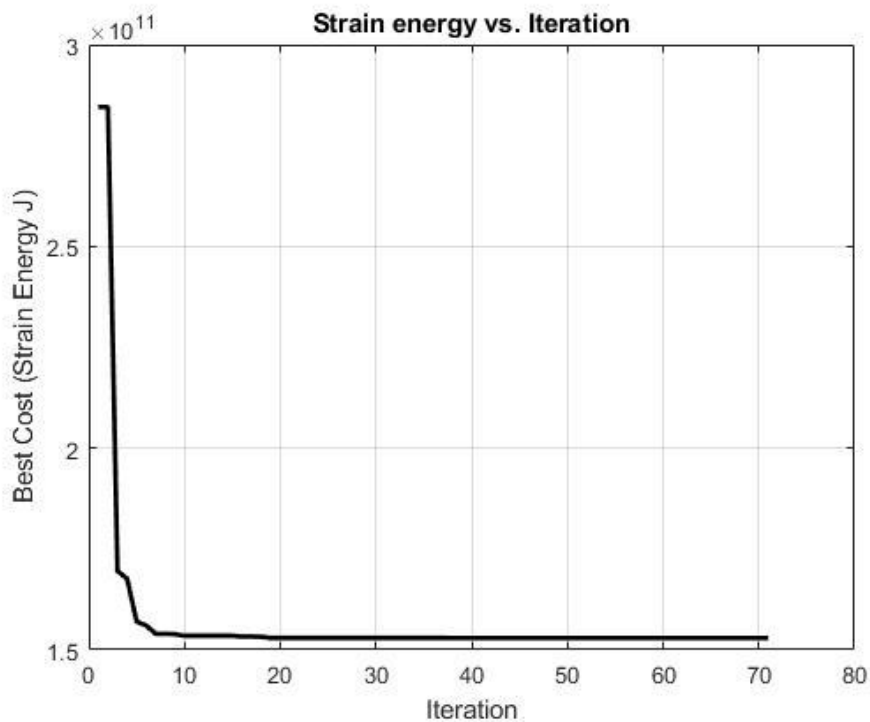


Figure 6.8 Variation of the strain energy with the iteration number for the four-layer flat panel of the verification case

6.1.2 Modelling and Buckling Analysis of an Isotropic Panel with MSC. Patran and MSC. Nastran

To verify the buckling analysis and buckling load factor calculation of MSC. Nastran, an isotropic flat panel is modelled in MSC. Patran and buckling analysis is done by MSC. Nastran. The verification problem is taken from MSC. Patran Reference Manual Part 6 [43]. The problem asks to find the critical buckling edge load of the rectangular panel (16x4) inches given in Figure 6.9.

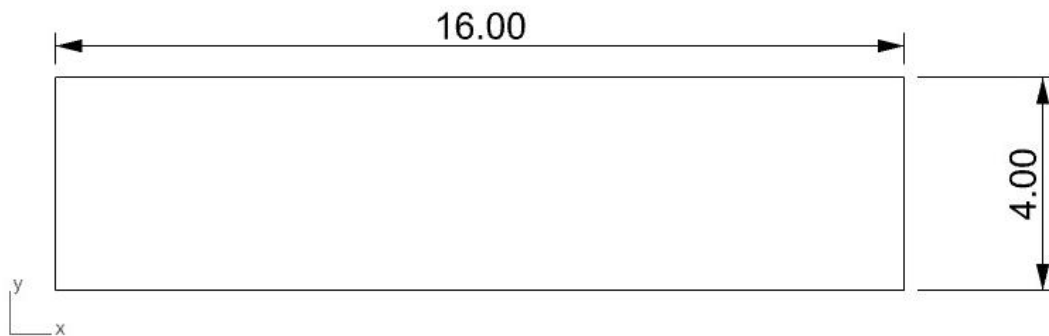


Figure 6.9 Flat panel dimensions for the buckling analysis of an isotropic flat panel. For simplicity, buckling analysis is done for a quarter of the panel. The boundary and load conditions are given in Figure 6.10. The panel is subject to biaxial load. For the quarter panel, at the left edge symmetry boundary conditions are imposed; displacement in the x-direction is zero ($u=0$), and rotations around the y-axis and z-axis are equal to zero ($R_y=R_z=0$). At the bottom edge, symmetry boundary conditions are also applied; displacement in the y-direction is zero ($v=0$), and rotations around the x-axis and z-axis are equal to zero ($R_x=R_z=0$). The displacement in the z-direction is taken as zero ($w=0$) along the right and top edges. Compressive edge pressures are modeled as distributed edge loads equal to 100 lb./inch. The panel material is an isotropic material, and the material properties are given in Table 6.6.

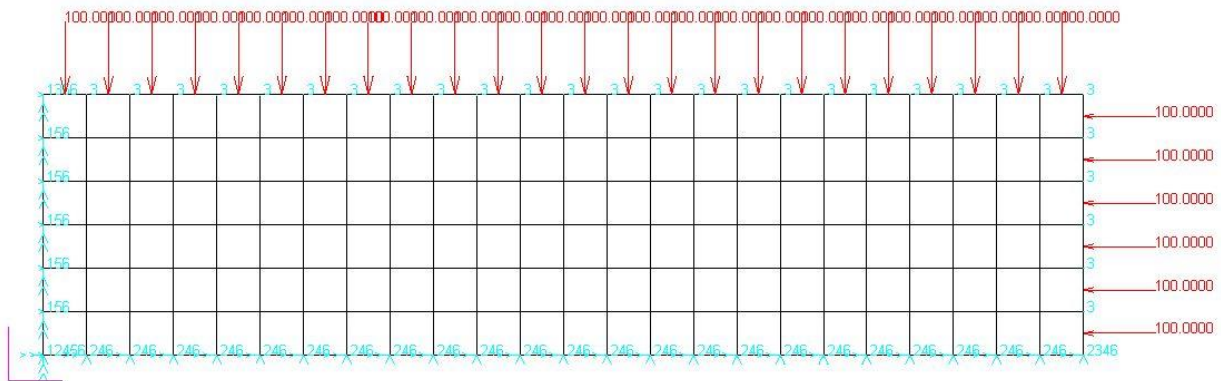


Figure 6.10 Quarter panel boundary conditions for the buckling analysis

Table 6.6 Material properties of the isotropic panel

E (Elastic Modulus)	10^7 Psi
ν (Poisson Ratio)	0.33
t(thickness)	0.1 inches

The buckling load factor is extracted from the MSC. Nastran output file. According to the analysis, the BLF turns out to be 6.133. Hence, the buckling load is equal to the applied load multiplied by the buckling load factor 6.133 which is equal to 613.3 lb/inch. Considering that the panel has a thickness of 0.1 inches, the theoretical calculations in the MSC. Patran Reference Manual Part 6 [43] yield that the panel's critical stress is 6133.13 Psi, which corresponds to a distributed edge load of 613.313 lb/inch [43]. The critical edge pressure calculated theoretically and determined by finite element analysis by MSC. Nastran are compared in Table 6.7.

Table 6.7 Comparison of the buckling stress calculated theoretically and by FEA in MSC. Nastran

Theory	6133.13 psi
MSC. Nastran	6133.25 psi

This example analysis shows that MSC. Nastran calculates the BLF very accurately.

6.2 Flat Panel Optimization

In this section, strain energy and failure index minimization of a cantilever flat panel with the dimensions of 3000mm x 1000mm (see Figure 6.1) under distributed bending load is studied. In the forthcoming subsections, different constraints are used for the analysis. The load condition is a distributed load in the in-plane bending direction, and the panel is clamped at the left edge of the panel, as seen in Figure 6.11. All rotations and translations are disabled on the left side of the panel. For the analyses, 736 elements (46x16) are used. The material properties of the composite material are given in Table 6.1. In the next subsections, 1 layered and 4 layered panels with a ply thickness of 0.183 mm are studied.

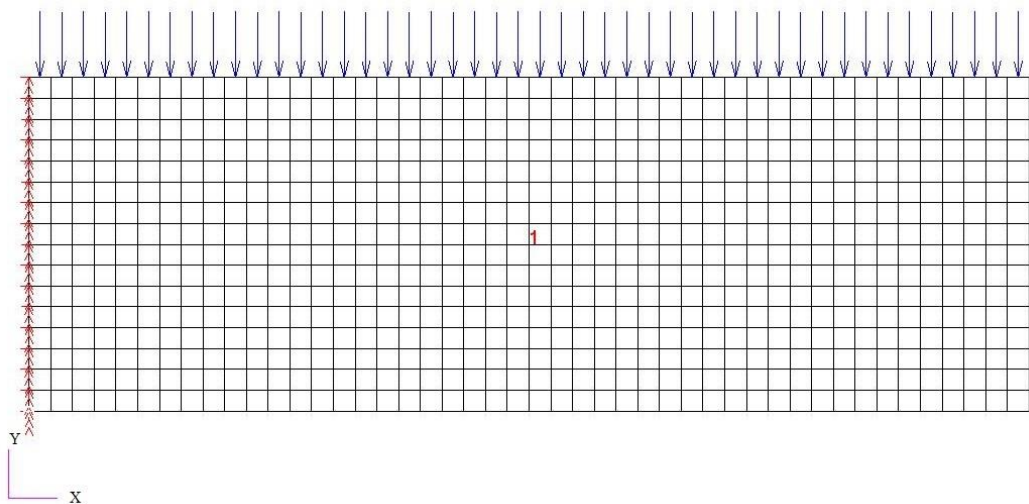


Figure 6.11 Loading and boundary conditions of the flat panel

For the flat panel cases, control points are the optimization variables and convergence tolerance are set as 10 mm. All optimization parameters are given in Table 6.3.

6.2.1 Strain Energy Minimization of the Flat Panel

Strain energy minimization of the flat panel is studied under the defined boundary and loading conditions. In the analysis, the NURBS fiber path is constrained by the specified minimum curvature. The minimum curvature of the path is defined as 50 mm. This value is defined as a generic value for showing the implementation of the curvature constraint is successful. Two distinct analyses with one layered and four-layered panels are performed.

For the PSO, first a reference fiber path is created in Rhino environment. Rhino representation of the reference fiber path is given in Figure 6.12. NURBS path is then created again in MATLAB as seen in Figure 6.13 by importing the NURBS curve properties from the created step file from the Rhino model.

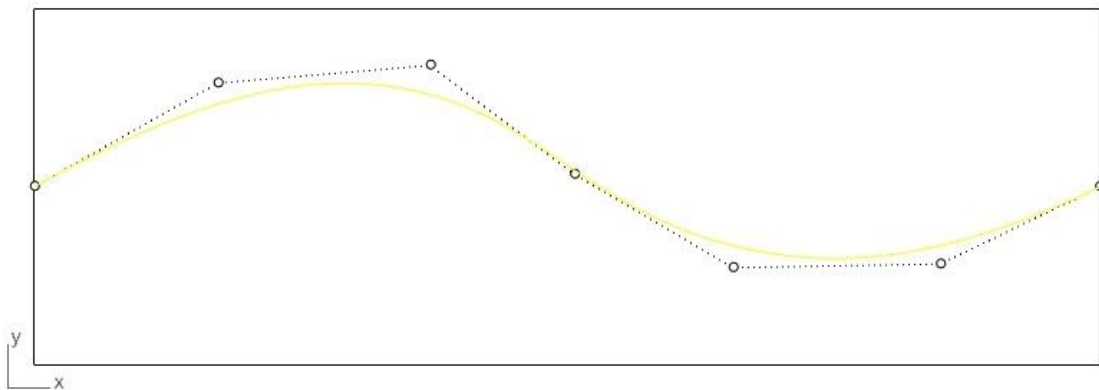


Figure 6.12 Reference NURBS path for flat panel created by Rhino

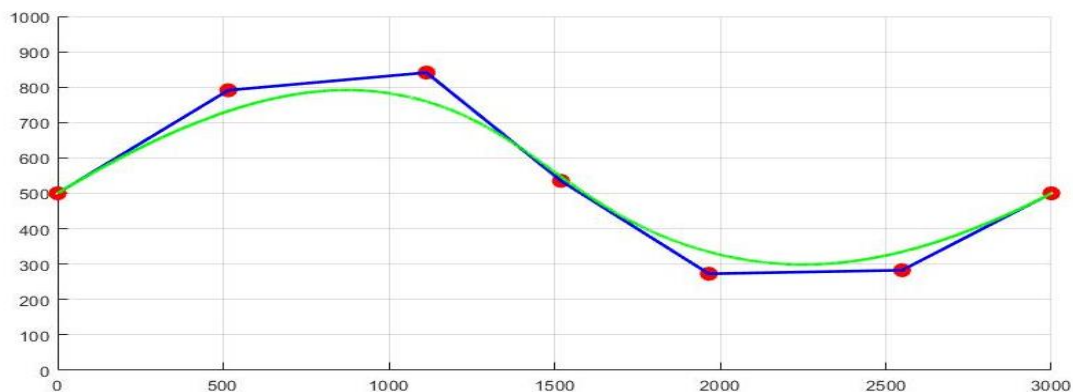


Figure 6.13 Flat panel reference path created by MATLAB

The NURBS reference path is defined by the knot vector and the weights given below, and control points are given in Table 6.8.

$$U=[0\ 0\ 0\ 0\ 0.25\ 0.5\ 0.75\ 1\ 1\ 1] \quad w=1.0$$

Table 6.8 Control points of the reference fiber path for the flat panel

Control points	x	0	515.48	1113.67	1519.77	1966.08	2549.32	3000
	y	500	791.23	841.07	535.29	272.80	282.77	500

6.2.1.1 One Layer Flat Panel Strain Energy Minimization

The flat panel strain energy minimization for the one-layer design is studied. The loading magnitude is 1kN/m and the panel consist of 1 layer with 0.183 mm ply. In Figure 6.14, the optimized path is shown as the purple line, and the initial reference path is shown as the green line. In Figure 6.15, the Rhino representation of the optimized path on the flat panel is shown. The optimized NURBS path’s control points are given in Table 6.10. The fibers are tried to align in the loading direction at the right of the plate. Because maximum strain is expected to see at the free edge.

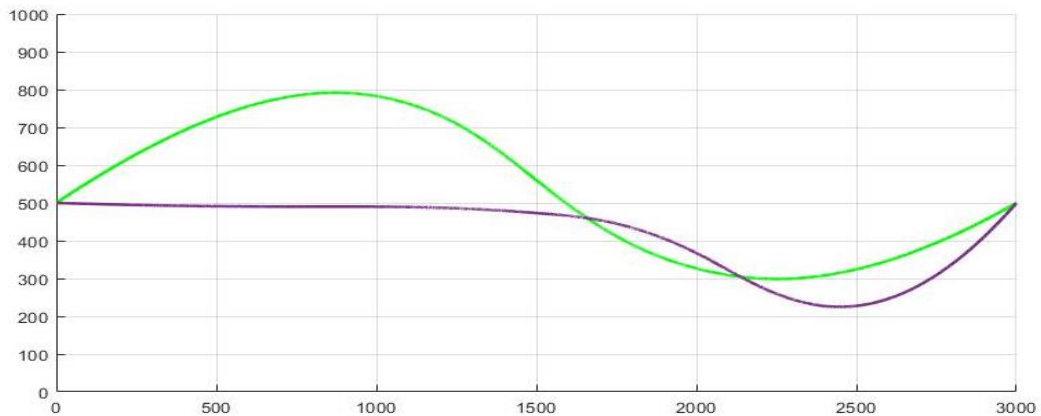


Figure 6.14 Strain energy optimized fiber path for the one-layer flat panel; Matlab representation

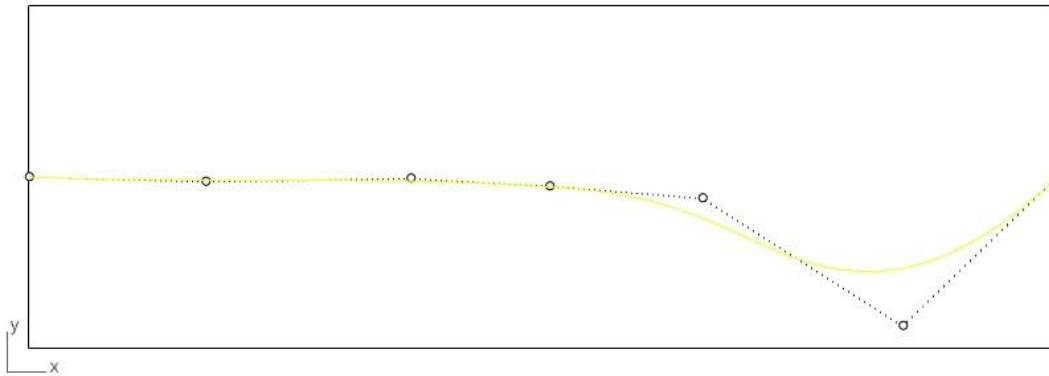


Figure 6.15 Strain energy optimized fiber path for the one-layer flat panel; Rhino representation

Table 6.9 Control points of the strain energy optimized fiber path for the one-layer flat panel

Control points	x	0	515.48	1113.67	1519.77	1966.08	2549.32	3000
	y	500	486.82	495.77	473.71	438.06	65.52	500

Before starting the optimization, a population with 25 particles are created by the algorithm as it is mentioned in section 6.1.1. The strain energy is reduced by 30 % compared to the strain energy of the best particle that is created in the first population. The strain energy with the best reference fiber path of the first population was 1.13 kJ, and for the panel with the optimized fiber path, strain energy is 0.79 kJ. Strain energy versus the iteration number plot during the optimization is given in Figure 6.16. It should be noted that the resulting fiber path is very similar to the fiber orientation distribution obtained by the discrete analysis done by the Setoodeh et al.[42]. Figure 6.17 shows the discrete fiber angle distribution obtained by cellular automata in the work of Setoodeh et al.[42]. However, since the present analysis is a continuous analysis and manufacturing constraint is used during the optimization, the optimized fiber path is smoother than the path found by the discrete analysis result in the study of Setoodeh et al. [42] in Figure 6.17. In PSO, again the iteration continues after the optimum result is reached until the specified convergence

criterion is satisfied. The algorithm stops after all particles converge within the tolerance limit given in Table 6.3.

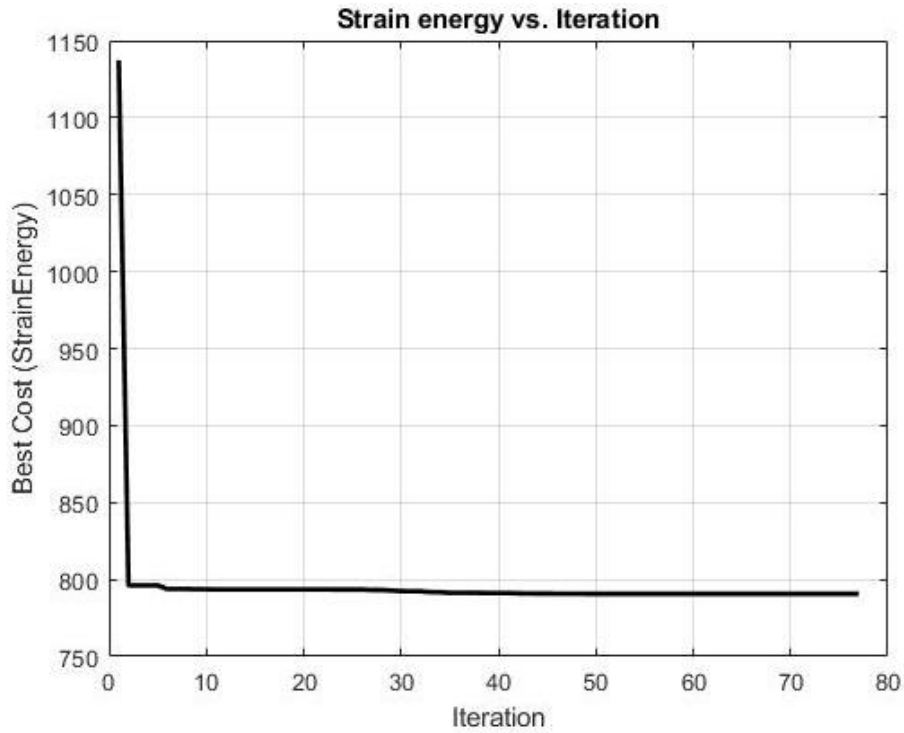


Figure 6.16 Strain energy versus the iteration number for the one-layer flat panel strain energy minimization problem

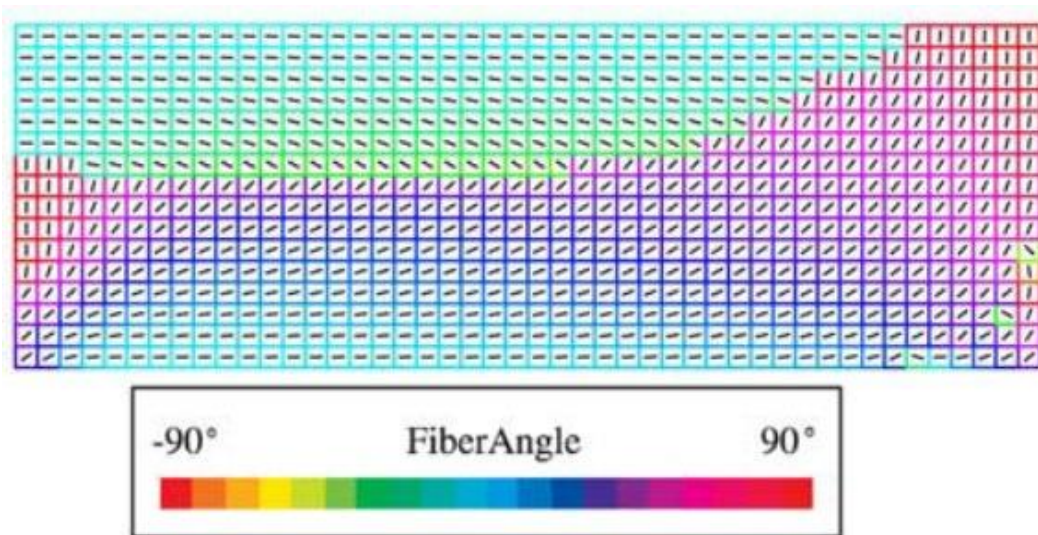


Figure 6.17 Setodeeh et al.'s work for fiber angle optimization with cellular automata [42]

6.2.1.2 Four Layer Flat Panel Strain Energy Minimization

In this case study, strain energy minimization of the flat panel is studied for a panel with 4-layers with a ply thickness of 0.183 mm. The loading magnitude is again 1kN/m. The stacking sequence of the panel is same as the one shown previously in Figure 6.2.

For the 4-layered panel, the initial reference fiber path is defined as same as shown in Figure 6.12 and Figure 6.13. For the four layered flat panel, the optimized fiber path is shown with the purple line, and the initial reference path is shown with the green line in Figure 6.18. Optimized opposite signed fiber paths are shown on the flat panel in Rhino in Figure 6.19. Control points of the optimized fiber path are given in Table 6.11. The fiber angles are aligned as like Figure 6.18 and Figure 6.19 because this case is midplane symmetric case. When the paths put on top of the other with respect to stacking sequence it is seen that fibers are tried to align in the loading direction.

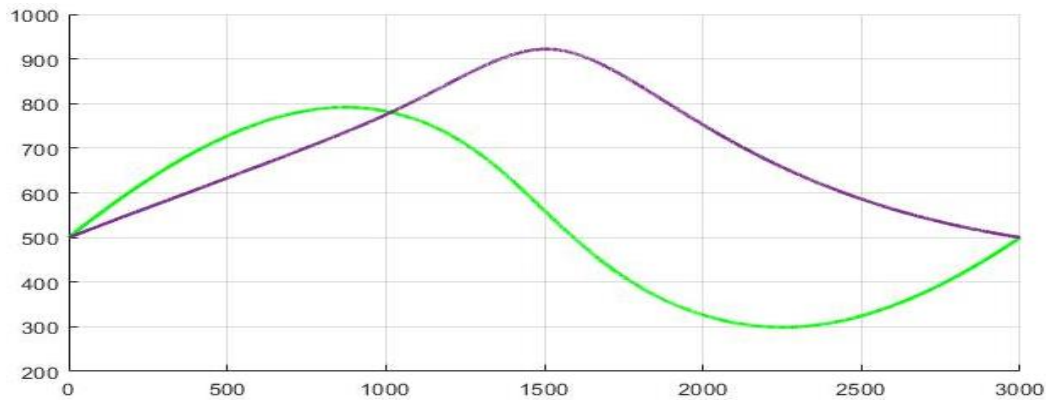


Figure 6.18 Strain energy optimized fiber path for the four-layer flat panel

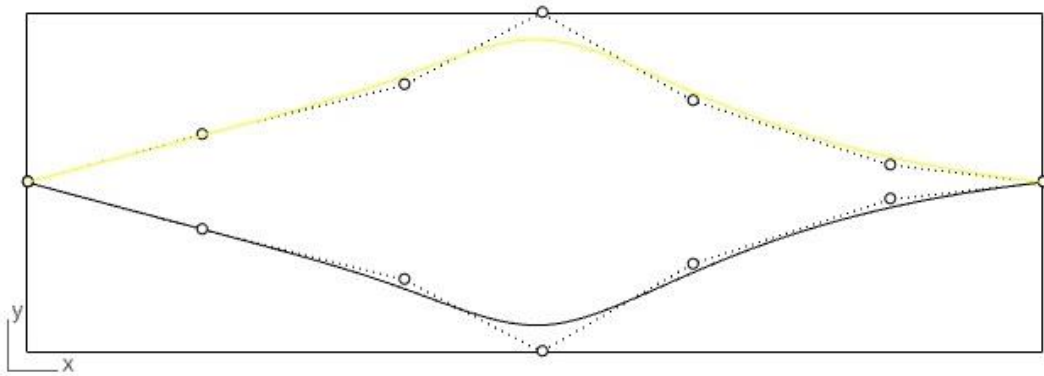


Figure 6.19 Strain energy optimized fiber path for the four-layer flat panel; Rhino representation

Table 6.10 Control points of the strain energy optimized fiber path for the four-layer flat panel

Control points	x	0	515.48	1113.67	1519.77	1966.08	2549.32	3000
	y	500	638.94	786.72	1000	741.29	550.83	500

In this case, the strain energy is reduced by 11.76 % compared to the flat panel with best reference fiber path in the initial population. The strain energy with the initial population's best reference fiber path was 170 J, and for the four-layered flat panel with the optimized fiber paths strain energy is 150 J. Variation of the strain energy with the iteration number is presented in Figure 6.20.

It should be noted that for the four layered flat panel, since the loading condition is the same as the one-layer flat panel and the number of layers is more and there are layers with symmetric fiber angles, percent decrease of the strain energy is not very high compared to the one-layer flat plate case.

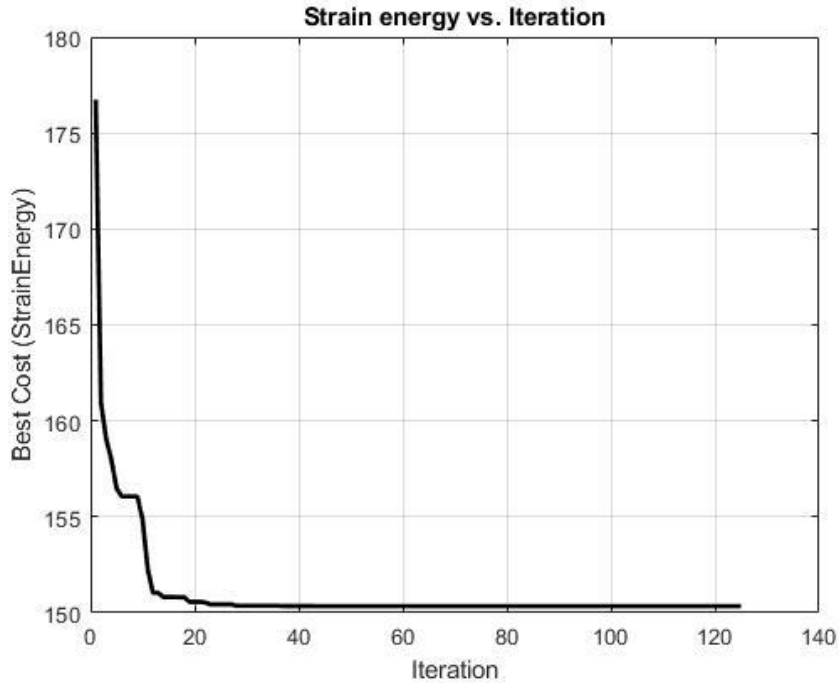


Figure 6.20 Strain energy versus the iteration number for the four-layer flat panel strain energy minimization problem

This case is also examined with the reference fiber path definition method of Gürdal and Olmedo’s work [3]. Design variables are defined as $T_0=0^\circ$, $T_1=45^\circ$ and $\phi = 0^\circ$ initially. In this method only T_0 and T_1 are used as design variables and ϕ is taken as constant ($\phi = 0^\circ$) . In this method, fiber angle is zero degree ($T_0=0^\circ$) at the center of the plate and changes linearly to $T_1=45^\circ$ at the right edge with antisymmetric path definition towards the left edge of the flat panel. The strain energy of the flat panel with these variables ($T_0=0^\circ$, $T_1=45^\circ$) is 220.71 J. After the initial population is randomly created in PSO, the strain energy of the panel with the best fiber path (the one with minimum strain energy) is 152.5 J. The strain energy of the flat panel with the optimum fiber path is determined as 149.09 J. Figure 6.21 shows the variation of the strain energy values with to the iteration number. For the best fiber path, design variables are determined as; $T_0=15.83^\circ$, $T_1=16.94^\circ$. The resultant positive and negative angled fiber paths with these optimized variables are shown in Figure 6.22.

When this result is compared with the optimum strain energy determined with the use of NURBS fiber path method that is used in this thesis, it is seen that the results are very close. There is 0.06% difference between the two optimized results; 150 J for the NURBS fiber path method and 152.5 J for the fiber defined by $T_0 - T_1$ definition. NURBS fiber path method gives slightly lower strain energy since more parameters (control points) exist in the path definition resulting in more design freedom. The $T_0 - T_1$ method described in Gürdal and Olmedo's work [3] is used in different studies [4], [7], [10], [15], [44] for different geometries under different loading and boundary conditions. By comparing the strain energy values and fiber path shapes it can be said that presented method gives results as good as the method in Reference 3. It should be noted that in the $T_0 - T_1$ method, fiber path definition is anti-symmetric with respect to the center of the panel as Figure 6.22 clearly shows this. Hence, $T_0 - T_1$ reference fiber method is restrictive; NURBS fiber path definition presents alternative paths since the control points can be selected anywhere in the panel. In the defined strain energy problem, one cannot see a definite advantage of the NURBS fiber path method over the $T_0 - T_1$ method, most probably due to the load and boundary conditions imposed; cantilevered plate under in-plane bending load. It is deemed that the NURBS fiber path definition makes a difference in problems involving complex loading and boundary conditions; because in such problems load paths may change sharply in the panel and this necessitates similar change in the fiber path which is not possible to generate via the $T_0 - T_1$ method which is based on linear change of fiber path along one of the axis of the panel.

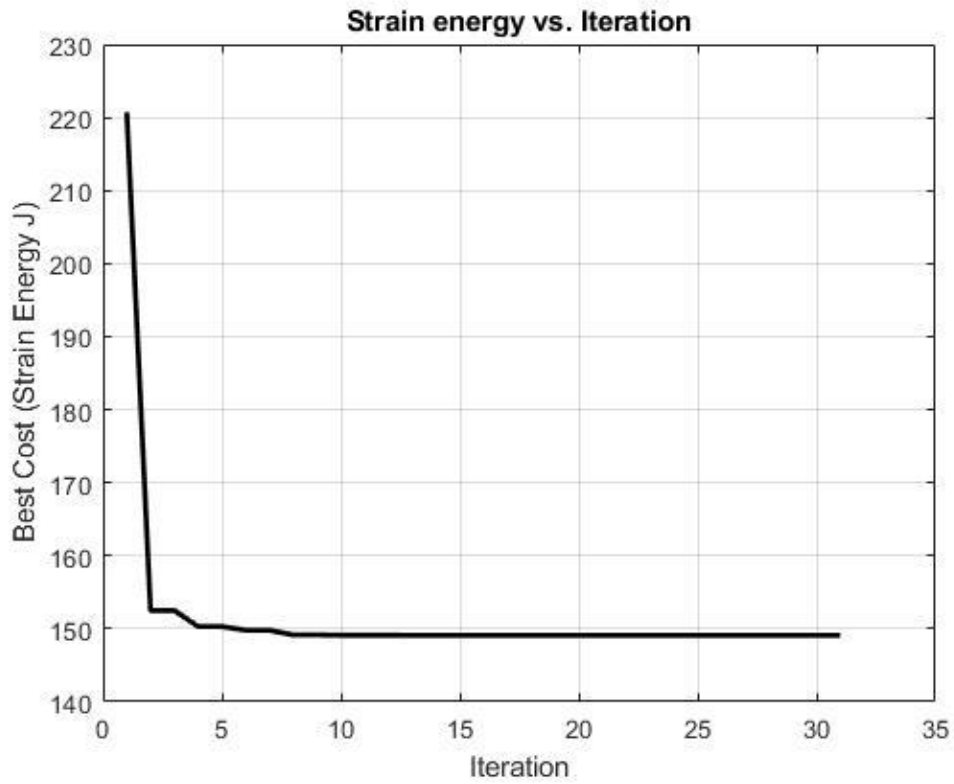


Figure 6.21 Strain energy versus the iteration number for the four-layer flat panel strain energy minimization problem solved with (T_0, T_1) fiber path definition method

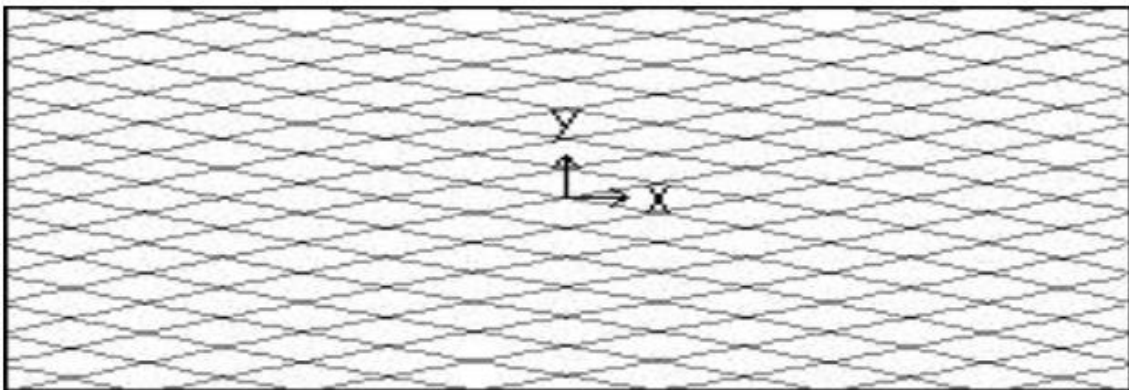


Figure 6.22 Strain energy optimized fiber path for the four-layer flat panel; solved with (T_0, T_1) fiber path definition method

6.2.1.3 Four Layered Flat Panel Strain Energy Minimization Constrained with Failure Index (FI)

In this section, strain energy minimization of a 4-layered flat panel under failure index constraint is studied. Tsai-Wu failure criterion is used as the FI constraint. The details of the Tsai-Wu criterion and failure index calculation is given in the section 5.2.3.2. The ply thickness is 0.183 mm as in previous cases. For this analysis, the only constraint is the FI, and the geometry constraint is not applied to the NURBS fiber path. During the analysis, FI values of all elements are calculated, however from the output of the finite element analysis only the maximum FI is extracted. If the maximum FI is greater than 1, then the algorithm automatically penalizes the objective function and makes the solution infeasible.

Again, the initial reference fiber path is same as defined in Figure 6.12 and Figure 6.13. The boundary conditions are same as in previous case studies; however, in this case the loading is changed to 2 kN/m. The optimized fiber path is presented with the purple line and the initial reference fiber path is shown with the green line in Figure 6.23. Optimized opposite signed fiber paths are represented on the flat panel in Rhino in Figure 6.24. The control points of the optimized path are given in Table 6.12.

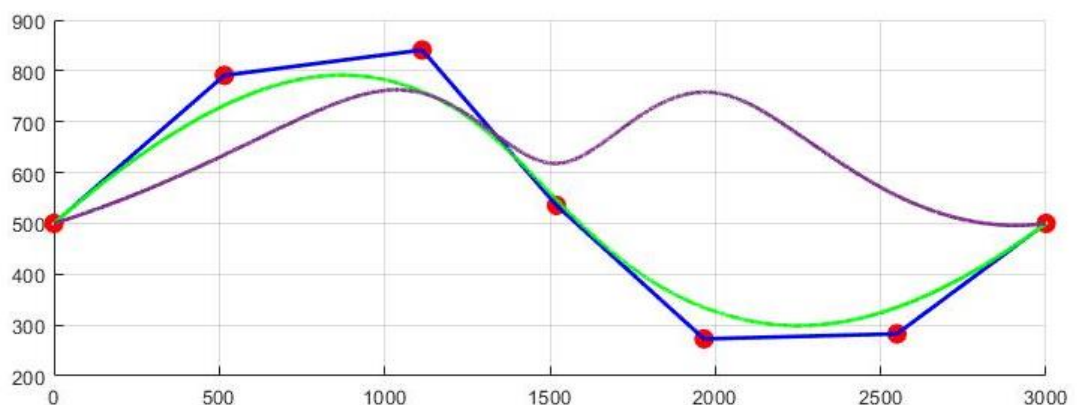


Figure 6.23 Strain energy optimized fiber path for the four-layer flat panel subject to FI constraint

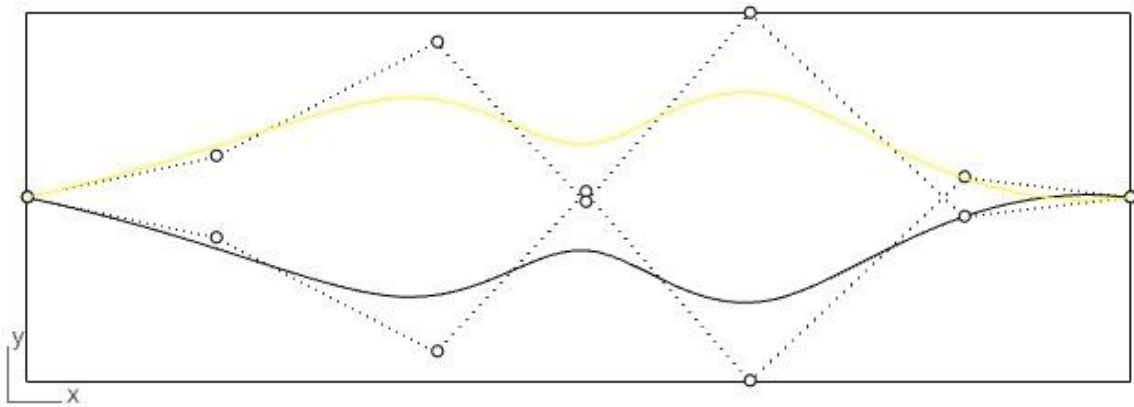


Figure 6.24 Rhino representation of strain energy optimized fiber path (yellow) and its opposite signed path (black) for the four-layer flat panel subject to FI constraint

Table 6.11 Control points of the strain energy optimized fiber path for the four-layer flat panel

Control points	x	0	515.48	1113.67	1519.77	1966.08	2549.32	3000
	y	500	609.916	920.63	486.18	1000	446.63	500

In this optimization, the magnitude of the external load is tuned for the flat panel with the initial reference fiber path such that at least one element has a failure index greater than one ($FI > 1$). The maximum FI in the initial population 1.72 and it is indicated in the FI plot in Figure 6.25. Maximum FI occurs in 1st ply in element 1 which is at the bottom left corner of the geometry in Figure 6.25. By making the maximum FI greater than 1 in the initial configuration, it aimed to see the algorithm's ability to penalize the infeasible design in terms of FI. After the optimization process, maximum FI reaches a value of $FI = 0.9756$. Figure 6.26 gives the FI plot of the optimized configuration. The maximum FI after the optimization occurs in the 1st ply in the bottom left corner element in Figure 6.24. It is guaranteed that all elements are in the safe zone, and their failure indices are below the critical value, which is "1". In this case, strain energy is reduced by 22.4% compared to the best reference fiber path of the initial population. The strain energy of the flat panel with the best

particle's fiber path of the initial population was 0.7941 kJ, and the flat panel with the optimized fiber path has a strain energy of 0.616 kJ. Variation of the strain energy with the iteration number is presented in Figure 6.27.



Figure 6.25 FI plot of the flat panel with the initial reference path under the given load and boundary conditions



Figure 6.26 FI plot of the flat panel with the optimized fiber path under the given load and boundary conditions

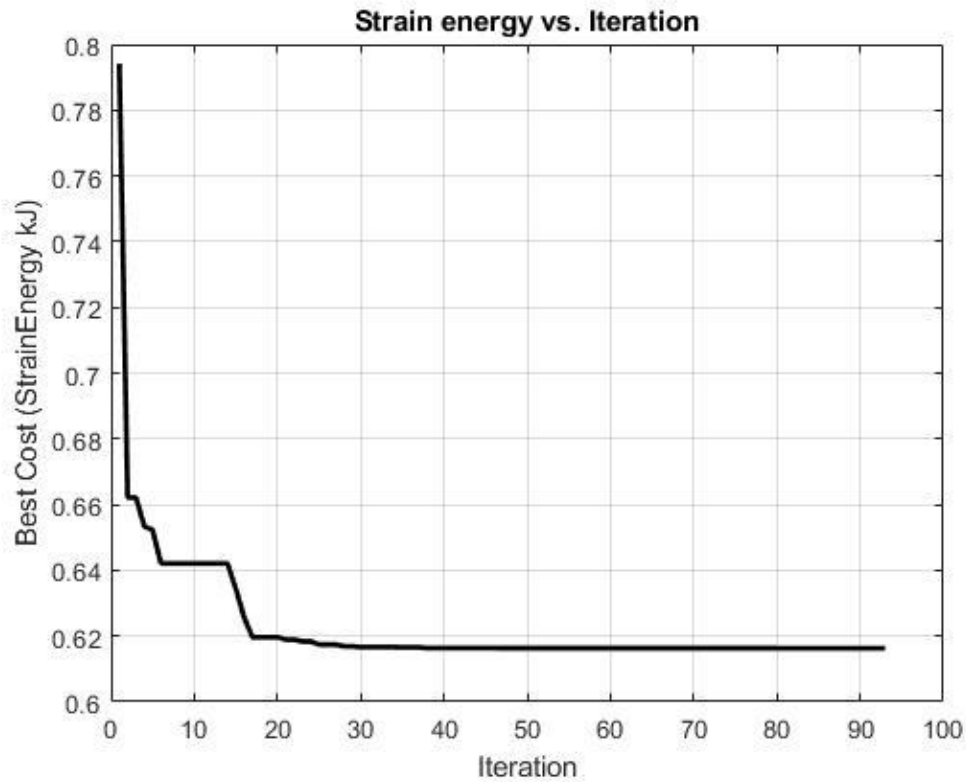


Figure 6.27 Strain energy versus the iteration number for the four-layer flat panel strain energy minimization problem with FI constraint

6.2.2 Failure Index (FI) Minimization of the Flat Panel

In this case study, failure index minimization of the flat panel is studied. Finite element solution performed by MSC. Nastran gives the FI of all plies as output along with the maximum failure index in the finite element model. FI minimization is achieved by optimizing the reference fiber path. Besides the objective function, FI is also used as constraint to guarantee that FI is under 1. If the maximum FI is greater than 1, algorithm penalizes the objective function value and makes that solution infeasible.

In the failure index minimization problem, the same flat panel with 4-layers is used as in section 6.2.1. The boundary conditions are the same as in section 6.2.1. However, the magnitude of the distributed load is changed to 2 kN/m. The initial

fiber path is the same as the one used in section 6.2.1, and it is given in Figure 6.12 and Figure 6.13.

The optimized fiber path for the failure index minimization problem of the 4-layer flat panel together with the initial reference fiber path is given in Figure 6.25. The purple line is the optimized fiber path, and the initial reference fiber path is presented as the green line in Figure 6.28. Figure 6.29 shows the optimized opposite signed fiber paths represented on the flat panel in Rhino. The control points of the optimized fiber path are given in Table 6.13.

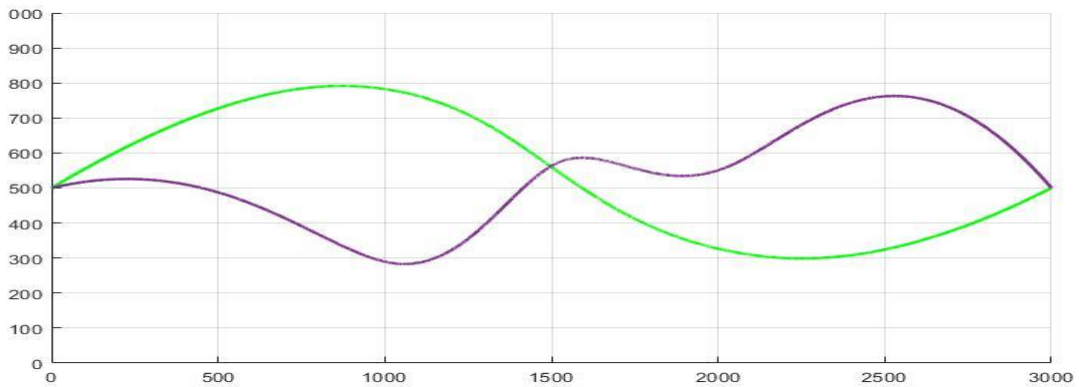


Figure 6.28 Failure index minimized fiber path for the four-layer flat panel; Matlab representation

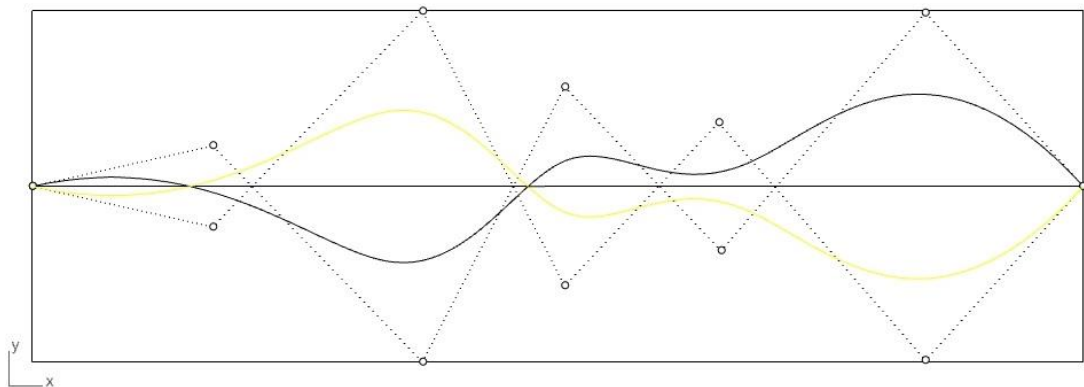


Figure 6.29 Failure index minimized fiber path for the four-layer flat panel; Rhino representation

Table 6.12 Control points of failure index minimized fiber path for the four-layer flat panel

Control points	x	0	515.48	1113.67	1519.77	1966.08	2549.32	3000
	y	500	615.43	0	783.47	316.75	995.00	500

In this case study, in the initial population the maximum failure index is 1.72. After the optimization process, the maximum FI reaches a value of FI=0.9517. It is guaranteed that all elements are in the safe zone, and their failure indices are under the critical value, which is “1”. In this case, there is a 44.6% reduction in the maximum FI value in the finite element model. Failure index variation with the iteration number for the four-layer flat panel is given in Figure 6.30.

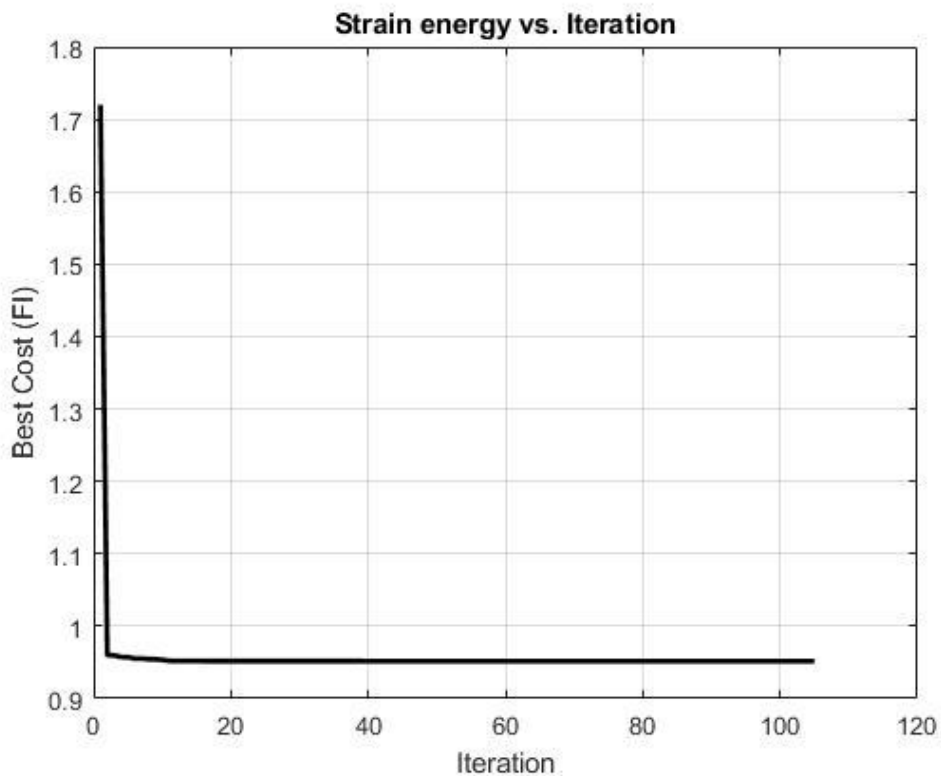


Figure 6.30 Strain energy versus the iteration number for the four-layer flat panel

6.3 Curved Panel Optimization

In this section, Buckling Load Factor (BLF) maximization and strain energy minimization of a curved panel with the dimensions given in Figure 6.31 are studied. The panel is a 4-layered panel with a ply thickness of 0.183 mm, and the stacking sequence is same as shown in Figure 6.2. Load and boundary conditions of the buckling load factor maximization problem and the strain energy minimization problem are different. For each case, the load and boundary conditions are described in the relevant sections. For the finite element analysis, 736 elements (46x16) are used. The material properties of the composite ply of the curved panel are given in Table 6.1.

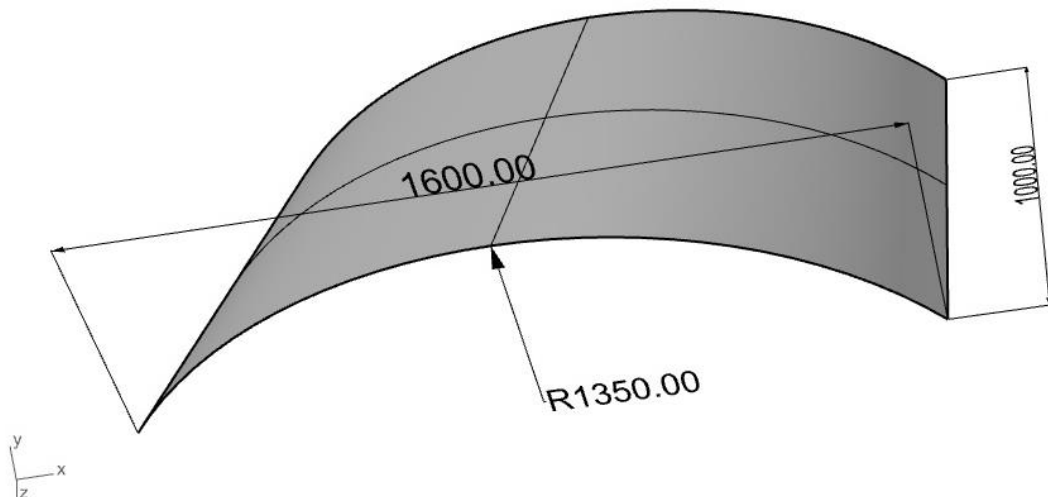


Figure 6.31 Curved panel dimensions (mm)

Before the optimization case studies, as in flat panel cases, a reference fiber path is created by using Rhino. The reference fiber path generated in Rhino is presented in Figure 6.32. The spline is created by projecting the 2D spline given in Figure 6.12 to the curved panel given in Figure 6.31.

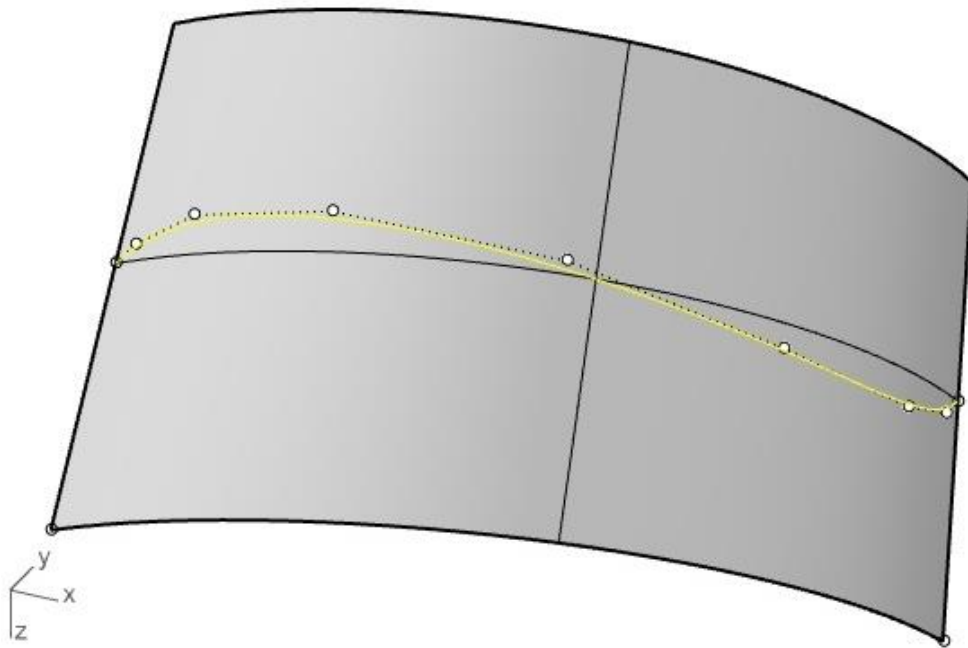


Figure 6.32 Reference NURBS path for the curved panel created by Rhino

The reference NURBS path has the control points given in Table 6.14. Knot vector and weights of the reference NURBS path are given below.

$$U=[0\ 0\ 0\ 0\ 0.0780\ 0.202\ 0.437\ 0.765\ 0.890\ 1\ 1\ 1\ 1]$$

$$w=1.0$$

Table 6.13 Control points of the reference fiber path for the curved panel

Control Points		
x	y	z
-800.00	0.00	500.00
-774.86	25.31	468.01
-689.84	100.37	424.30
-466.24	231.25	427.59
-60.479	330.94	487.75
363.89	274.90	562.94
659.88	122.99	578.87
764.40	36.07	544.62
800.00	0.00	500.00

For the curved panel cases, control points are also taken as the optimization variables and convergence tolerance is set as 10 mm as the flat panel case. All optimization parameters are given in Table 6.3.

6.3.1 Buckling Load Factor (BLF) Maximization of the Curved Panel

The curved panel BLF maximization is done for the 4-layered composite laminate. Stacking sequence of the 4-layered composite curved panel is given in Figure 6.2. The load that is applied is a distributed load of 3.5 N/m as shown in Figure 6.33. The curved panel is clamped from the left side such that all rotations and translations are disabled on the left side of the panel.

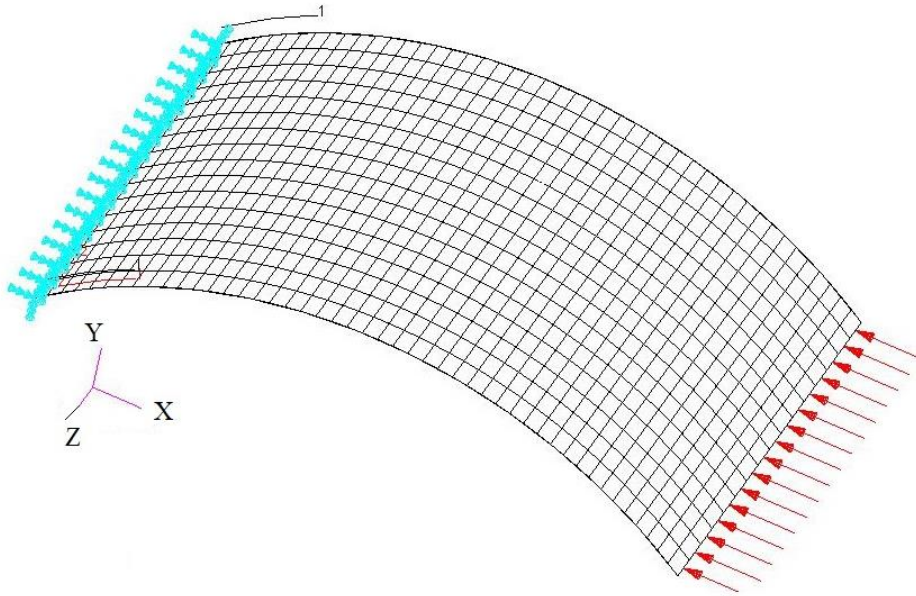


Figure 6.33 MSC. Patran model of the curved panel for the BLF maximization case study

The optimized fiber path for the configuration with the maximum BLF is given in Figure 6.34 as the yellow line, and the initial reference fiber path is presented in the figure as the black line. Control points of the optimized fiber path are given in Table 6.14.

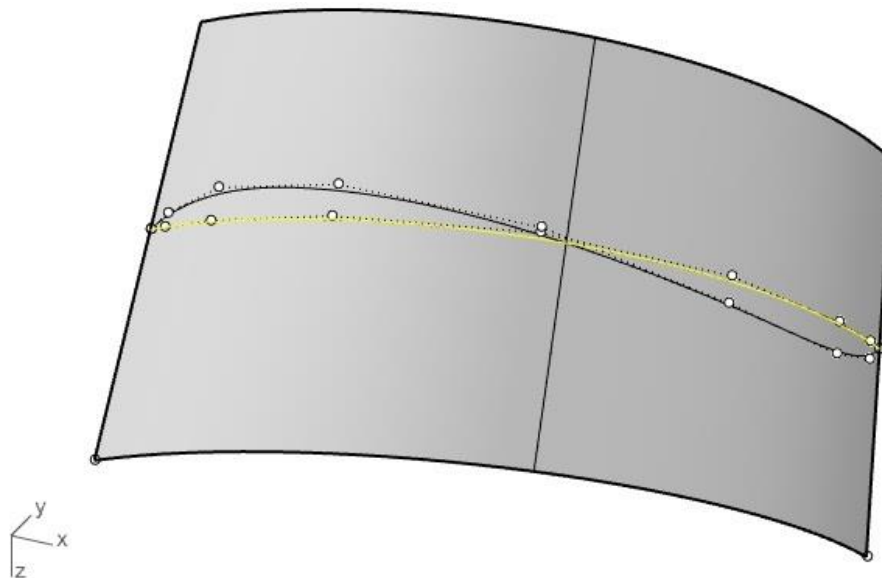


Figure 6.34 BLF optimized fiber path for the four-layer curved panel

Table 6.14 Control points of the BLF optimized fiber path for the four-layer curved panel

Control Points		
x	y	z
-800.00	0.00	500.00
-774.86	25.31	499.86
-689.84	100.37	500.25
-466.24	231.25	499.73
-60.479	330.94	500.38
363.89	274.90	499.37
659.88	122.99	501.55
764.40	36.07	497.96
800.00	0.00	500.00

In the optimized configuration, the BLF increased by 20.93% compared to the BLF of the curved panel with the initial reference fiber path. The maximum BLF among the the initially created population's reference paths is 0.9236, and with the optimized path, BLF is 1.1174. Variation of the BLF with the iteration number is given in Figure 6.35. In the optimized configuration, variation of the fiber angle of the continuous path is between 1.59° and -1.01° . The results show that fibers are aligned along the loading direction. This fiber path is expected because fibers are most powerful in the fibers' longitudinal direction. The first buckling mode shape of the curved panel with the initial reference fiber path is given in Figure 6.36. In Figure 6.37 gives the buckling mode shape of the curved panel with the optimized fiber path. It is noted that since the optimum fiber path aligns itself with the direction of

the loading, first buckling mode shape shows a symmetric deformation pattern with respect to the longer edge of the curved panel.

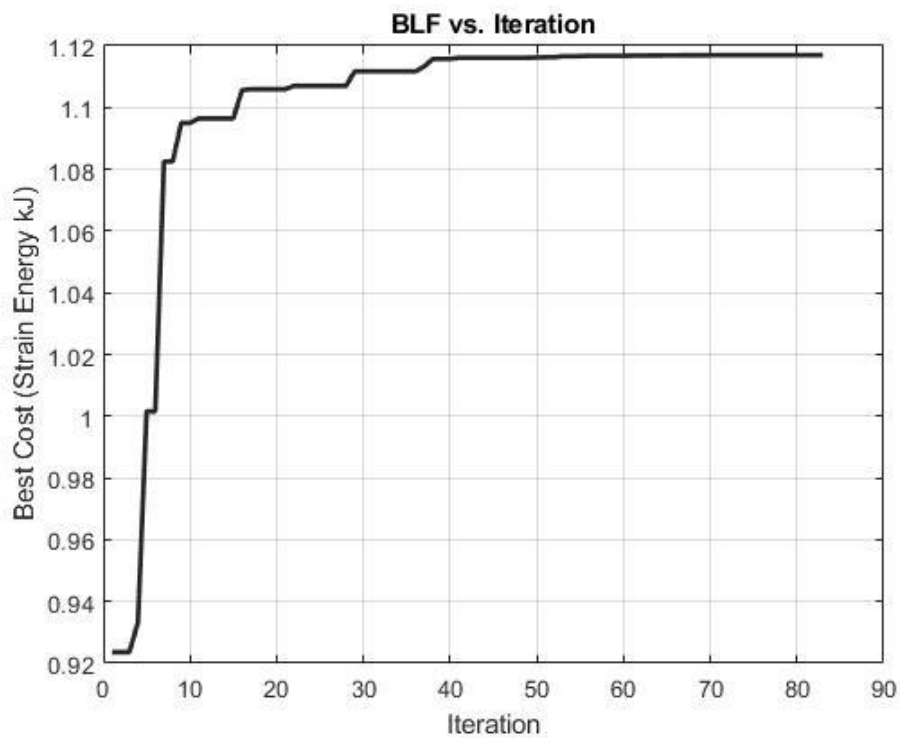


Figure 6.35 Variation of the BLF with the iteration number for the BLF maximization of the curved panel

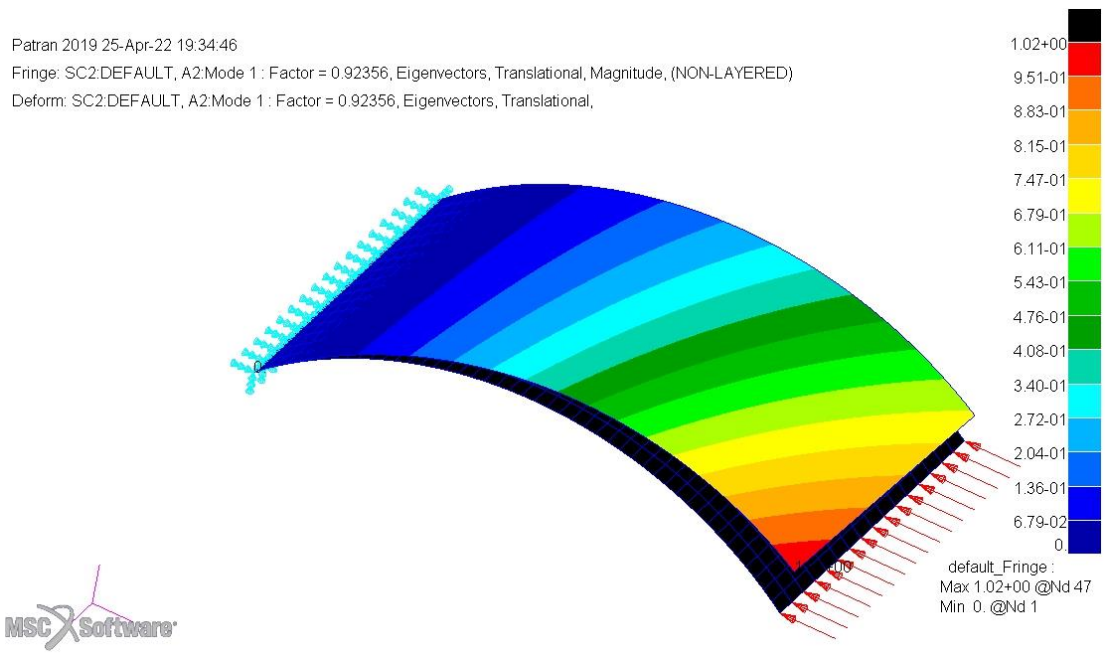


Figure 6.36 First buckling mode shape of the curved panel with the initial reference fiber path

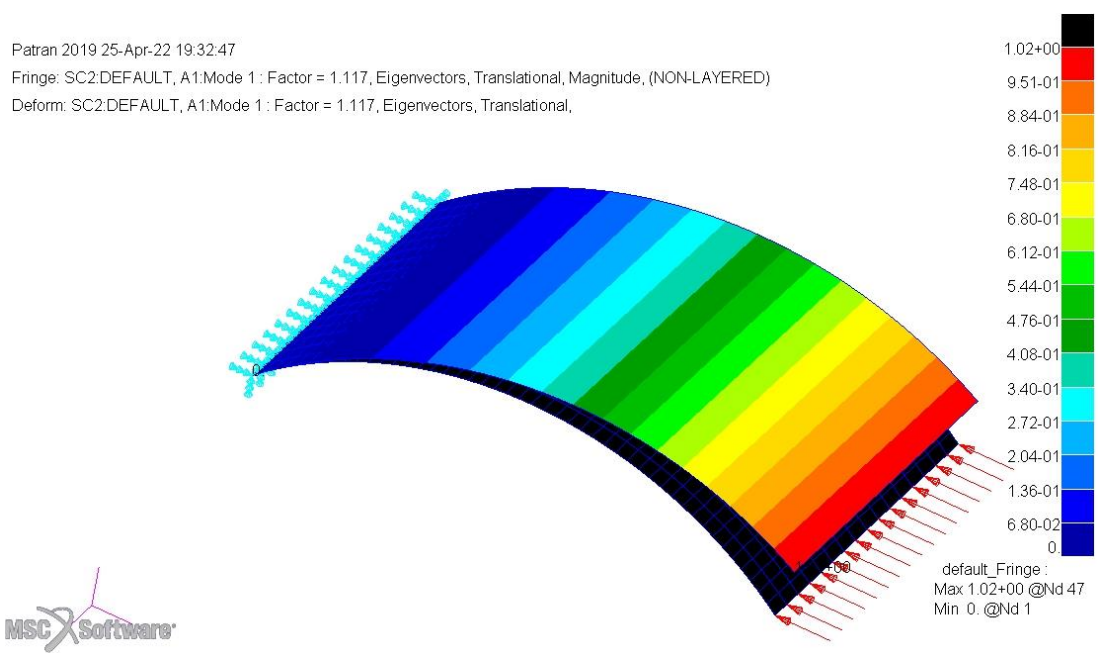


Figure 6.37 First buckling mode shape of the curved panel with the optimized fiber path

Another curved panel BLF maximization is done for the 4-layered composite laminate with different boundary conditions. Stacking sequence of the 4-layered

composite curved panel is given in Figure 6.2. For defining load and boundary conditions cylindrical coordinate frame is used. The load that is applied is a distributed load of 1 kN/m as shown in Figure 6.38. The curved panel has following boundary conditions. On the right side all translations are disabled ($u_R = u_T = u_Z = 0$) and rotations are disabled ($R_R = R_T = R_Z = 0$). On the curved sides of the panel only the T and Z translation is disabled ($u_T = u_Z = 0$). All other translations and rotations are set free ($u_R = R_R = R_T = R_Z \neq 0$). On the left side from where the load is applied, only the T and Z translation is disabled ($u_T = u_Z = 0$) and rotation around R axis is disabled ($R_R = 0$). All other translations and rotations are set free ($u_R = R_T = R_Z \neq 0$).

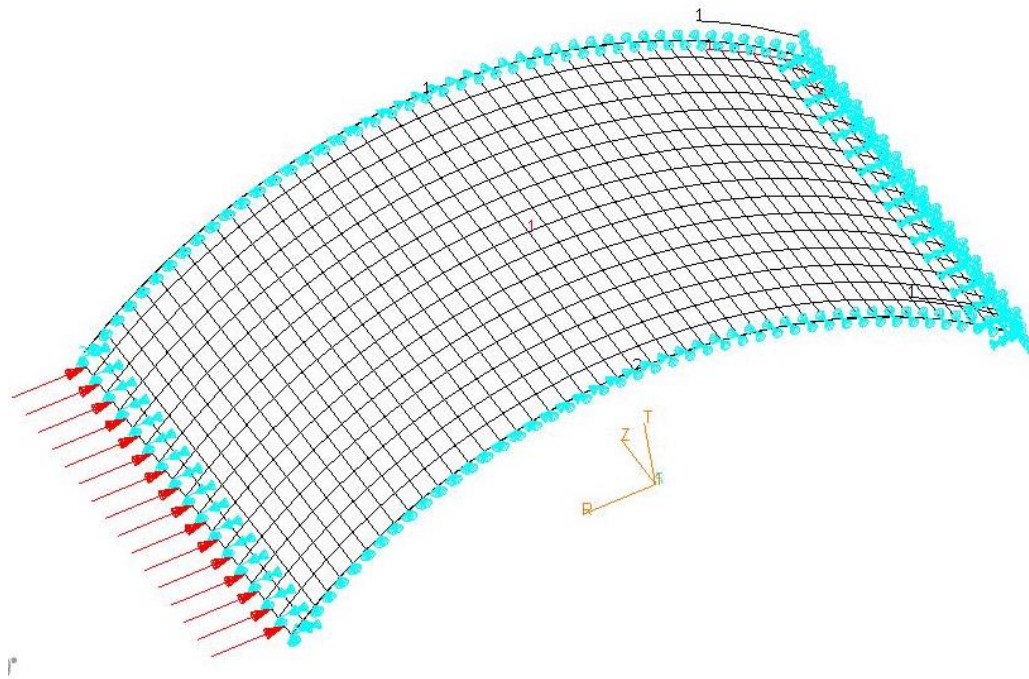


Figure 6.38 MSC. Patran model of the curved panel for the BLF maximization case study

The optimized fiber path for the configuration with the maximum BLF is given in Figure 6.39 as the yellow line, and the initial reference fiber path is presented in the figure as the black line. Control points of the optimized fiber path are given in Table 6.15.

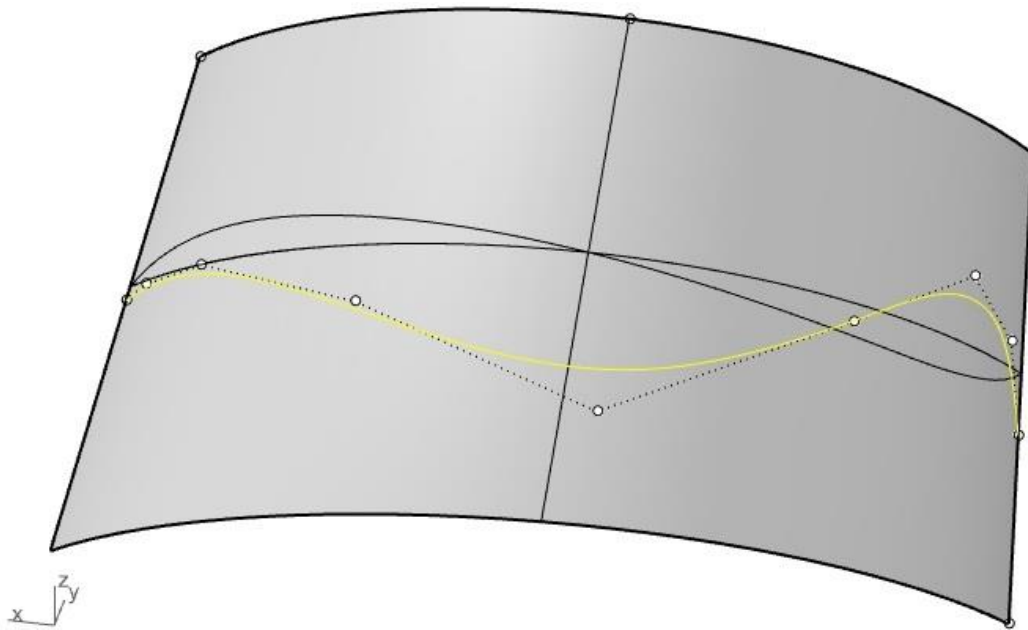


Figure 6.39 BLF optimized fiber path for the four-layer curved panel

Table 6.15 Control points of the BLF optimized fiber path for the four-layer curved panel

Control Points		
x	y	z
-800.00	0.00	369.83
-774.86	25.31	552.96
-689.84	100.37	644.474
-466.24	231.25	453.24
-60.479	330.94	187.03
363.89	274.90	374.51
659.88	122.99	493.35
764.40	36.07	489.34
800.00	0.00	472.07

In the optimized configuration, the BLF increased by 34.46% compared to the BLF of the curved panel with the initial reference fiber path. The best BLF value of the curved panel with the initial population's best particle's reference path was 0.79 and with the optimized path, BLF is 1.0623. Variation of the BLF with the iteration number is given in Figure 6.40.

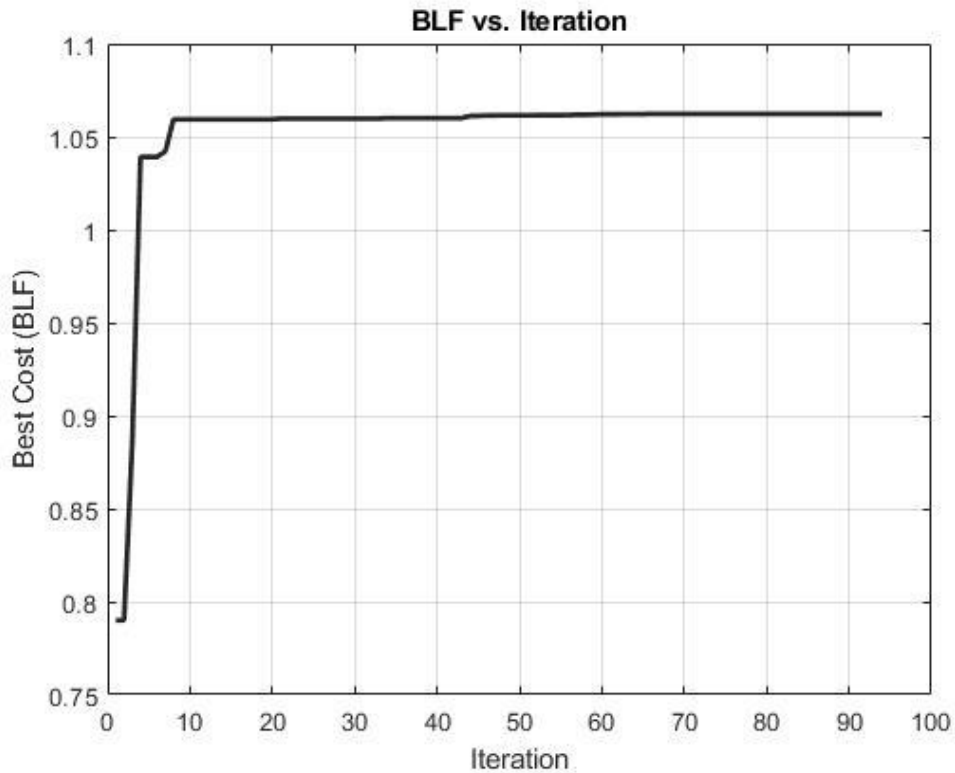


Figure 6.40 Variation of the BLF with the iteration number for the BLF maximization of the curved panel

6.3.2 Strain Energy Minimization of the Curved Panel

In this section strain energy minimization is studied for the described curved panel in Figure 6.31. In this case, the panel is under variable pressure load from the concave face as shown in Figure 6.41. The pressure load increases linearly from 1 atm on the left edge to 10 atm at the centerline parallel to the z-axis and decreases from 10 atm to 1 atm at the right edge. On the right and left short sides all translations are disabled ($u_R = u_T = u_Z = 0$) and rotation around R axis is disabled ($R_R = 0$). On the curved sides of the panel only the T and Z translation is disabled ($u_T = u_Z = 0$) and rotation around T axis is disabled ($R_t = 0$). All other translations and rotations are set free ($u_R = R_R = R_Z \neq 0$).

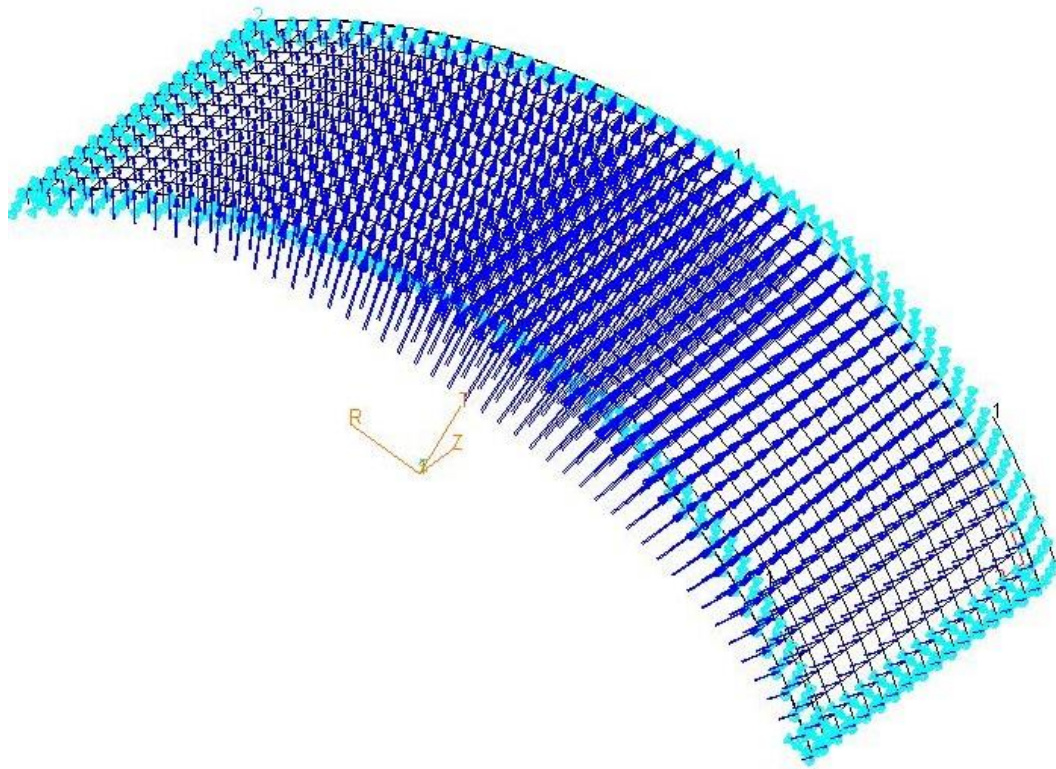


Figure 6.41 MSC. Patran model of the curved panel for the strain energy maximization case study

The reference fiber layup path is given in Figure 6.32. The control points are defined in Table 6.14. Correspondent knots and weights are same as in previous case studies.

The optimized path of the curved panel with the minimum strain energy is shown in Figure 6.42 as the yellow spline, and the initial reference path is presented in the figure as the black spline. The control points of the optimized fiber path are given in Table 6.16.

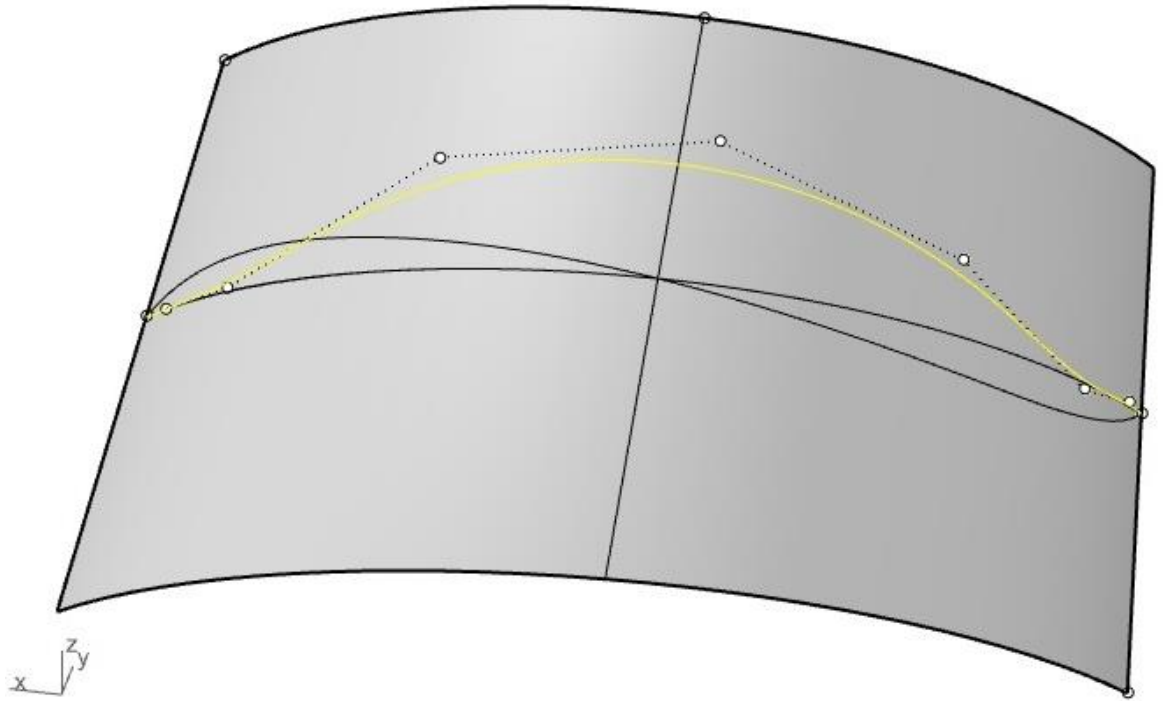


Figure 6.42 Fiber paths for the curved panel; reference fiber path and the fiber path with minimum strain energy

Table 6.16 Control points of fiber path for four-layer flat panel with minimum strain energy

Control Points		
x	y	z
-800.00	0.00	500
-774.86	25.31	505.65
-689.84	100.37	483.15
-466.24	231.25	630.59
-60.479	330.94	743.37
363.89	274.90	689.87
659.88	122.99	501.35
764.40	36.07	498.00
800.00	0.00	500

In this case study, the strain energy in the optimum configuration is reduced by 24.3 % compared to the strain energy of the curved panel with the initial reference fiber path. The strain energy of the curved panel with the initial fiber path was 0.19 kJ, and the strain energy of the curved panel with the optimized fiber path is 0.143 kJ. Variation of the strain energy with the iteration number for the curved panel is given in Figure 6.43.

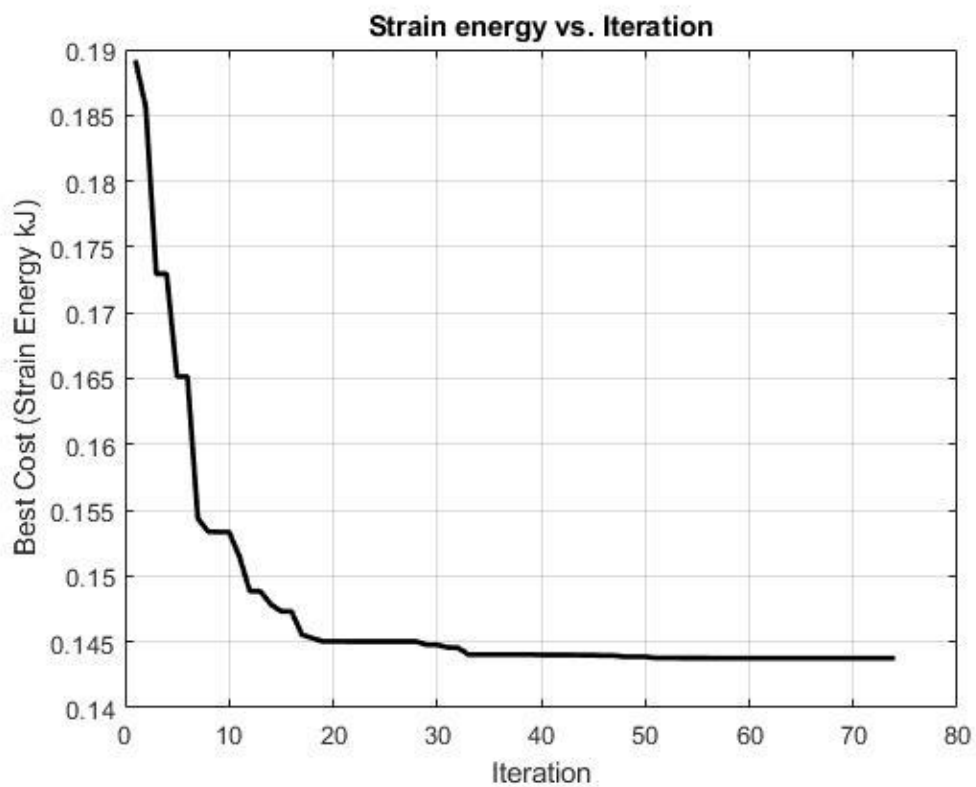


Figure 6.43 Variation of the strain energy with the iteration number for the curved panel strain energy minimization case study

6.3.3 Strain Energy Minimization of the Curved Panel with Failure Index (FI) constraint

In this section for the same curved panel given in Figure 6.31, strain energy minimization of the curved panel is performed subject to FI constraint. The panel is four layered panel, and the stacking sequence is same as shown in Figure 6.2. The panel is under the effect of variable pressure load from the concave face. The pressure load increases linearly from 1.2 atm at the short edges and 12 atm at the center line ($R=0$) with symmetric behavior with respect the z axis passing from the center of the panel. The boundary conditions are same as previous case in section 6.3.2.

For this analysis the only constraint is the FI, and the geometry constraint is not applied to the NURBS fiber path. If FI is greater than 1, objective function is automatically penalized by the algorithm and the solution is made infeasible.

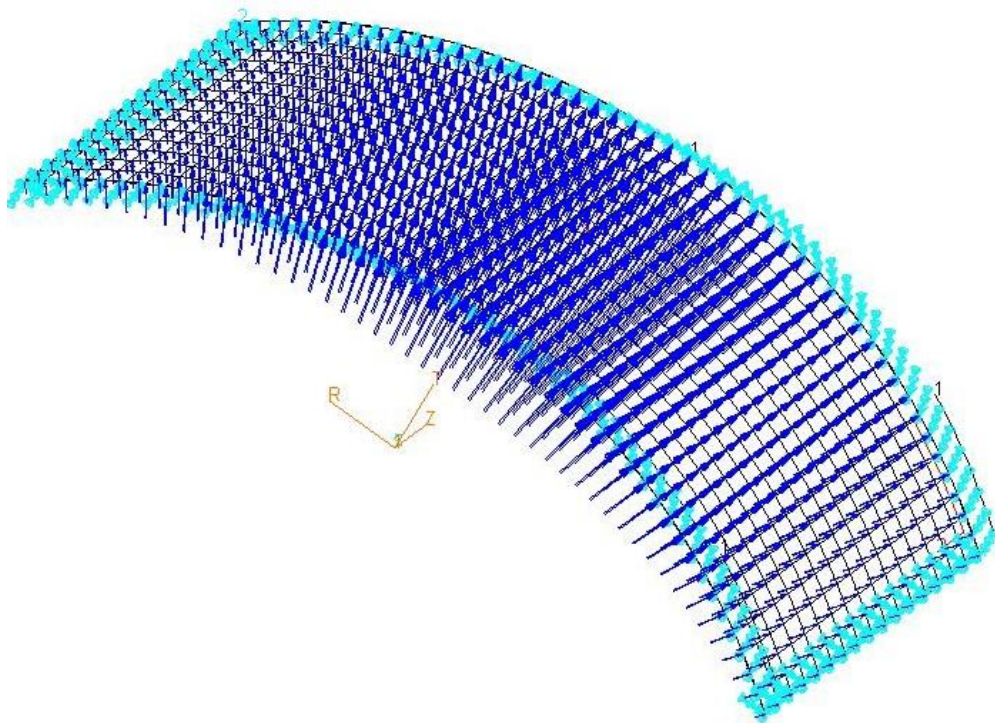


Figure 6.44 MSC. Patran model of the curved panel for the strain energy maximization case study constrained with FI

The reference fiber layup path is given in Figure 6.32 also the control points of the reference fiber path are defined in Table 6.14 with the correspondent knots and weights defined as mentioned before.

The optimized fiber path of the curved panel with FI constraint is given in Figure 6.45 as the yellow line and the initial reference path is presented in the figure as the black line. Control points are given in Table 6.17.

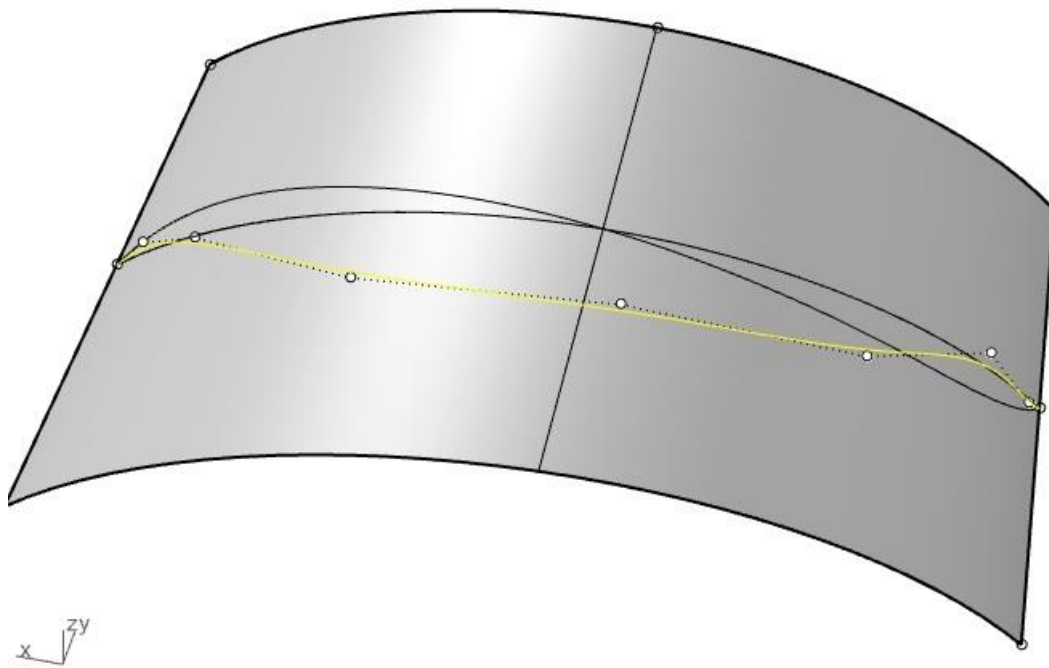


Figure 6.45 Rhino representation of the fiber paths for the four-layer curved panel ; reference fiber path and the fiber path with minimum strain energy

Table 6.17 Control points of the fiber path for four-layer curved panel with minimum strain energy subject to FI constraint

Control Points		
x	y	z
-800.00	0.00	500
-774.86	25.31	490.10
-689.84	100.37	530.64
-466.24	231.25	373.65
-60.479	330.94	320.24
363.89	274.90	332.54
659.88	122.99	486.02
764.40	36.07	527.53
800.00	0.00	500

In this optimization, the magnitude of the external load is tuned for the curved panel. The load tuned as at least one element of the created VSC structures with the initial populations candidate reference fiber paths has FI greater than one ($FI > 1$). As it can be seen in Figure 6.46 the maximum FI in this case is 1.24 for the best fiber path in the initial population. The maximum FI occurs in 46th element of the mesh in the 1st ply. By making the maximum FI greater than 1 in the initial configuration, it aimed to see the algorithm's ability to penalize the infeasible design in terms of FI. After the optimization process, maximum FI reaches a value of $FI = 0.31$ at the 31st element's 1st ply. Figure 6.47 gives the FI plot of the optimized configuration. In this case, the strain energy is reduced by of 24 % compared to the strain energy of the curved panel with the initial reference fiber path. The strain energy of the curved panel with the initial reference fiber path was 0.2724 kJ and the strain energy of the curved panel with the optimized fiber path is 0.2117 kJ. Variation of the strain energy with the iteration number for the strain energy minimization of the curved panel with FI constraint is given in Figure 6.48. In Figure 6.48, it is seen that first 2

strain energy values are 0.2724 kJ. This is because the reference fiber paths that do not violate the FI constraint is found after the 2nd iteration.

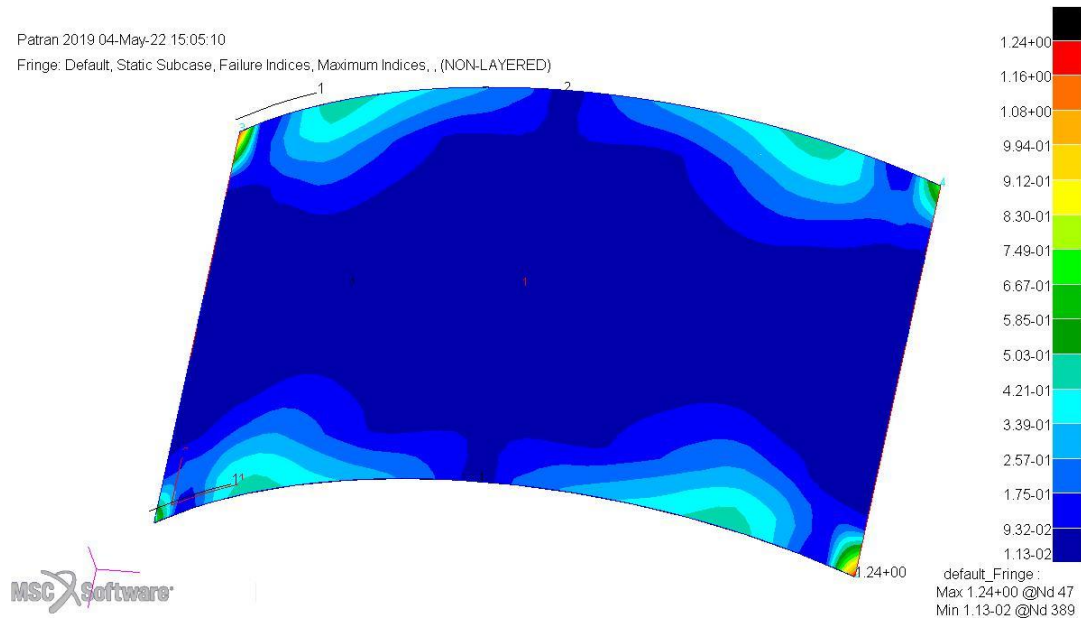


Figure 6.46 FI plot of the curved panel with the initial reference path under the given load and boundary conditions

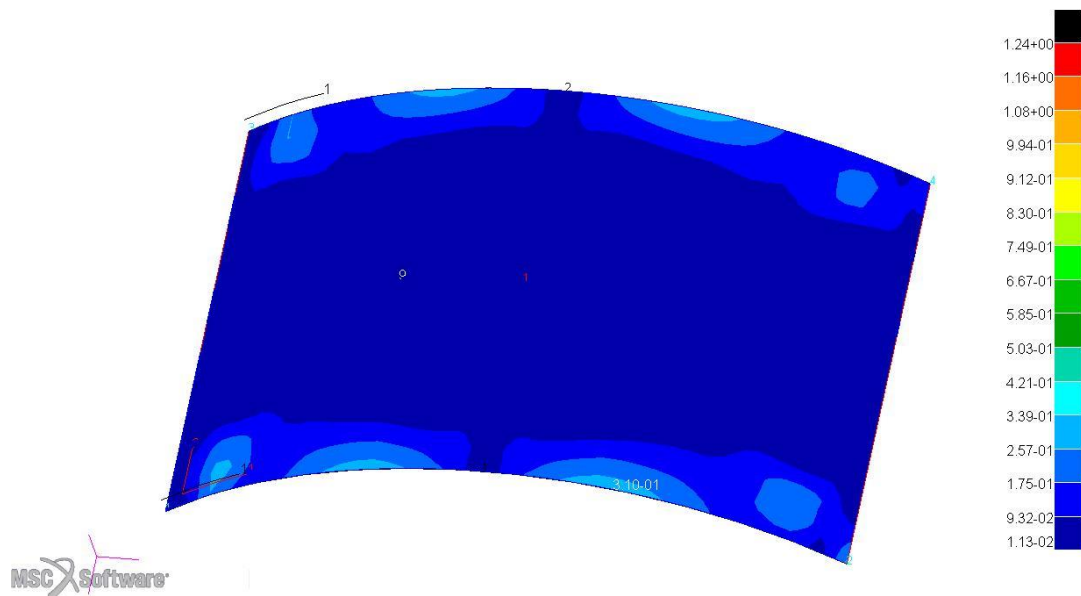


Figure 6.47 FI plot of the optimized curved panel under the given load and boundary conditions

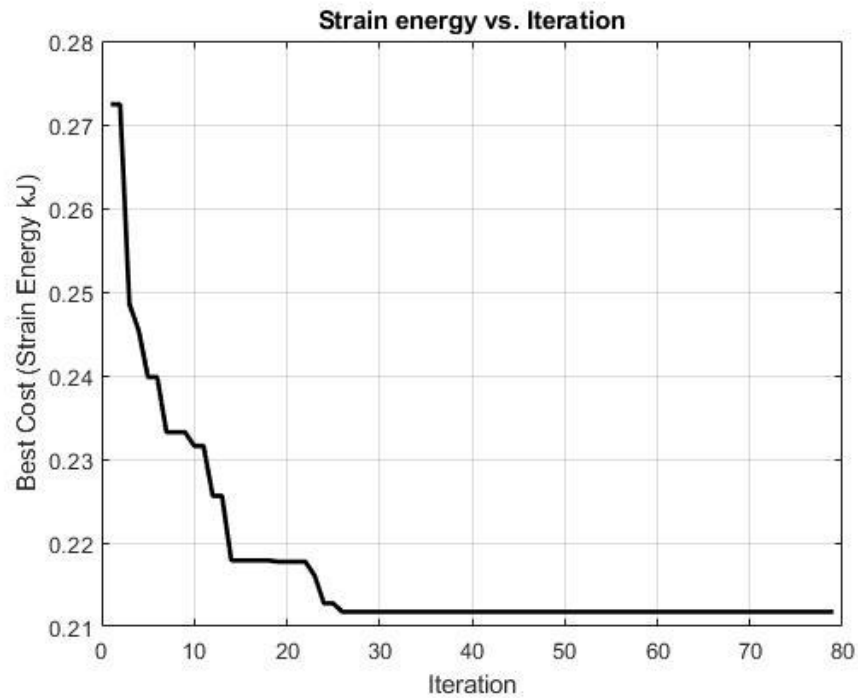


Figure 6.48 Variation of the strain energy with the iteration number for the strain energy minimization of the curved panel with FI constraint

6.4 Discussions

The developed method is verified for the strain energy minimization problem using a flat panel that is under compression. In the verification case with the referred boundary and loading conditions, it was expected that the optimum fiber path must converge to a straight line. This is because the maximum stiffness is achieved in the loading direction by the fibers parallel to the load. By the alignment of fibers parallel to the loading direction, minimum strain energy is achieved.

As outputs of the study firstly, flat panels are examined. For one layered and four layered flat panels strain energy minimization is studied. There are two constraints which are used separately to bound the feasible search space of the objective function. In the first case, strain energy minimization of one layered flat panel

constrained with fiber curvature is examined. The strain energy is reduced by 30 % compared to the best fiber path in the initial population. This study shows that the fiber path is very similar to the discrete analysis done by Setoodeh et al. [42]. In this case fibers are aligned in the loading direction at the right of the plate. Because maximum strain is expected to occur near the free edge. Moreover, very similar behavior can be seen in the study of Setoodeh et al. [42].

In the work of Setoodeh et al. different mesh sizes are examined. In Figure 6.49, it is seen that the total variation of the fiber angle in discrete elements throughout the cantilever beam has not changed with the mesh size. For the developed method in this study, an optimization for finer mesh with a mesh of 301x101 is also performed. In this study, it is seen that the behavior of the optimized fiber layup path has not changed. The optimized strain energy values for the course mesh and fine mesh cases are also very close. This study with 301x101 mesh density is added to Appendix D.

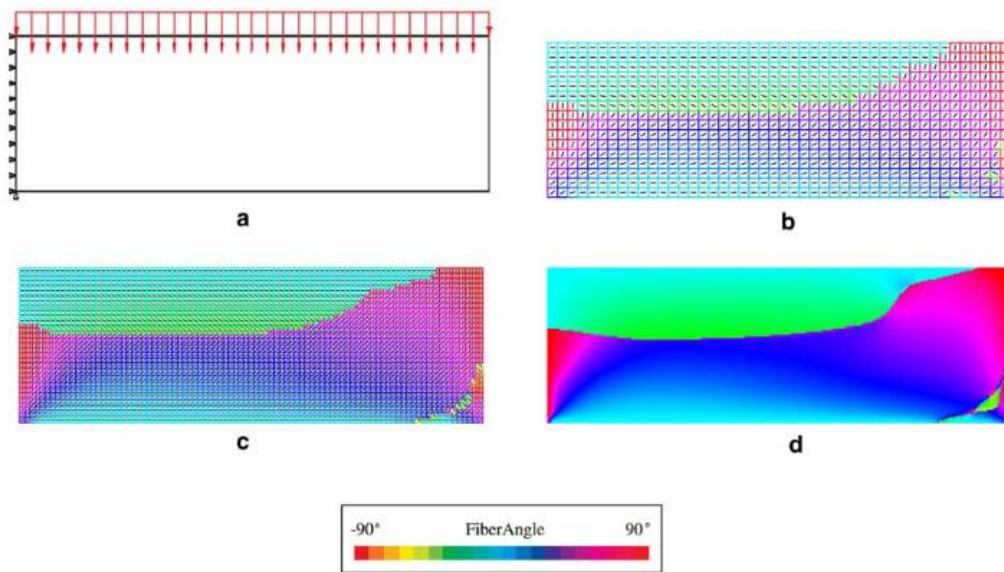


Figure 6.49 Short cantilever design with different meshes(a) Uniformly distributed loaded short cantilever beam; (b)46 x16 mesh; (c) 91 x31 mesh; (d) 301x101 mesh [42]

The second optimization case was the strain energy minimization of the flat panel composed of 4-layers with the same ply thickness and load and boundary conditions as the single layer flat panel. In this case 11.76% decrease in the strain energy is achieved as a result of fiber path optimization. It should be noted that compared to the one-layer flat plate case, since the number of layers is more and there are layers with symmetric fiber angles, percent decrease of the strain energy is not as high as the single layer case. The result in this case is compared with the result found by using the fiber path definition given in Reference 3 which is referred to as the $T_0 - T_1$ method in this study. It is seen that the strain energy results of the panel with optimized paths are very close, and optimum fiber paths are very similar.

Third case study was on the strain energy minimization of the 4- layered flat panel constraint by the FI. In this case, the magnitude of the distributed load is tuned such that at least one element in the flat panel with the initial reference fiber path has a FI greater than one ($FI > 1$). The maximum FI in this case was 1.72 and maximum FI reaches a value of $FI = 0.9756$ after the optimization. In this case, strain energy is reduced by 22.4% compared to the best fiber path configuration in the initially created swarm.

Last case for flat panel optimizations is the FI minimization of the flat panel with 4-layers. In this analysis, FI is in the objective function and in the constraint. In the initial configuration, the maximum failure index was greater than one ($FI > 1$), and it was $FI = 1.72$. After the optimization process, the maximum FI reaches a value of $FI = 0.9517$. It is guaranteed that all elements are in the safe zone, and their failure index is under the critical value, which is "1". In this case, 44% reduction is achieved in the maximum FI.

To show that the developed optimization methodology is applicable to the curved panels, two objective functions are used. For the four layered curved panel, buckling load factor maximization and strain energy minimization are studied. In these case

studies, two constraints are used separately to bound the feasible search space of the objective function.

In the first case study of the curved panel, BLF of the curved panel is maximized when it is constrained with the fiber curvature. Two different curved panels with different boundary conditions are optimized. It is shown that for the first configuration the BLF increased by 20.93% compared to the BLF of the curved panel with the initial reference fiber path. For the second configuration BLF increased by 34.46% compared to the BLF of the curved panel with the best layup path in the initial population.

Second case study of the curved panel is the strain energy minimization. The curved panel considered is subjected variable pressure load from the concave face. Under these conditions the strain energy in the optimum configuration is reduced by 24.3% compared to the strain energy of the curved panel with the best layup path in the initial population.

The third case study of the curved panel is very similar to the second case except that in this case FI is the constraint of the optimization, and to make FI greater than 1 in the initial configuration the loading is tuned. In this case, the strain energy is reduced by of 22.4 % compared to the strain energy of the curved panel with the initial reference fiber path.

CHAPTER 7

CONCLUSION AND FUTURE WORK

This thesis presents a method that utilizes NURBS based fiber path to construct variable stiffness composite structures in 3D. In this study, structural optimization method is developed to optimize panels under the presented circumstances. In this chapter the final words and lessons learned are discussed.

Studies on the VSC structures started with research on different manufacturing techniques of VSC structures. Different methods are used to manufacture VSC composite structures. DiNardo [8] worked on the internally dropped plies. In the study conducted by Leissa and Martin [9] volume fraction of the straight and parallel fibers is increased continuously towards the one end of the ply. The third method to manufacture variable stiffness composite structures is spatially varying the orientation of fibers in a layer of the composite structure by continuously placing the composite prepreg tows over the surface following a curved reference path. Nagendra et al. [16] worked on a different method to define the fiber path on surfaces. To define the fiber path, NURBS is used. Because NURBS has superior control capability of the spline and flexibility, and it is used in commercial design tools [17]. The study of Nagendra et al. [16] is the inspiration of the work presented in this thesis. It is the first study that NURBS is used for constructing VSC composites. Theoretical and experimental studies showed that optimizing the lay-up path of the composite fibers increase the mechanical performance of VSC structures.

In this thesis study, an optimization methodology utilizing the NURBS reference fiber path is developed. To define the NURBS path in 3D, basics of NURBS are reviewed. NURBS has superior ability to represent curves, hence CAD tools use NURBS as infrastructure to model geometries. In the third chapter ability of NURBS in representing the conical shapes is presented. For this reason, NURBS are used to

represent VSC fiber paths. In the fifth chapter, method to define NURBS fiber paths in the analysis model and optimization algorithm is presented.

In addition to defining the fiber layup path and structural analysis of composite structures, this study includes optimization of the composite structure. Thus, one of the main parts of the study is utilizing an optimization method. PSO is chosen in this study because it is very efficient in global search. Furthermore, it is simple to implement and has very few algorithm parameters to tune. In the developed method, during the optimization iterations many structural analyses must be done; thus an optimization method that is time efficient and easy to apply is desired to be used for the optimization.

In the developed method, reference fiber paths on the relevant geometries are created by the Rhino software. Creating the reference fiber path by Rhino was very practical for this study. In Rhino, the panels can be modelled easily, and the reference path can be drawn as a NURBS on the panel geometry. Defining the fiber path visually and seeing the locations of the control points helps to understand NURBS better. Besides the ease of visualization, Rhino also gives an output document which includes NURBS parameters. By using this file and extracting the data, suitable reference NURBS paths are easily created in MATLAB environment.

In the developed optimization methodology, after creating the reference fiber path, all the processes to optimize the fiber path for the defined boundary and load conditions are automatized. Based on the objective function given as an input to the method, optimization process automatically starts. During the optimization, fiber angles are written to the analysis input file automatically. MSC. Nastran is automatically called by the developed algorithm and finite element analysis is performed. Outputs are taken from the MSC. Nastran's output file for evaluation.

The results showed that fiber layup path optimization according to the objective function can be done by developed method for VSC structures. In the study, firstly, it is demonstrated that methodology is efficient in the fiber layup path optimization of VSC flat panels. The comparison between the fiber layup path of one layer flat panel strain energy minimization case and results of similar previous study overlaps. Moreover, a mesh dependence study has been conducted on this case and results showed that the fiber layup path is not dependent on the mesh size. For four layer flat panel strain energy minimization case, it is seen that the results of the current method and $T_0 - T_1$ method come out to be very close. This shows that even a definite advantage of the NURBS fiber path method cannot be seen; this is probably because of the used load and boundary conditions cantilevered plate under in-plane bending load. In the curved panel cases, as it is stated in the motivation of the study, the layup path is defined directly on the 3D surface by using the NURBS layup path definition. The optimization results show that used objective functions can be improved compared to the best particle that is created in the first population of the optimization cases.

This study showed that NURBS can be utilized to optimize the VSC structures. It is possible to optimize a specific response or responses of a composite structure much more effectively than the straight fiber case. In the study it is shown that compared to the classical T_0, T_1 method NURBS reference path presents advantages in the optimization of VSC structures. The presented case studies show that the developed method optimizes VSC flat and curved panels effectively. In all cases, compared to the initial reference path, there is an upturn regarding the studied objective function. Defining the fiber layup path with NURBS to manufacture VSC has a great potential. It is thought that in the future, fiber placement technology will be the primary production method of composite structures. With the fiber placement machines, it is possible to optimize a specific response or responses of a composite structure much more effectively than the straight fiber case using the stacking sequence optimization. It is also very efficient because computer-aided design tools use

NURBS in their background. Adding the method that is presented in the study to the 3D composite design tools defining the fiber paths can be very efficient.

In the future, the current work can be improved in many ways. They are listed below:

- In the future more NURBS parameters can be added to the optimization process. Besides the control points, knots and weights can be added to the optimization. During the development phase of the method, knot vector is also tried to be used as an optimization variable. However, due to the constraints of the knot values in the knot vector, it is seen that convergence to an optimum is computationally heavy. This problem can be solved by giving some basic constraint and penalties to the inappropriate knot values.
- This study can be applied to the multiple curvature structures. Many structures in aerospace industry have multiple curvatures and it can be shown that the developed method can optimize mechanical properties of the structure by using NURBS easily.
- By manufacturing the geometries with optimized paths, the finite element analysis results can be verified

REFERENCES

- [1] M. P. Groover, *Fundamentals of Modern Manufacturing*. John WILEY & SONS, INC.
- [2] Hexcel composite Inc., “Hexcel Products.”
<https://www.hexcel.com/Products/Carbon-Fiber/>
- [3] Z. Gurdal and R. Olmedo, “In-plane response of laminates with spatially varying fiber orientations - Variable stiffness concept,” *AIAA Journal*, vol. 31, no. 4, pp. 751–758, 1993, doi: 10.2514/3.11613.
- [4] C. Waldhart, “Analysis of Tow-Placed, Variable-Stiffness Laminates,” Thesis, Virginia Polytechnic Institute and State University, 1996.
- [5] S. Talukder, “Mathematical Modelling and Applications of Particle Swarm Optimization,” Blekinge Institute of Technology, 2011.
- [6] R. McNeel, “Rhinoceros 3D.” 2010.
- [7] H. İnci, “Discrete Fiber Angle and Continuous Fiber Path Optimization in Composite Structures,” Middle East Technical University, 2012.
- [8] M. T. Dinardo, “Buckling and Postbuckling Behavior of Laminated Composite Plates with Ply Dropoffs,” Master Thesis, Massachusetts Institute of Technology, 1986.
- [9] A. W. Leissa and A. F. Martin, “Vibration and buckling of rectangular composite plates with variable fiber spacing,” *Composite Structures*, vol. 14, no. 4, pp. 339–357, Jan. 1990, doi: 10.1016/0263-8223(90)90014-6.

- [10] P. T. Langley, “Finite element modeling of tow-placed variable-stiffness composite laminates,” Master Thesis, Virginia Polytechnic Institute and State University, 1999.
- [11] A. A. G. COOPER, “Trajectorial Fiber Reinforcement of Composite Structures,” PhD Thesis, University Of Washington St. Louis, 1972.
- [12] N. J. Hoff and C. Muser, “Stress Concentration Factors for Cylindrically Orthotropic Plates,” *Journal of Composite Materials*, vol. 16, no. 4, pp. 313–317, 1982, doi: 10.1177/002199838201600405.
- [13] M. W. Hyer and R. F. Charette, “Innovative Design Of The Composite Use Of Design Format Structures : Curvilinear In Composite Structure Design,” 1989.
- [14] M. W. Hyer and H. H. Lee, “The use of curvilinear fiber format to improve buckling resistance of composite plates with central circular holes,” *Composite Structures*, vol. 18, no. 3, pp. 239–261, Jan. 1991, doi: 10.1016/0263-8223(91)90035-W.
- [15] S. GÜLDÜ, “Analysis and Optimization Of Cylindrical Structures Manufactured By Automated Fiber Placement Technique,” Masters Thesis, Middle East Technical University, 2014.
- [16] S. Nagendra, S. Kodiyalam, J. Davis, and V. Parthasarathy, “Optimization of tow fiber paths for composite design,” Apr. 1995. doi: 10.2514/6.1995-1275.
- [17] T. N. Nguyen, “Isogeometric Finite Element Analysis based on Bézier Extraction of NURBS and T-Splines,” 2011.
- [18] Z. Gürdal, B. F. Tatting, and C. K. Wu, “Variable stiffness composite panels: Effects of stiffness variation on the in-plane and buckling response,” *Composites Part A: Applied Science and Manufacturing*, vol. 39, no. 5, pp. 911–922, 2008, doi: 10.1016/j.compositesa.2007.11.015.

- [19] D. H. J. A. Lukaszewicz, C. Ward, and K. D. Potter, “The engineering aspects of automated prepreg layup: History, present and future,” *Composites Part B: Engineering*, vol. 43, no. 3, pp. 997–1009, 2012, doi: 10.1016/j.compositesb.2011.12.003.
- [20] R. Matsuzaki, K. Mitsui, Y. Hirano, A. Todoroki, and Y. Suzuki, “Optimization of curvilinear fiber orientation of composite plates and its experimental validation,” *Composite Structures*, vol. 255, no. July 2020, p. 112956, 2021, doi: 10.1016/j.compstruct.2020.112956.
- [21] P. Hao *et al.*, “Design of manufacturable fiber path for variable-stiffness panels based on lamination parameters,” *Composite Structures*, vol. 219, no. March, pp. 158–169, 2019, doi: 10.1016/j.compstruct.2019.03.075.
- [22] O. Coskun and H. S. Turkmen, “Multi-objective optimization of variable stiffness laminated plates modeled using Bézier curves,” *Composite Structures*, vol. 279, no. June 2021, p. 114814, 2022, doi: 10.1016/j.compstruct.2021.114814.
- [23] D. F. Rogers, *An Introduction to NURBS*, vol. 1. Morgan Kaufmann, 2001.
- [24] L. Piegl and W. Tiller, *The NURBS book*, vol. 35, no. 02. Springer, 1997.
- [25] D. T. T. Do and J. Lee, “An automatically connected graph representation based on B-splines for structural topology optimization,” *Structural and Multidisciplinary Optimization*, vol. 59, no. 6, pp. 2023–2040, 2019, doi: 10.1007/s00158-018-2170-5.
- [26] M. G. Cox, “The numerical evaluation of b-splines,” *IMA Journal of Applied Mathematics (Institute of Mathematics and Its Applications)*, vol. 10, no. 2, pp. 134–149, 1972, doi: 10.1093/imamat/10.2.134.
- [27] C. de Boor, “On Calculating with B-Splines,” *Journal of Approximation Theory*, vol. 6, pp. 50–62, 1972.

- [28] E. Guilbert and H. Lin, “Isobathymetric line simplification with conflict removal based on a B-spline snake model,” *Marine Geodesy*, vol. 30, no. 1–2, pp. 169–195, 2007, doi: 10.1080/01490410701296697.
- [29] M. Hoffmann and I. Juhasz, “Shape control of cubic B-spline and NURBS curves by knot modifications,” in *Proceedings Fifth International Conference on Information Visualisation*, 2001, pp. 63–68. doi: 10.1109/IV.2001.942040.
- [30] K. E. Parsopoulos, *Handbook of Heuristics*. Springer International Publishing AG, 2016, pp. 1–47. doi: 10.1007/978-3-319-07153-4.
- [31] S. Sengupta, S. Basak, and R. A. Peters, “Particle Swarm Optimization: A survey of historical and recent developments with hybridization perspectives,” *arXiv*, 2018, doi: 10.3390/make1010010.
- [32] J. Kennedy and R. Eberhart, “Particle swarm optimization,” in *Proceedings of ICNN’95 - International Conference on Neural Networks*, 1995, vol. 4, pp. 1942–1948. doi: 10.1109/ICNN.1995.488968.
- [33] D. M. Spink, “NURBS tool box.” 2010.
- [34] MSC Software, “PATRAN.” 2019.
- [35] MSC Software, “MSC NASTRAN.” 2019.
- [36] J. Arora, *Introduction to Optimum Design*, 3rd ed. Iowa City: Elsevier, 2012. doi: 10.1016/C2009-0-61700-1.
- [37] K. Deb, *Optimization for Engineering Design Algorithms and Examples*. PHI Learning Pvt. Ltd, 2012.
- [38] R. C. Hibbeler and S. Fan, *Mechanics of materials (8th edition in SI units)*. Pearson, 2011.
- [39] A. K. Kaw, *Micromechanics of Composite Materials*. Boca Raton, FL: Taylor & Francis, 2006.

- [40] C. S. Lopes, Z. Gürdal, and P. P. Camanho, “Variable-stiffness composite panels: Buckling and first-ply failure improvements over straight-fibre laminates,” *Computers and Structures*, vol. 86, no. 9, pp. 897–907, 2008, doi: 10.1016/j.compstruc.2007.04.016.
- [41] J. P. Hurley, “Design of Variable Stiffness Composite Panels for Maximum Strength,” 2017.
- [42] S. Setoodeh, Z. Gürdal, and L. T. Watson, “Design of variable-stiffness composite layers using cellular automata,” *Computer Methods in Applied Mechanics and Engineering*, vol. 195, no. 9–12, pp. 836–851, 2006, doi: 10.1016/j.cma.2005.03.005.
- [43] MSC.Software, “MSC.Patran Reference Manual,” 2012.2., MSC.Software, 2011.
- [44] M. A. Luersen, C. A. Steeves, and P. B. Nair, “Curved fiber paths optimization of a composite cylindrical shell via Kriging-based approach,” *Journal of composite Materials*, vol. 49, no. 29, pp. 3583–3597, 2015, doi: 10.1177/0021998314568168.

APPENDICES

A. Example Rhino Step File

ISO-10303-21;

HEADER;

/* Generated by software containing ST-Developer

* from STEP Tools, Inc. (www.steptools.com)

*/

/* OPTION: using custom schema-name function */

FILE_DESCRIPTION(

/* description */ ("),

/* implementation_level */ '2;1');

FILE_NAME(

/* name */ '3dcurve',

/* time_stamp */ '2021-07-06T17:50:05+03:00',

/* author */ ("),

/* organization */ ("),

/* preprocessor_version */ 'ST-DEVELOPER v16.5',

/* originating_system */ "",

/* authorisation */ "");

FILE_SCHEMA (('AUTOMOTIVE_DESIGN'));

```

ENDSEC;

DATA;

#10=SHAPE_REPRESENTATION_RELATIONSHIP("","#33,#12);

#11=GEOMETRIC_CURVE_SET('curve_set_0',(#14));

#12=GEOMETRICALLY_BOUNDED_WIREFRAME_SHAPE_REPRESENTATION(
'wireframe_rep_0',(#11,#35),#32);

#13=PRESENTATION_LAYER_ASSIGNMENT('Default',(#14));

#14=B_SPLINE_CURVE_WITH_KNOTS("3,(#41,#42,#43,#44,#45,#46,#47,#48,
#49),
.UNSPECIFIED.,.F.,.F.,(4,1,1,1,1,1,4),(0.,147.304636887528,382.990865511633,
825.393092062741,1444.88456930339,1680.57869626113,1886.79622641132),.U
NSPECIFIED.);

#15=SHAPE_DEFINITION_REPRESENTATION(#16,#33);

#16=PRODUCT_DEFINITION_SHAPE('Document',"#18);

#17=PRODUCT_DEFINITION_CONTEXT('3D Mechanical Parts',#22,'design');

#18=PRODUCT_DEFINITION('A','First version',#19,#17);

#19=PRODUCT_DEFINITION_FORMATION_WITH_SPECIFIED_SOURCE('
A',
'First version',#24,.MADE.);

#20=PRODUCT_RELATED_PRODUCT_CATEGORY('tool','tool',(#24));

#21=APPLICATION_PROTOCOL_DEFINITION('Draft International Standard',
'automotive_design',1999,#22);

```

```

#22=APPLICATION_CONTEXT(
'data for automotive mechanical design processes');
#23=PRODUCT_CONTEXT('3D Mechanical Parts',#22,'mechanical');
#24=PRODUCT('Document','Document','Rhino converted to STEP',(#23));
#25=(
LENGTH_UNIT()
NAMED_UNIT(*)
SI_UNIT(.MILLI.,METRE.)
);
#26=(
NAMED_UNIT(*)
PLANE_ANGLE_UNIT()
SI_UNIT($,.RADIAN.)
);
#27=DIMENSIONAL_EXPONENTS(0.,0.,0.,0.,0.,0.,0.);
#28=PLANE_ANGLE_MEASURE_WITH_UNIT(PLANE_ANGLE_MEASURE(
0.01745329252),#26);
#29=(
CONVERSION_BASED_UNIT('DEGREES',#28)
NAMED_UNIT(#27)
PLANE_ANGLE_UNIT()
);

```

```

#30=(
NAMED_UNIT(*)
SI_UNIT($,.STERADIAN.)
SOLID_ANGLE_UNIT()
);
#31=UNCERTAINTY_MEASURE_WITH_UNIT(LENGTH_MEASURE(0.001),
#25,
'DISTANCE_ACCURACY_VALUE',
'Maximum model space distance between geometric entities at asserted c
onnectivities');
#32=(
GEOMETRIC_REPRESENTATION_CONTEXT(3)
GLOBAL_UNCERTAINTY_ASSIGNED_CONTEXT((#31))
GLOBAL_UNIT_ASSIGNED_CONTEXT((#30,#29,#25))
REPRESENTATION_CONTEXT('ID1','3D')
);
#33=SHAPE_REPRESENTATION('Document',(#34,#35),#32);
#34=AXIS2_PLACEMENT_3D("#40,#36,#37);
#35=AXIS2_PLACEMENT_3D("#50,#38,#39);
#36=DIRECTION(",(0.,0.,1.));
#37=DIRECTION(",(1.,0.,0.));
#38=DIRECTION(",(0.,0.,1.));

```

```

#39=DIRECTION("(1.,0.,0.));

#40=CARTESIAN_POINT("(0.,0.,0.));

#41=CARTESIAN_POINT("(-800.000000000001,0.,500.));

#42=CARTESIAN_POINT("(-774.867490670939,25.3175694229778,468.01));

#43=CARTESIAN_POINT("(-689.843902912201,100.370320585827,424.30));

#44=CARTESIAN_POINT("(-466.247995835935,231.259369892784,427.59));

#45=CARTESIAN_POINT("(-60.4793998790345,330.940396115973,487.75));

#46=CARTESIAN_POINT("(363.898123597787,274.907293578569,562.94));

#47=CARTESIAN_POINT("(659.88771881709,122.996240681861,578.87));

#48=CARTESIAN_POINT("(764.405552511706,36.0760911057276,544.62));

#49=CARTESIAN_POINT("(800.000000000002,0.,500.000000000001));

#50=CARTESIAN_POINT("(0.,0.,0.));

#51=(

GEOMETRIC_REPRESENTATION_CONTEXT(2)

PARAMETRIC_REPRESENTATION_CONTEXT()

REPRESENTATION_CONTEXT('pspace',")

);

ENDSEC;

END-ISO-10303-21;

```

B. Nastran Input File

Description of the MSC. Nastran input file which is prepared to perform mechanical optimization of composite panels' .fiber path.

```

$ Direct Text Input for File Management Section
$ Direct Text Input for Executive Control
$ Linear Static Analysis, Database
SOL 101
CEND
$ Direct Text Input for Global Case Control Data
TITLE = MSC.Nastran job created on 19-Jan-21 at 22:40:31
ECHO = NONE
SUBCASE 1
  SUBTITLE=Default
  ECHO = NONE
  SPC = 2
  LOAD = 2
  ESE (THRESH=0.5)=ALL
$   STRAIN (SORT1,REAL,VONMISES,STRCUR,BILIN)=ALL
  STRESS (SORT1,REAL,VONMISES,BILIN)=ALL
$ Direct Text Input for this Subcase
BEGIN BULK
$ Direct Text Input for Bulk Data
PARAM  POST      0
PARAM  NOCOMPS  1
PARAM  NUMOUT2  -3
PARAM  EST      -1
$ Elements and Element Properties for region : shell
$ Composite Property Reference Material: carbonfiberlaminate
$ Composite Material Description :
PCOMP  1          5000.    TSAI
      1          0.183    15.05    NO
      2          0.183   -15.05    NO
      3          0.183   -15.05    NO
      4          0.183    15.05    NO
PCOMP  2          5000.    TSAI
      5          0.183    14.99    NO
      6          0.183   -14.99    NO
      7          0.183   -14.99    NO
      8          0.183    14.99    NO
PCOMP  3          5000.    TSAI
      9          0.183    14.95    NO
     10          0.183   -14.95    NO
     11          0.183   -14.95    NO
     12          0.183    14.95    NO

```

} Output Requests
} PCOMP 1 with 4 layers midplane symmetric

} P_{lv}
} Orientation

The PCOMP property entry may be used when the element is a composite consisting of layers of unidirectional fibers. The information on the PCOMP entry includes the thickness, orientation, and material identification of each layer. The detail explanation of PCOMP card is given below.

1	2	3	4	5	6	7	8	9	10
PCOMP	PID	Z0	NSM	SB	FT	TREF	GE	LAM	
PCOMP	1			5000.0	HILL	0.0			
	MID1	T1	THETA1	SOUT1	MID2	T2	THETA2	SOUT2	
	1	0.0054	0.0	YES	1	0.0054	45.0	YES	
	MID3	T3	THETA3	SOUT3	etc.				
	1	0.0054	90.0						

- Z0 is composite offset.
 - Use default = -(composite thickness)/2
- NSM is nonstructural mass
- SB is allowable interlaminar shear stress
 - Put as Bonding Shear Stress in Patran 2D Orthotropic Material
 - Required for failure indices
- FT is the ply failure theorem
 - Required for failure indices
- TREF is reference temperature
 - Overrides TREFs on ply MAT8s
- GE is element damping
 - Overrides GE on ply MAT8s
- LAM is layup options
- MIDi is ply material ID
 - MAT8 ID
- Ti is ply thickness
- THETAi is ply angle
- SOUTi is data recovery option

MAT8 cards define the material properties. Each MAT8 cards refer to the MID number of the PCOMP cards layers. In this example there are 736 elements with 4 layers. Thus, there are 2944 MAT8 cards are created.

```

MAT8 2934 134000. 16750. 2070. 1160. 132.7 199.8 117.1
      .3 5862.5
MAT8 2935 134000. 16750. 2070. 1160. 132.7 199.8 117.1
      .3 5862.5
MAT8 2936 134000. 16750. 2070. 1160. 132.7 199.8 117.1
      .3 5862.5
MAT8 2937 134000. 16750. 2070. 1160. 132.7 199.8 117.1
      .3 5862.5
MAT8 2938 134000. 16750. 2070. 1160. 132.7 199.8 117.1
      .3 5862.5
MAT8 2939 134000. 16750. 2070. 1160. 132.7 199.8 117.1
      .3 5862.5
MAT8 2940 134000. 16750. 2070. 1160. 132.7 199.8 117.1
      .3 5862.5
MAT8 2941 134000. 16750. 2070. 1160. 132.7 199.8 117.1
      .3 5862.5
MAT8 2942 134000. 16750. 2070. 1160. 132.7 199.8 117.1
      .3 5862.5
MAT8 2943 134000. 16750. 2070. 1160. 132.7 199.8 117.1
      .3 5862.5
MAT8 2944 134000. 16750. 2070. 1160. 132.7 199.8 117.1
      .3 5862.5

```

The CQUAD4 Cards refers to the elements of Finite Elements Analysis.

EID is the element identification number (integer>0)

PID is identification number of a PSHELL or PCOMP property entry which is created for each element.

GRID is the grid point identification numbers of connection points.

```

CQUAD4 , 725 , 725 , 740 , 741 , 788 , 787
CQUAD4 , 726 , 726 , 741 , 742 , 789 , 788
CQUAD4 , 727 , 727 , 742 , 743 , 790 , 789
CQUAD4 , 728 , 728 , 743 , 744 , 791 , 790
CQUAD4 , 729 , 729 , 744 , 745 , 792 , 791
CQUAD4 , 730 , 730 , 745 , 746 , 793 , 792
CQUAD4 , 731 , 731 , 746 , 747 , 794 , 793
CQUAD4 , 732 , 732 , 747 , 748 , 795 , 794
CQUAD4 , 733 , 733 , 748 , 749 , 796 , 795
CQUAD4 , 734 , 734 , 749 , 750 , 797 , 796
CQUAD4 , 735 , 735 , 750 , 751 , 798 , 797
CQUAD4 , 736 , 736 , 751 , 752 , 799 , 798

```

1	2	3	4	5	6	7
CQUAD4	EID	PID	GRID1	GRID2	GRID3	GRID4

\$ Nodes of the Entire Model

```

GRID 1 0. 0.
GRID 2 65.22 0. 0.
GRID 3 130.43 0. 0.
GRID 4 195.65 0. 0.
GRID 5 260.87 0. 0.
GRID 6 326.09 0. 0.
GRID 7 391.3 0. 0.
GRID 8 456.52 0. 0.
GRID 9 521.74 0. 0.
GRID 10 586.96 0. 0.
GRID 11 652.17 0. 0.
GRID 12 717.39 0. 0.
GRID 13 782.61 0. 0.
GRID 14 847.83 0. 0.
GRID 15 913.04 0. 0.
GRID 16 978.26 0. 0.
GRID 17 1043.48 0. 0.
GRID 18 1108.7 0. 0.
GRID 19 1173.91 0. 0.
GRID 20 1239.13 0. 0.
GRID 21 1304.35 0. 0.
GRID 22 1369.57 0. 0.
GRID 23 1434.78 0. 0.

```


CQUAD4 card has information about, PCOMP card number. PCOMP card has information about the material, thickness, and orientation angle. MAT8 card is defined for the used material.

C. Example of an optimization iteration

In this appendix, an optimization iteration is described in more detail to clarify the issues related with the use the NURBS and PSO parameters. The example is from the strain energy minimization of the flat panel which is under in-plane bending load.

Figure C.1 shows the finite element model of the flat panel which is under in-plane bending load.

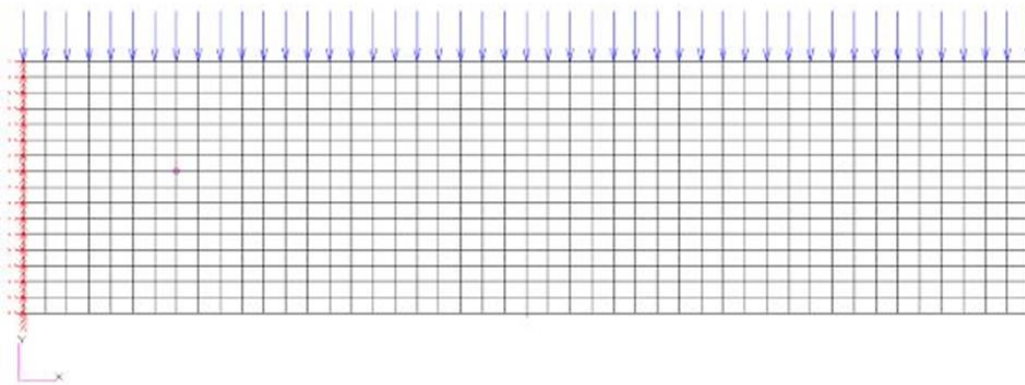


Figure C.1 Finite element of the flat panel

Figure C.2 shows the initial reference NURBS path created by Rhino for the flat panel given in Figure C.1.

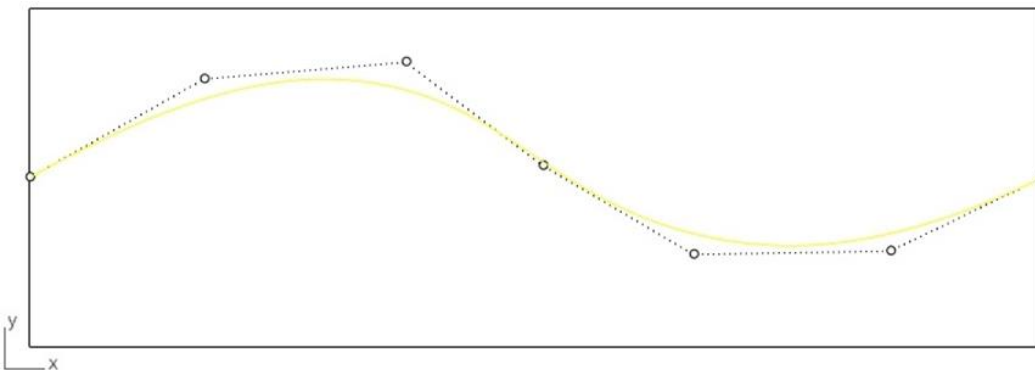


Figure C.2 Initial reference NURBS path created by Rhino for the flat panel

Coordinates of the control points of the initial reference fiber path are given in Table C.1.

Table C.1 Coordinates of the control points of the initial reference fiber path

Control points	x	0	515.48	1113.67	1519.77	1966.08	2549.32	3000
	y	500	791.23	841.07	535.29	272.80	282.77	500
	z	0	0	0	0	0	0	0

In the shifted fiber path method, only the y coordinates of the NURBS are changed since y is the shifting direction. Hence, all finite elements having element centers at a fixed x coordinate but different y coordinates have the fiber angle. Since the flat panel is on the x-y plane, z coordinates of the control points of the reference NURBS curve are all zero. In the PSO optimization, design variables are taken as the coordinates of the control points. Thus, the particles are matrices of order $3 \times m$ which include the coordinates (x_m, y_m, z_m) of the m control points. In the particular example, number of control points is 7, hence order of the matrices, which are the particles in the PSO, is 3×7 .

The search space X for this optimization problem is the values that y coordinates can take, and the search space is bounded by the length of the short edge of the rectangle which is 1000 mm. So the y coordinates of the control points can take values between [0,1000]. Since there is only a change in the y-direction, the dimension of the search space is 1 ($d=1$).

As the first step in PSO, twenty five empty particles ($n=25$) are created and the velocities of the particles and the objective functions (strain energy) are initialized. One of those particles in the initial population is initialized with the coordinates of the control points of the reference fiber path, and for the others, y coordinates of the particles are randomly created and x coordinates are taken as the x coordinates of the control points of the reference fiber path. So, in the initial population there are twenty

five 3x7 matrices (x,y and z coordinates of the control points) that store the coordinates of the control points. In iteration t , a particle is denoted as $\mathbf{x}_i^{(t)}$ with the subscript i denoting the particle number and in this problem range of i is 1-25.

In the initialization process, each particle's velocity vector is initialized as zeros vector of size 7. For each particle, through the course of the PSO run velocities are updated according to the Equation (C.1).

$$v_{ij}^{(t+1)} = w * v_{ij}^{(t)} + c_1 r_1 (p_{ij}^{(t)} - x_{ij}^{(t)}) + c_2 r_2 (p_{gj}^{(t)} - x_{ij}^{(t)}) \quad (C.1)$$

In the first iteration, for each particle ($i=1-n$) objective functions are also initialized as zero. When the iterations start, according to positions of the particles, the objective functions are evaluated.

In this problem, total strain energy of the flat panel, read from the output file of MSC. Nastran FE solver, is the objective function. This strain energy is calculated based on the loading applied to the panel and the created reference fiber path according to which fiber angle of each finite element is determined. So for each particle, one strain energy value is calculated, and since the population consists of 25 particles, there are 25 objective function values in a population in iteration t . $\mathbf{p}_i^{(t)}$ is the position vector of the i^{th} particle at the t^{th} iteration.

In each iteration, PSO algorithm uses the global best objective value ever visited in the search space. Since the example problem is a minimization problem, best value in the swarm is initialized as infinity and the particle positions are initialized as empty vector. After the first iteration, in each iteration, 25 strain energy values are calculated. Each objective function value (of $m=25$ particles) are compared with the previous global best value. After this comparison, the minimum strain energy value is taken as the current global best and stored to use in the next iteration, and the corresponding position of this strain energy is taken as $\mathbf{p}_g^{(t+1)}$. This global best value is stored and updated whenever better global best is found during the course of iterations.

In Figure C.3, MATLAB structure after the termination of the optimization is given. “Fields” column is the particle number from 1 to 25. “Position” column consists of position of each particle given as 3x7 matrices (x,y and z coordinates of the control points). “Velocity” column is a vector of size 7 with first and last value being equal to 0. Since the positions of the first and last control points do not change, first and last values of the velocity vector are zero. The column named as “Best” contains MATLAB structure arrays that stores the best objective value and the corresponding position of each particle ever visited.

In the optimization algorithm, a convergence tolerance is defined. PSO continues until all particles’ position vectors are within a defined tolerance. The tolerance is 10 mm in this example because control points are the optimization variables. Consequently, as seen in Figure C.3, after the termination of the optimization all objective values are very close to each other.

In Figure C.4, MATLAB structure that contains the best position and cost after the termination of iterations is shown.

. This structure is updated if better results are found through the course of PSO.

Fields	Position	Cost	Velocity	Best
1	3x7 double	7.9067e+05	[0,1.4601,0.0213,-0.0228,5.1137,32.2749,0]	1x1 struct
2	3x7 double	7.9067e+05	[0,0.0536,-0.2532,0.0278,-0.6330,-0.1780,0]	1x1 struct
3	3x7 double	7.9067e+05	[0,-0.0439,-0.0187,-0.4230,-0.0843,0.2629,0]	1x1 struct
4	3x7 double	7.9067e+05	[0,-0.2490,1.2490,0.3292,-1.1753,0.1396,0]	1x1 struct
5	3x7 double	7.9067e+05	[0,0.1326,0.0270,-0.0638,-0.7004,0.3300,0]	1x1 struct
6	3x7 double	7.9067e+05	[0,-0.1368,0.3032,-0.0390,-0.3405,-0.1059,0]	1x1 struct
7	3x7 double	7.9067e+05	[0,-0.1753,-0.6302,-0.4437,-0.0650,-3.9345,0]	1x1 struct
8	3x7 double	7.9067e+05	[0,-0.1204,0.0237,-0.0063,0.3831,0.8500,0]	1x1 struct
9	3x7 double	7.9068e+05	[0,1.7364,-1.7591,-0.1816,0.7751,-1.3182,0]	1x1 struct
10	3x7 double	7.9067e+05	[0,0.4176,-0.1972,0.0567,0.0289,-0.2469,0]	1x1 struct
11	3x7 double	7.9067e+05	[0,-2.5741,-0.7897,0.2885,-7.5142e-04,0.8033,0]	1x1 struct
12	3x7 double	790666	[0,-0.0368,0.0047,-0.0474,1.2223,-0.0954,0]	1x1 struct
13	3x7 double	7.9067e+05	[0,0.0703,0.3593,-0.0585,-0.0408,0.0305,0]	1x1 struct
14	3x7 double	7.9067e+05	[0,0.0332,-1.3967,0.2859,1.7042,-0.3530,0]	1x1 struct
15	3x7 double	7.9067e+05	[0,0.1524,-0.1307,3.8695,-0.0291,-3.2139,0]	1x1 struct
16	3x7 double	7.9070e+05	[0,-0.3003,0.1134,-28.9986,0.4676,2.9907,0]	1x1 struct
17	3x7 double	7.9068e+05	[0,0.0837,7.9307,-0.2675,1.0548,-4.1236,0]	1x1 struct
18	3x7 double	7.9067e+05	[0,0.2478,0.0243,-0.2954,-0.4160,0.1169,0]	1x1 struct
19	3x7 double	790666	[0,-0.1904,-0.0570,-1.8330,2.3715,-0.5047,0]	1x1 struct
20	3x7 double	790670	[0,0.2365,3.8216,-0.7673,4.2178,0.1126,0]	1x1 struct
21	3x7 double	7.9067e+05	[0,-0.2213,0.4091,0.4440,-1.5327,1.9602,0]	1x1 struct
22	3x7 double	7.9067e+05	[0,-0.1820,0.9601,0.6898,0.0701,-1.7208,0]	1x1 struct
23	3x7 double	7.9067e+05	[0,0.1567,-0.0056,-0.0704,-0.0688,0.0056,0]	1x1 struct
24	3x7 double	7.9067e+05	[0,-0.0992,-0.0122,0.1813,0.9019,-8.5518,0]	1x1 struct
25	3x7 double	7.9067e+05	[0,-0.4684,-0.1707,-1.0646,6.8875,5.2862,0]	1x1 struct

Figure C.3 MATLAB particle structure after the termination of optimization

Field ▲	Value
Position	3x7 double
Cost	7.9067e+05

Figure C.4 MATLAB structure that contains the best position and cost after the termination of iterations

As an example of position, cost and velocity fields of particle 6 given in Figure C.3 is presented in Table C.2.

Table C.2 Position, cost and velocity fields for particle 6 in Figure C.3

Final Optimization Results for Particle 6							
Position X	0	515.48	1113.67	1519.77	1966.08	2549.32	3000
Position Y	500	486.87	495.48	473.31	437.97	65.74	500
Velocity	0	-0.13678	0.30317	-0.038994	-0.34049	-0.10588	0
Cost	7.906665 x 10 ⁵						

Best position and cost fields in Figure C.4 is presented in Table C.3

Table C.3 Position, cost and velocity fields for best solution in Figure c.4

Best particle and the corresponding cost							
Position X	0	515.48	1113.67	1519.77	1966.08	2549.32	3000
Position Y	500	486.82	495.77	473.71	438.06	65.52	500
Cost	7.9067 x 10 ⁵						

D. One Layer Flat Panel Strain Energy Minimization with Fine Mesh

In this appendix, results one layer flat panel strain energy minimization is examined with fine mesh density. In the finite element model, a mesh of 301x101 mesh is used. The fiber layup path and the optimization iteration results are presented below.

The loading magnitude is 1kN/m and the panel consists of 1 layer with a 0.183 mm thick ply. In Figure D.1, the optimized path is shown as the purple line, and the initial reference path is shown as the green line. The optimized control points of NURBS path are given in Table D.1.

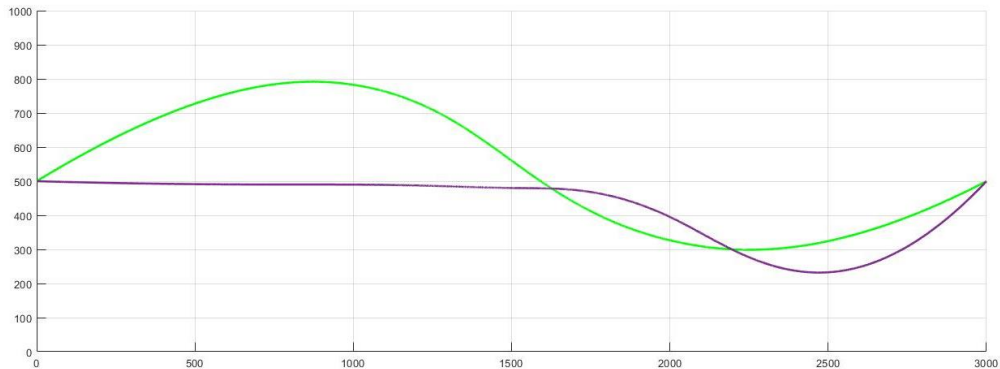


Figure D.1 Strain energy optimized fiber path for the one-layer flat panel with 301x101 mesh density; Matlab representation

Table D.1 Control points of the strain energy optimized fiber path for the one-layer flat panel with 301x101 mesh density

Control points	x	0	515.48	1113.67	1519.77	1966.08	2549.32	3000
	y	500	486.52	493.89	474.01	488.06	57.32	500

The strain energy is reduced by 50.48% compared to the strain energy of the best particle that is created in the first population. The strain energy with the best reference fiber path of the first population was 1.60 kJ, and for the panel with the

optimized fiber path, strain energy is 0.79 kJ. Strain energy versus the iteration number plot during the optimization is given in Figure D.2

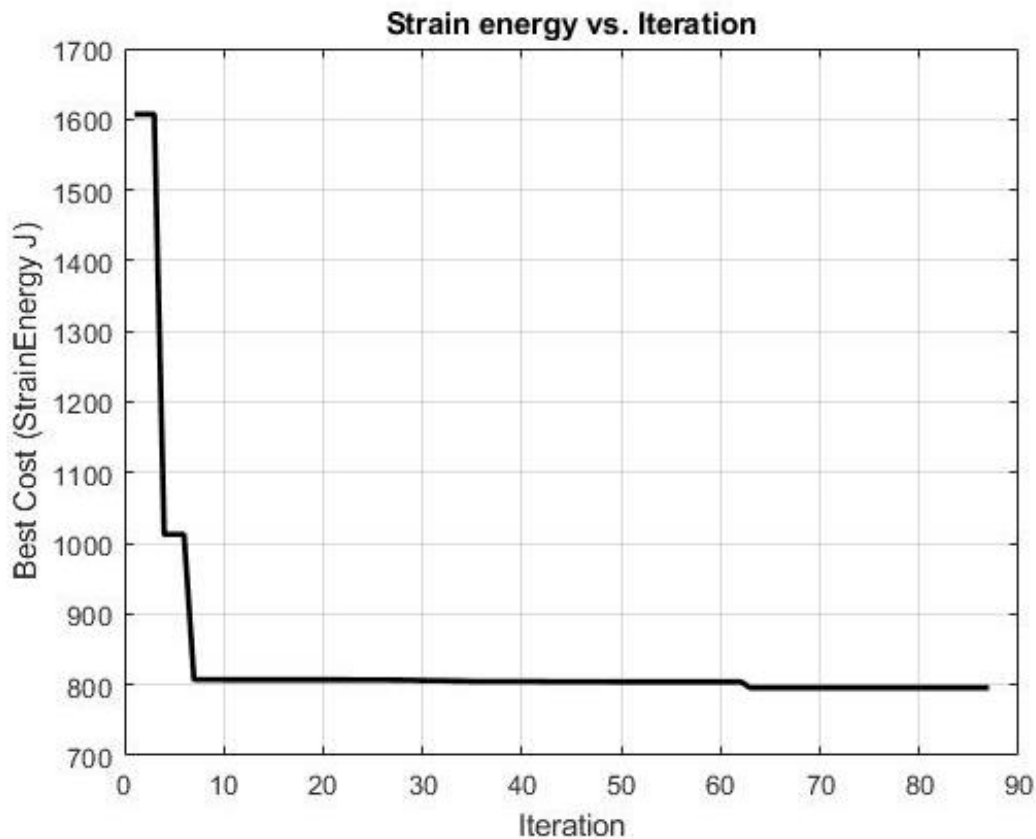


Figure D.2 Strain energy versus the iteration number for the one-layer flat panel strain energy minimization problem 301x101 mesh density

When the results of the one layer flat panel strain energy minimization with fine mesh and the coarse mesh are compared, it is seen that in Table D.2 that y coordinates of control points of the fiber layup paths are slightly different. However, the values of the control points are very close, and the shape of the layup paths are very similar as it can be seen in the Figure D.3. Although the coordinates of the control points are changed, the final optimized strain energy values came out as same (0.79 kJ).

Table D.2 Control points obtained with fine mesh and the coarse mesh for the one layer flat panel strain energy minimization problem

x coordinates of the fiber path in both mesh sizes	y coordinates of fiber path with fine mesh	y coordinates of fiber path with coarse mesh
0	500	500
515.48	486.52	486.82
1113.67	493.89	495.77
1519.77	474.01	473.71
1966.08	488.06	438.06
2549.32	57.32	65.52
3000	500	500

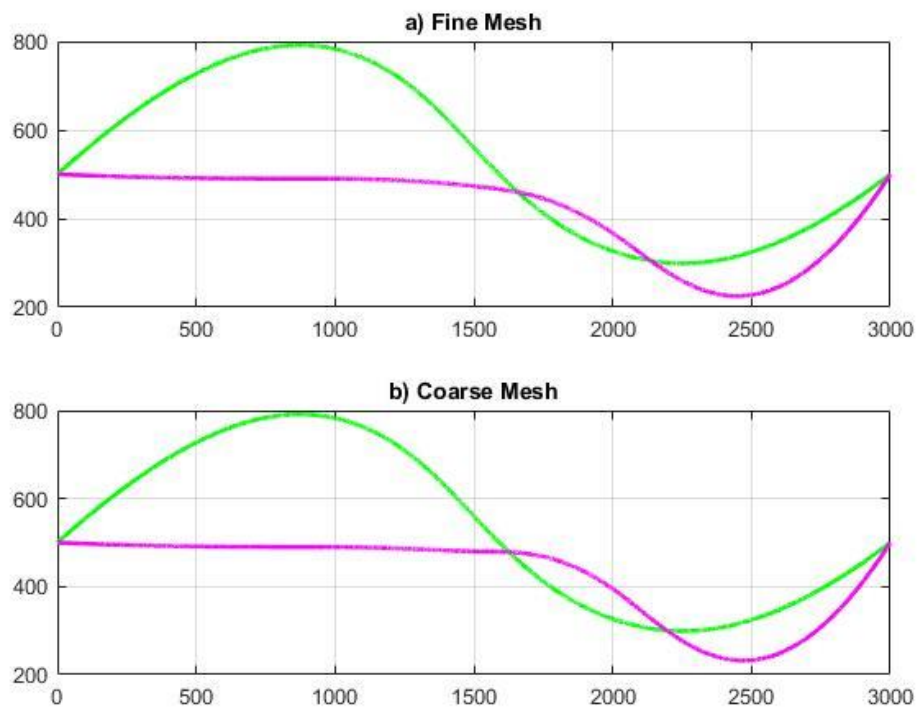


Figure D.3 One layer flat panel strain energy minimization fiber paths a) fiber path after optimization with fine mesh b) fiber path after optimization with coarse mesh